ÇUKUROVA UNIVERSITY
INSTITUTE OF NATURAL AND APPLIED SCIENCES

PhD THESIS

Merve Nilay AYDIN

FAULT-TOLERANT SLIDING MODE CONTROL DESIGN FOR AN ELECTROMECHANICAL SYSTEM

DEPARTMENT OF COMPUTER ENGINEERING

ADANA-2022

ABSTRACT

PhD THESIS

FAULT-TOLERANT SLIDING MODE CONTROL DESIGN FOR AN ELECTROMECHANICAL SYSTEM

Merve Nilay AYDIN

ÇUKUROVA UNIVERSITY
INSTITUTE OF NATURAL AND APPLIED SCIENCES
DEPARTMENT OF COMPUTER ENGINEERING

Supervisor : Prof. Dr. Ramazan ÇOBAN
Year: 2022, Pages: 109
Juries : Prof. Dr. Ramazan ÇOBAN
: Prof. Dr. M. Fatih AKAY
: Prof. Dr. Ahmet TEKE
: Assoc. Prof. Dr. Sertan ALKAN
: Asst. Prof. Dr. İpek ABASIKELEŞ TURGUT

The purpose of this thesis is to propose an adaptive dynamic proportional–integral–derivative sliding surface based second-order fault-tolerant sliding mode controller for speed control of an electromechanical system under uncertainties and disturbances. The sliding-mode control technique is a robust control scheme that obtains the desired output with a concept of changing the controller's structure in response to change the state of the system. The online adaption skill of adaptive control makes it superior to sliding mode control in terms of constant or slowly-varying parameters for a non-linear dynamical system having uncertainties. Fault-tolerant control schemes are utilized commonly in safety-critical systems. This study aims to show how to utilize the robust properties of second-order adaptive dynamic sliding-mode control on the problem of component fault. The control design process prioritizes, even in the existence of the unsuitable conditions, providing the closed-loop stability for overall system. The Lyapunov theorem is used for affirming the design and stability of the closed-loop system. The presented adaptive dynamic first and second-order fault-tolerant sliding-mode controllers and the traditional sliding-mode controller are compared with each other and the results are discussed. The experimental results of the proposed fault-tolerant controller, concerning parametric uncertainties and disturbances, acquire suitable tracking performance and show more robustness than the traditional sliding-mode control.

Key Words: Fault tolerant control, sliding mode control, nonlinear control, electromechanical system

ÖZ

DOKTORA TEZİ

ELEKTROMEKANİK BİR SİSTEM İÇİN HATA-TOLERANSLI KAYAN KİPLİ KONTROL TASARIMI

Merve Nilay AYDIN

ÇUKUROVA ÜNİVERSİTESİ
FEN BİLİMLERİ ENSTİTÜSÜ
BİLGİSAYAR MÜHENDİSLİĞİ ANABİLİM DALI

Danışman : Prof. Dr. Ramazan ÇOBAN
Yıl: 2022, Sayfa: 109
Juri : Prof. Dr. Ramazan ÇOBAN
: Prof. Dr. M. Fatih AKAY
: Prof. Dr. Ahmet TEKE
: Doç. Dr. Sertan ALKAN
: Dr.Öğr. Üyesi İpek ABASIKELEŞ TURGUT

Bu tezin amacı, belirsizlikler ve bozulmalar altında bir elektromekanik sistemin hız kontrolü için uyarlanabilir dinamik oransal-integral-türevsel kayan yüzey tabanlı ikinci dereceden hata toleranslı kayan kipli kontrolcü tasarlamaktır. Kayan kipli kontrol tekniği, sistemin durumunu değiştirmeye yanıt olarak kontrolcü yapısını değiştirme mantığıyla çalışan gürbüz bir kontrol yöntemidir. Uyarlanabilir kontrolün çevrim içi uyarlama becerisi, belirsizliklere sahip doğrusal olmayan dinamik bir sistem için sabit veya yavaş değişen parametreler açısından onu kayan kipli kontrolden üstün kılar. Hataya dayanıklı kontrol, güvenlik açısından kritik sistemlerde yaygın olarak kullanılmaktadır. Bu çalışma, ikinci dereceden uyarlanabilir dinamik kayan kipli kontrolün gürbüz özelliklerinin bileşen hatası probleminde nasıl kullanılacağını göstermeyi amaçlamaktadır. Kontrol tasarım süreci, uygun olmayan koşulların varlığında bile tüm sistem için kapalı döngü kararlılığı sağlamaya öncelik verir. Lyapunov teoremi, kapalı döngü sistemin tasarımını ve kararlılığını doğrulamak için kullanılmıştır. Sunulan uyarlanabilir dinamik birinci ve ikinci dereceden hata toleranslı kayan kipli kontrolcüler ve geleneksel kayan kipli kontrolcü birbiriyle karşılaştırılmış ve sonuçlar tartışılmıştır. Önerilen hata toleranslı kontrolcünün deneysel sonuçları, parametrik belirsizlikler ve bozulmalar karşısında, uygun referans izleme performansı elde ettiğini ve geleneksel kayan kipli kontrolcüden daha gürbüz olduğunu göstermiştir.

Anahtar Kelimeler: Hata toleranslı kontrol, kayan kipli kontrol, doğrusal olmayan kontrol, elektromekanik sistem;

EXPANDED ABSTRACT

In this thesis, an adaptive dynamic proportional–integral–derivative sliding surface based second-order fault-tolerant sliding mode controller is proposed for speed control of an electromechanical system under uncertainties and disturbances.

Control of non-linear systems is a related field of study in control engineering. In control of non-linear systems, some approximated mathematical models are used for controller design. These approximations might cause some unknown disorders and uncertainties during the control design process. Recently for the control of non-linear systems many design techniques have raised such as sliding mode control, fault-tolerant control and adaptive control. Safety-critical systems commonly utilize fault-tolerant schemes.

Sliding mode control is named in control theory as a particular type of variable structure control. It is a robust control scheme that obtains the desired output with a concept of changing the controller's structure in response to change the state of the system. Robustness measures the performance of being able to overcome the issues of disturbances and uncertainties for a control system.

In the matter of handling parametric or non-parametric uncertainties, in comparison with sliding-mode control, the adaptive control methodology can attain further flexibility for adjusting unknown non-linear dynamical systems due to generally containing an adaptive estimation approach which plays an essential role in learning.

There are many different design methodologies in the literature in order to the design of fault-tolerant controllers. In this study, because of their advantages, adaptive sliding mode control and fault- tolerant control are used together to increase the stability, reliability and survivability of safety-critical systems.

In this thesis, to eliminate the chattering which arises from undesirable occurrence of oscillations on switching control part with finite frequency and amplitude, higher-order sliding modes technique is used. In this study because the

fault function is added on the system parameters model based high-order sliding mode algorithm is used. Hence, the proposed adaptive method for controlling the uncertain system is proportional-integral-derivative sliding surface based fault tolerant control.

Fault can occur on one or more parameters of a system and cause serious damage. Hence, under fault condition, it is aimed to improve performance of the controller by making the designed controller a second-order and better results are obtained as expected. A lot of different fault cases are considered to occur under load.

In order to confirm the system robustness, the presented adaptive first-order and second-order fault-tolerant controllers are applied to the real electromechanical system and compared with the traditional sliding mode control. To test the performances of the designed and proposed controllers, control input and speed responses are considered and compared with each other.

The second-order adaptive dynamic fault tolerant controller, according to the rise time and settling time, is much better than the first-order adaptive dynamic fault tolerant controller. Also, the second-order adaptive dynamic fault tolerant controller significantly eliminates the chattering in comparison with the first-order adaptive dynamic fault tolerant controller.

GENİŞLETİLMİŞ ÖZET

Bu tezde, belirsizlikler ve bozucular altında bir elektromekanik sistemin hız kontrolünü yapmak için uyarlanabilir, dinamik, oransal-integral-türevsel kayan yüzey tabanlı ikinci dereceden hata toleranslı kayan kipli kontrol yöntemi önerilmiştir.

Doğrusal olmayan sistemlerin kontrolü, kontrol mühendisliği ile ilgili bir çalışma alanıdır. Doğrusal olmayan sistemlerin kontrolünde, kontrolcü tasarımı için bazı yaklaşık matematiksel modeller kullanılır. Bu tahmini kullanımlar, kontrol tasarım sürecinde bazı bilinmeyen bozukluklara ve belirsizliklere neden olabilmektedir. Son zamanlarda doğrusal olmayan sistemlerin kontrolü için kayan kipli kontrol, hata toleranslı kontrol ve uyarlanabilir kontrol gibi birçok tasarım tekniği gündeme gelmiştir. Güvenliğin kritik önem taşıdığı sistemlerde genellikle hata toleranslı yöntemler kullanır.

Kayan kipli kontrol, kontrol teorisinde değişken yapılı kontrol türü olarak adlandırılır. Sistem durumunun değişmesine yanıt olarak kontrolör yapısını değiştirme konseptiyle istenen çıktıyı elde eden gürbüz bir kontrol metodudur. Gürbüzlük, bir kontrol sistemi için gürültü ve belirsizlik sorunlarının üstesinden gelme performansıdır.

Parametrik veya parametrik olmayan belirsizliklerin ele alınması konusunda, doğrusal olmayan dinamik sistemlerin denetimi için uyarlamalı kontrol uyarlanabilir bir tahmin yaklaşımı içerdiğinden dolayı kayan kipli kontrole kıyasla daha esnek olmaktadır.

Hataya dayanıklı kontrolörlerin tasarımı için literatürde birçok farklı tasarım metodolojisi bulunmaktadır. Bu çalışmada, avantajları nedeniyle, uyarlanabilir kayan kipli kontrol ve hata toleranslı kontrol güvenlik açısından kritik sistemlerin kararlılığını, güvenilirliğini ve sürekliliğini artırmak için birlikte kullanılmıştır.

Bu tezde, sonlu frekanslı ve genlikli anahtarlama kontrol parçası üzerinde istenmeyen salınımların meydana gelmesinden kaynaklanan çatırdamaları gidermek için yüksek dereceli kayan kipli kontrol tekniği kullanılmıştır. Ayrıca sistem parametrelerine hata fonksiyonu eklendiğinden dolayı model tabanlı yüksek dereceli kayan kipli kontrol algoritması kullanılmıştır. Böylece belirsizlik içeren sistemi kontrol etmek için orantısal-integral-türev kayan yüzey tabanlı hata toleranslı uyarlamalı bir kontrol yöntemi önerilmiştir.

Tasarlanan kontrolcünün ikinci derece haline getirilmesiyle kontrolcünün iyileştirilmesi amaçlanmaktadır ve beklendiği gibi birinci derece kontrolcüye göre daha iyi sonuçlar elde edilmiştir.

Sistemin gürbüzlüğünü doğrulamak için sunulan uyarlanabilir birinci dereceden ve ikinci dereceden hata toleranslı kontrolcüler gerçek elektromekanik bir sisteme uygulanmış ve geleneksel kayan kipli kontrolcüyle karşılaştırılmıştır.

Tasarlanan ve önerilen kontrolcülerin performanslarını test etmek için kontrol işaretleri ve hız cevapları incelenmiş ve birbirleriyle kıyaslanmıştır.

Yükselme zamanı ve yerleşme zamanına göre ikinci dereceden-uyarlanabilir-dinamik-hata toleranslı kontrolcü, birinci dereceden-uyarlanabilir-dinamik-hata toleranslı kontrolcüden çok daha iyi performans göstermiştir. Ayrıca, ikinci dereceden-uyarlanabilir-dinamik-hata toleranslı kontrolcü, birinci dereceden-uyarlanabilir-dinamik-hata toleranslı kontrolcüye kıyasla çatırdamayı önemli ölçüde ortadan kaldırmıştır.

ACKNOWLEDGEMENTS

I would like to express my sincere gratitude to my advisor Prof. Dr. Ramazan ÇOBAN for his supervision guidance, encouragements, patience, motivation, useful suggestions and his valuable time for this work.

I would like to thank members of PhD thesis jury, Prof. Dr. M. Fatih AKAY, Prof. Dr. Ahmet TEKE, Assoc. Prof. Dr. Sertan ALKAN, Asst. Prof. Dr. İpek ABASIKELEŞ TURGUT for their suggestions and corrections.

I would like to thank my great family for their support. I would like to express my warmest gratitude to my wonderful mother, who supported me with both love and encouragement throughout my whole life. Her endless love has kept me strong in every challenge I have struggled. Nothing I have succeed would have been possible without her presence.

I would like to thank my dear friend Bilal İşçimen, who has supported me since the day we met, regardless of the subject.

Also, I would like to thank my smart dog Tarçın, who is with me for the last two and a half years and supported me with his loving attitudes.

CONTENTS **PAGE**

LIST OF TABLES **PAGE**

LIST OF FIGURES **PAGE**

1. INTRODUCTION

Control is a crucial part of the new technologies underlying current developments. It has a place in devices from washing machines to passenger aircraft, from cell phones to oil refineries. Therefore, position and speed controls of these systems are required to high accuracy. And lately, controls of such systems have been commonly applied in various applications (Susperregui et al., 2007; Park and Park, 2009; Kalayci and Yigit, 2015). Through current control methods, the sliding mode control (SMC) in spite of the uncertainty in the system and changes on the parameters is a robust control technique that provides dynamic behavior when the appropriate conditions are fulfilled (Tan and Packard, 2008). Sliding mode control method, introduced in the beginning of 1950's by Emelyanov, has gained significantly value with fast developing switching technology since Utkin's article first published in 1977. It has been commonly applied in various applications (Yu and Kaynak, 2009).

Sliding mode control has been mentioned as subject by many of the studies in recent years. Also, it has taken a significant part in application of control theory problems (Susperregui et al., 2007; Park and Park, 2009; Kalayci and Yigit, 2015; Aydin and Coban, 2016). In one of the studies, two sliding mode control approaches have been applied to the angular reference tracking of DC motor. Suitability of both applications is determined by the experimental and simulation results (Susperregui et al., 2007). In another study, sliding mode control is used in linear position control. The sliding surface is determined by the method of placing roots. The performance of the control is analyzed experimentally (Park and Park, 2009). In a research, some sliding mode control techniques used in practice are considered theoretically and experimentally on a variety of real systems. A variety of simulation and experimental results are obtained from these studies. After the results are evaluated, new conclusions have been reached (Kalayci and Yigit, 2015). In another study, the Precision Modular Servo (PMS) is considered as a test bed and the sliding mode controller is designed to control the real time speed of this electromechanical system (Aydin and Coban, 2016). The traditional (first-order) SMC despite of some advantages may be obstructed by 'chattering'. Chattering caused by switching control part of the SMC can be defined as undesirable occurrence of oscillations with finite frequency and amplitude (Utkin and Lee, 2006). To overcome the chattering, two approaches have been offered in the literature.

The first approach is to use smooth switching control term such as tangent function and saturation function in place of signum function in the switching control term. And the second is "higher-order sliding modes" (HOSMC), first introduced by Levant (Levant, 1993). Several HOSMC algorithms have been developed (Levant, 2003). Among them, the Super-Twisting Algorithm (STA) provides easy application due to without requirement of the derivative of the sliding surface.

STA is preferable because of easy implementation and eliminating the chattering (Xu, 2014). STA second-order sliding mode control has been aforementioned as subject by many of the studies in recent years. Also, it has taken a significant part in application of control theory problems (Lin and Chiang, 2013; Langlois et al., 2015; Quintero-Manríquez and Felix, 2014; Mahjoub et al., 2015; Aydin and Coban, 2017). In one of the studies, STA second-order sliding mode controller is designed and implemented for synchronous reluctance motor. The study is intended to decrease the chattering phenomenon. The controller's performance is confirmed by simulations and experiments. The study shows that the controller is robust against chattering phenomenon (Lin and Chiang, 2013). In another study, super-twisting algorithm controller is designed for DC Motor position controller. The controller is based on a disturbance observer. Simulation results, compared to other existing control design, prove the effectivity of the controller and the controller has reduced the chattering phenomenon (Langlois et al., 2015). In a research, super twisting algorithm second-order sliding mode speed controller is proposed and applied on Brushless DC Motor. Lyapunov function is used to demonstrate stability of the system. Simulation and experimental results are compared under condition of the same control strategy (Quintero-Manríquez and Felix, 2014). In a research, first-order and second-order sliding mode controllers are proposed. To overcome the chattering phenomenon, modified super-twisting algorithm is designed. The Lyapunov function is used to ensure stability of the system. Simulation results show that the approaches are efficient (Mahjoub et al., 2015). In another study, the Precision Modular Servo (PMS) is considered as a test bed and super-twisting algorithm second-order sliding mode controller (STASMC) is designed to control the real time speed of the electromechanical system. The Lyapunov function is used to guarantee stability of the system (Aydin and Coban, 2017).

Control applications aim to preserve the output of a process under condition of unexpected disorders. In control applications, it is crucial to minimize the tracking error when tracking a reference signal. It is a useful example for design, testing, and comparing of different control techniques. Due to the convenience, control of non-linear systems is a related field of study in control engineering. One of the most known research is the control of the DC motors. Approximated mathematical models are used for controller design. These approximations might cause some unknown disorders and uncertainties during the control design process (Alwi and Edwards, 2008a). These control design process prioritizes, even in the existence of the aforementioned unsuitable conditions, providing the closed-loop stability for overall system. Additionally, availability, reliability, and operating safety of the system have significant importance.

Safety-critical systems commonly utilize fault-tolerant control (FTC) schemes. Maintaining the system stability is major aim of the FTC schemes in order to achieve a satisfactory performance despite faults and failures within the system (Wang et al., 2012). There are many studies in the literature proposing novel designs for fault-tolerant controllers. This study presents the usage of the robust properties of adaptive sliding mode control within the FTC framework. This will also provide increasing the stability, reliability, and survivability of critical safety systems (Edwards et al., 2010). As mentioned above, SMC is named in control theory as a particular type of variable structure control (Yu and Kaynak, 2009; Zhao et al., 2014). It is a robust control scheme that obtains the desired output with a concept of changing the controller's structure in response to change the state of the system. Robustness measures the performance of being able to overcome the issues of disturbances and uncertainties for a control system (Young et al., 1996). This is the main reason for using the SMC in many practical applications like automotive, induction motors, automotive climate control, diesel engine, alternator (Utkin et al., 2009), DC motors (Aydin and Coban, 2016; Aydin and Coban, 2017), submarines (Walcko et al., 2003), electrical drives (Akpolat and Gokbulut, 2003).

SMC exploits the lower and upper bounds to handle uncertainties and disturbances without parameter adaption. In contrast to SMC, the adaptive control (AC) method utilizes parameter adaption for managing parametric uncertainties without the need to use their lower and upper bounds. The online adaption skill of AC makes it superior to SMC in terms of constant or slowly-varying parameters for a non-linear dynamical system having uncertainties. In the matter of handling parametric or non-parametric uncertainties, in comparison with SMC, the AC methodology can attain further flexibility for adjusting unknown non-linear dynamical systems due to generally containing an adaptive estimation approach that is playing an essential role in learning (Coban, 2017). There are many different design model propositions in the literature in order to the design of fault-tolerant controllers. In this study, because of their advantages, adaptive sliding mode control and FTC are used to together increase the stability, reliability, and survivability of the system to be controlled.

Faults are commonly considered under three main types in literature. These are actuator faults, sensor faults and component faults.

There are a lot of studies which mention fault-tolerant control and most of them present fault-tolerant controller designs for actuators or sensors (Zhao et al., 2014; An et al., 2015; Gao et al., 2018; Alwi and Edwards, 2006; Sharifi et al., 2010; Hu and Xiao, 2011; Edwards et al., 2012; Li et al., 2013; Almedia and Araujo, 2013; Hamayun et al., 2016). However, despite of the existence of some studies (Fekih and Pilla, 2007; Hitachi, 2009; Edwards et al., 2010; Li and Liu, 2012; Wang et al., 2012; Zhao et al., 2014), component fault is apparently studied less than faults of actuator and sensor. Because of this reason, this study focuses on the component fault.

There are some previous studies on fault-tolerant control in the literature. In one of the studies, an online sliding mode fault-tolerant controller is designed. When a fault occurs, the controller redistributes the control signal to other actuators using the actuator efficiency level (Alwi and Edwards, 2006). In research, the finite-time fault-tolerant trajectory tracking of fully actuated marine vehicles is investigated in the presence of parametric uncertainties, external disturbances, actuator faults, and input saturation. A adaptive finite-time sliding mode control scheme is used by combining the homogeneous integral sliding mode manifold, the fast terminal sliding mode control, and the adaptation technique (Yao, 2020). In one of the studies develops an enhanced robust fault tolerant control using a novel adaptive fuzzy proportional-integral-derivative-based nonsingular fast terminal sliding mode control for a class of second-order uncertain nonlinear systems (Van, 2018). There is another study on quadrotor vehicle control under damage and actuator fault conditions. In the study, the fault-tolerant controller which is a sliding mode based is designed and tested (Li et al., 2013). In research, the attitude stabilization of a flexible spacecraft is the subject of the study. A fault tolerant sliding mode control is proposed for achieving actuator effectivity under conditions of partial loss. The control designs are evaluated using numerical simulation comparisons (Hu and Xiao, 2011). A different study validates and derives a fault-tolerant controller using sliding mode techniques. The derived controller is used in a multi-motor electric vehicle. The study shows that individual motor drive failures could be handled directly without the need to reconfigure the controller (Almedia and Araujo, 2013). In one of the studies, fault-tolerant sliding mode control is designed for an uncertain MIMO aircraft model. Computer experiments have illustrated the application of the proposed approach and it is shown that the designed method is effective (Fekih and Pilla, 2007). Another study introduces a linearized aircraft model and offers of a sliding mode control based damaged-tolerant controller. Simulation study proves that the techniques are practical and have advantages (Zhao et al., 2014). However, there is neither any test nor experiment on the designed first-order controller. In research, an adaptive dynamic PID sliding surface-based second-order fault-tolerant sliding mode controller for speed control of an electromechanical system is designed. The Lyapunov theorem is used for affirming the design and stability of the closed-loop system. Experimental results show that the control system with the designed controller is easily implemented (Aydin and Coban, 2022).

In this thesis, an adaptive dynamic PID surface based second-order fault-tolerant sliding mode controller is proposed for controlling the electromechanical system. Additionally, adaptive dynamic first-order fault-tolerant sliding mode controller is designed to compare with the proposed controller. In order to change the physical parameters in the system, the system is loaded with a magnet. The amount of load added to the system is adjusted according to the location of the magnet. This added load amount has been adapted and calculated with the given formula.

Contributions in this thesis are listed as follows:

1) To ensure the stability and reliability of the system under different degrees of damage with the designed controller.
2) To make the controller 2nd order to avoid the chattering problem and increase the performance.

3) There are some other research studies which are based on simulation. This study deals with not only a new theoretical design but also experimental validation on a real physical system. Experimental results indicate that the control system with the proposed controller is easily implemented and has higher tracking precision and considerable robustness to uncertainties compared with the existing controllers.
4) To show that the designed controller can be applied on more complex and more risk-prone real-time systems by applying to a relatively simple but real-time system.

In this thesis, we propose a new type of SMC for an electromechanical system with uncertainties and faults. We proceed by solving the problems that arise during the SMC design phases, step by step. In the most basic SMC's, there is the chattering problem. This can be solved either with help of the saturation function or with help of the high-order (second-order) SMC. Second-order SMC is preferred because it gives better results than the SMC with the saturation function. There are two ways to make the controller second-order. The first of these; non-model based algorithm (super-twisting algorithm) SOSMC, latter model-based algorithm (PID surface-based) SOSMC. Since our system contains faults and this fault is on system parameters, model-based PID based SOSMC, which uses system parameters, is preferred instead of non-model based SOSMC, which does not use system parameters. Adaptive PID based SOSMC has been chosen to determine the limits of the uncertainties in the system. In addition, fault-tolerant adaptive PID based SOSMC has been selected to find the fault added to the system. The problems are thus solved step by step.

The rest of the thesis is organized as follows: Experimental set-up, system description, and mathematical model are given in Chapter 2. In Chapter 3, theoretical backgrounds of the traditional SMC and the fault-tolerant approach are explained. The adaptive dynamic first-order fault-tolerant sliding mode control and

PID sliding surface-based adaptive dynamic second-order fault-tolerant sliding mode control design is presented in Chapter 4. In Chapter 5, experimental results are presented. Conclusions are drawn in Chapter 6.

2. EXPERIMENTAL SET-UP

The description of the Precision Modular Servo (PMS) setup in this section refers mostly to the mechanical part and the control aspect. Figure 2.1 shows that the Precision Modular Servo (PMS) setup which consists of a digital encoder, servo-amplifier, preamplifier, output potentiometer, brushed dc motor, power supply, attenuator, gearbox/tachometer, digital encoder, and analog control interface units. The setup allows designers to test their controllers in real-time (Kesarkar et al., 2013).

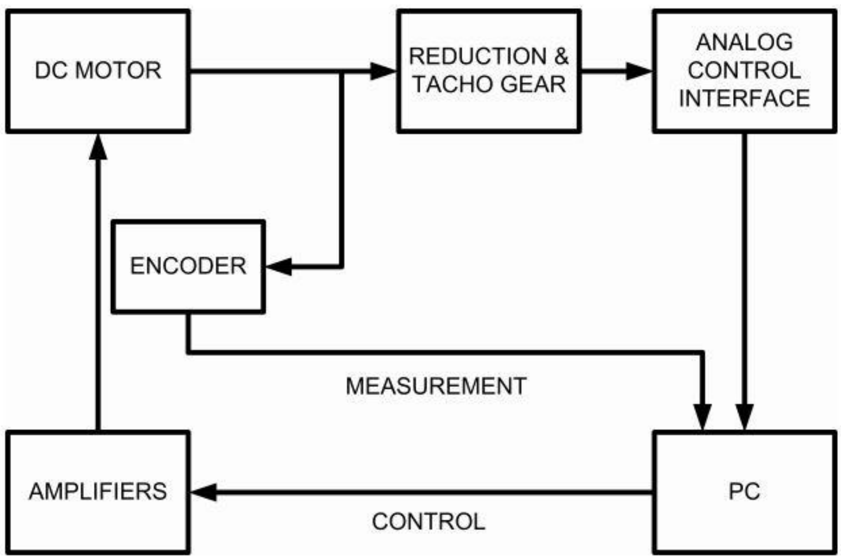

Figure 2.1. Precision modular servo setup (Feedback Instruments, 2006).

The electromechanical system consists of mainly electrical and mechanical units. Data acquisition card transmits the input-output signals in the system to the computer. The output speed, which is measured by a tachometer, provides an output voltage proportional to the speed. Digital encoder measures precisely the motor angular position. The I/O board receives the digital data from the encoder.

Preamplifier supplies the correct signal range to the servo amplifier which provides the controlled power to the DC motor. An interface unit is employed to scale the analog input and output to the I/O board in the computer to the correct operating range. The attenuator sets the input to the motor control circuit to the correct operating level. The output potentiometer is used as a visual display of the motor (gearbox shaft) position. The electromechanical system under consideration operates at control (input) voltage in the range -2.5 V and +2.5 V with a maximum no-load speed of 4050 rpm (Feedback Instruments, 2006).

In order to design any control algorithms one must first understand the physical background behind the process and carry out identification experiments. The next section explains the modelling process of the PMS. Every control project starts with plant modelling so as much information as possible is given about the process itself. The mechanical-electrical model of the servo motor is presented in Figure 2.2.

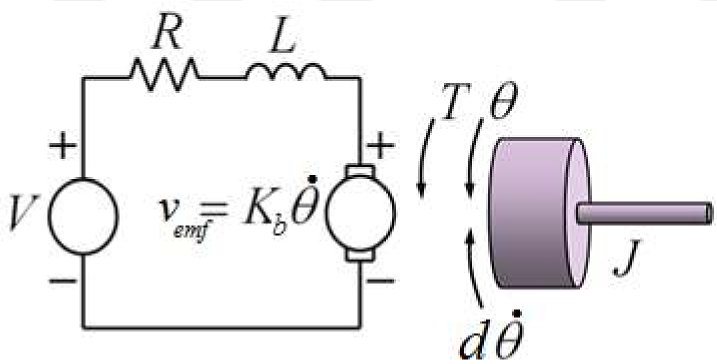

Figure 2.2. The mechanical-electrical model of the servo motor (Feedback Instruments, 2006).

The DC brushed servo motor model in the Precision Modular Servo (PMS) can be represented by electrical and mechanical equations. The torque τ produced by the DC servo motor is related to the motor current $i(t)$

$$\tau = K_t i(t) \tag{2.1}$$

where K_t is the torque constant. The induced electromotive force v_{emf} is a voltage related to the angular shaft speed $\dot{\theta}(t)$

$$v_{emf} = K_b \dot{\theta}(t) \tag{2.2}$$

where K_b is an electromotive force constant related to physical attribute of the motor. Using Newton's law the mechanical dynamics can be determined as

$$J_m \ddot{\theta}(t) = \sum \tau_i = -d_m \dot{\theta}(t) + K_t i(t) \tag{2.3}$$

where d_m is linear approximation of the viscous friction constant. The equations managing the behavior of the electrical model are

$$u(t) - v_{emf} = L \frac{di(t)}{dt} + Ri(t) \tag{2.4}$$

where $u(t)$ is the control signal. Substituting Equation (2.2) into Equation (2.4), we can get

$$u(t) = L \frac{di(\mathrm{t})}{dt} + Ri(\mathrm{t}) + K_b \dot{\theta}(t). \tag{2.5}$$

Equation (2.3) and Equation (2.5) generate the two fundamental differential equations. The state space form is

$$\ddot{\theta}(t) = -\frac{d_m}{J_m}\dot{\theta}(t) + \frac{K_t}{J_m}i(t), \tag{2.6}$$

$$\frac{di(\mathrm{t})}{dt} = -\frac{R}{L}i(\mathrm{t}) - \frac{K_b}{L}\dot{\theta}(t) + \frac{1}{L}u(t) \tag{2.7}$$

where J_m is the constant of moment of inertia; $\dot{\theta}(t)$ is angular shaft velocity; L is inductance; R is resistance; t is the time. We can write the state and output equations in the following:

$$\frac{d}{dt}\begin{bmatrix} \dot{\theta}(t) \\ i(t) \end{bmatrix} = \begin{bmatrix} \frac{-d_m}{J_m} & \frac{K_t}{J_m} \\ \frac{-K_b}{L} & \frac{-R}{L} \end{bmatrix} \begin{bmatrix} \dot{\theta}(t) \\ i(t) \end{bmatrix} + \begin{bmatrix} 0 \\ \frac{1}{L} \end{bmatrix} u(t). \tag{2.8}$$

Mechanical and electrical parts influence a viscous friction and moment of inertia of the dc motor. Because of the load effects on the real experimental system, moment of inertia J_t and viscous friction d_k are added in the motor model equations. A complete mathematical model of the electromechanical system can be derived using mechanical and electrical equations. By Kirchhoff's voltage and Newton's rotational motion laws one has

$$(J_m + J_t)\ddot{\theta}(t) = -(d_m + d_k)\dot{\theta}(t) + K_t i(t), \tag{2.9}$$

$$u(t) = L\frac{di(t)}{dt} + Ri(t) + K_b\dot{\theta}(t). \tag{2.10}$$

One can write Equation (2.6) and Equation (2.7) in the following form respectively:

$$\frac{d\dot{\theta}(t)}{dt} = -\frac{\left(d_m + d_k\right)}{\left(J_m + J_t\right)}\dot{\theta}(t) + \frac{K_t}{\left(J_m + J_t\right)}i(t), \tag{2.11}$$

$$\frac{di(t)}{dt} = -\frac{R}{L}i(t) - \frac{K_b}{L}\dot{\theta}(t) + \frac{1}{L}u(t). \tag{2.12}$$

Let us use $\omega(t)$ instead of $\dot{\theta}(t)$ in Equation (2.11) and then take its Laplace transform:

$$S\omega(S) = -\frac{\left(d_m + d_k\right)}{\left(J_m + J_t\right)}\omega(S) + \frac{K_t}{\left(J_m + J_t\right)}i(S), \tag{2.13}$$

$$i(S) = \frac{K_b}{\left(SL + R\right)}\omega(S) + \frac{1}{\left(SL + R\right)}u(S). \tag{2.14}$$

Substituting Equation (2.14) into Equation (2.13), the following equation is obtained:

$$S^2\omega(S) = -\left[\frac{R}{L} + \frac{\left(d_m + d_k\right)}{\left(J_m + J_t\right)}\right]S\omega(S) - \frac{\left(d_m + d_k\right)R + K_t K_b}{L\left(J_m + J_t\right)}\omega(S) + \frac{K_t}{L\left(J_m + J_t\right)}u(S). \tag{2.15}$$

Taking the inverse Laplace transform of Equation (2.15) and then including the additional gain K_{amp} introduced by the amplifiers and converting the motor angular velocity from rad/s to rpm, the following equation is obtained:

$$\begin{aligned}\ddot{\omega}(t) = &-\left[\frac{R}{L} + \frac{(d_m + d_k)}{(J_m + J_t)}\right]\dot{\omega}(t) \\ &- \frac{(d_m + d_k)R + K_t K_b}{L(J_m + J_t)}\omega(t) + \frac{K_{amp} K_t T_{rpm}}{L(J_m + J_t)}u(t)\end{aligned} \tag{2.16}$$

where $T_{rpm} = \dfrac{60}{2\pi}$ and $K_{amp} = 9.6$.

The servo motor model parameters are presented in Table 2.1 but moment of inertia J_t and viscous friction d_k due to the load effects of some electrical and mechanical parts on the real electromechanical system are determined experimentally (Coban, 2017). With the help of the experimentally determined value of these parameters, response of the basic motor model gets closer to that of the real electromechanical system. Despite there still exists a difference between responses of the real system and model, it is rejected by a robust controller to be designed in the succeeding subsections.

Table 2.1. DC motor system parameters (Feedback Instruments, 2006).

Parameter	Meaning	Unit	Value
J_m	Moments Of Inertia	kgm^2	$0.0000140kgm^2$
K_t	Torque Constant	Nm/A	$0.052\,Nm/A$
K_b	Electromotive Force constant	VS/rad	$0.057\,VS/rad$
d_m	Viscous Friction constant	Nms/rad	$0.000001\,Nms/rad$
R	Resistance	Ω	2.5Ω
L	Inductance	H	$0.0025H$

The electromechanical system composing of the model with unmatched uncertainties, dead-zone nonlinearity and disturbances can be modelled as a class of nonlinear dynamical system in Equation (2.17) (Kesarkar et al., 2013). A photograph of the Precision Modular Servo (PMS) setup where we applied our experimental work is shown in Figure 2.3.

$$\ddot{\omega}(t) = -\left[\frac{R}{L} + \frac{(d_m + d_k)}{(J_m + J_t)}\right]\dot{\omega}(t) - \frac{(d_m + d_k)R + K_t K_b}{L(J_m + J_t)}\omega(t) + \frac{K_{amp} K_t T_{rpm}}{L(J_m + J_t)}u(t) + d(x,t) \tag{2.17}$$

where $d(x,t)$ is the sum of uncertainties and disturbances. Taking $x = [x_1, x_2]^T = [\omega, \dot{\omega}]^T$ as the state vector, the following general nonlinear dynamical equation is obtained:

$$\dot{x}_1(t) = x_2(t)$$
$$\dot{x}_2(t) = f(x,t) + g(x,t)u(t) + d(x,t) \tag{2.18}$$

where $f(x,t) = -\left[\frac{R}{L} + \frac{(d_m + d_k)}{(J_m + J_t)}\right]x_2(t) - \left[\frac{(d_m + d_k)R + K_t K_b}{L(J_m + J_t)}\right]x_1(t)$;

$g(x,t) = \frac{K_{amp} K_t T_{rpm}}{L(J_m + J_t)}$ is constant and has positive sign; $d(x,t) \le d_{\max}$ and $d_{\max}$ is a positive unknown coefficient (Coban, 2019).

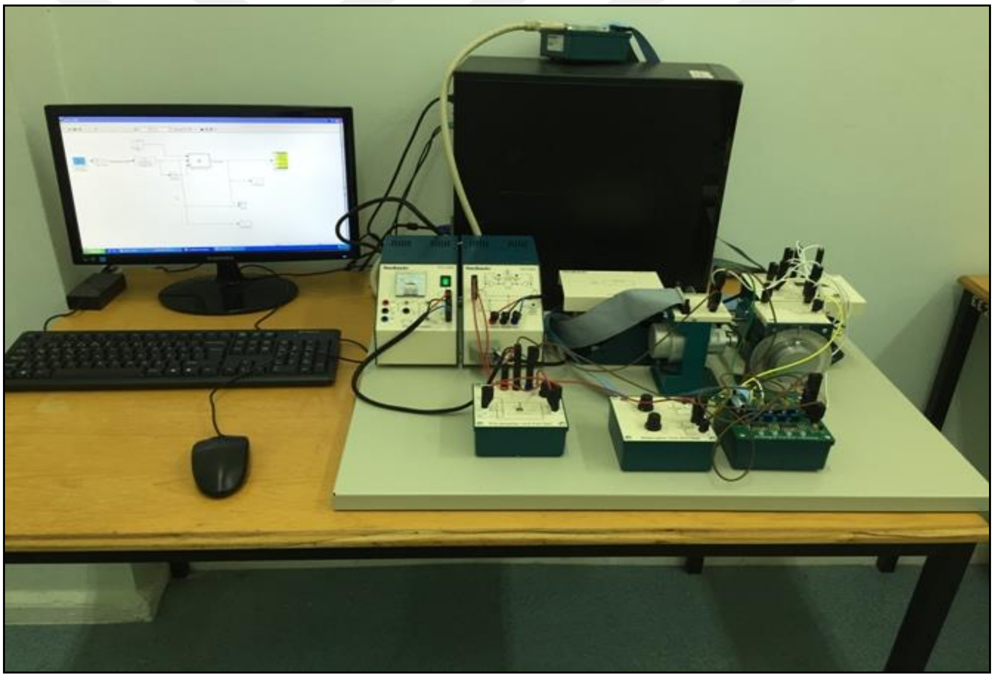

Figure 2.3. A picture of the experimental set-up.

3. DESIGN METHODS

3.1. First Order (Traditional) Sliding Mode Control

Sliding mode control (SMC) is named in control theory as a particular type of variable structure control (Zhao et al, 2014; Yu and Kaynak, 2009). It is a robust control scheme that obtains desired output with a concept of changing controller's structure in response in order to change the state of the system. For a control system, performance of being able to overcome the issues of disturbances and uncertainties is measured by the robustness. A high-speed control action is used to switch between different structures of the controller and the trajectory of the system is forced to move from any initial state to a user-specified sliding surface in the state-space at all subsequent time (Young et al, 1996).

Sliding mode control is an area which contains extensive studies performed for over 50 years (Zhao et al, 2014). It can be said that the first study was performed by Vadim I. Utkin (Utkin, 1977). Since that study, the control research community has shown a significant interest in sliding mode control (Zhao et al, 2014). It is considered one of the most powerful solutions for many practical control designs due to its simple design providing multiple adaptable capabilities. This is the main reason for using the SMC in many practical applications like automotive, induction motors, automotive climate control, diesel engine, alternator (Utkin et al, 2009), DC motors (Aydin and Coban,2016; Aydin and Coban, 2017), submarines (Walcko et al, 2003), electrical drives (Akpolat and Gokbulut, 2003).

Sliding mode controllers can provide advantages with robust and systematic designs (Utkin, 1977). Sliding control methods are usually designed for the systems of relative degree of one (Utkin et al, 2009). The control input has a relative degree of one with respect to control because it appears in the first derivative of the sliding function. The mentioned method of the sliding control is named as traditional SMC or first-order SMC.

A traditional SMC design procedure includes two main phases and consist of two major steps (Yu and Kaynak, 2009): The first step is the reaching phase which the system states are forced from an initial condition to a pre-defined sliding surface. The second step is the sliding mode phase. In this phase the system states are restricted to stay on the sliding surface and slides on the surface to an equilibrium.

These two phases correspond to the following two main design steps: The first step is the switching manifold selection in which a set of switching manifolds with desirable dynamical characteristics is selected. The second step is the discontinuous control design in which a discontinuous control strategy is designed in order to ensure the finite time reachability of the switching manifolds (Yu and Kaynak, 2009).

Switching control and equivalent control are two exact control laws for a traditional sliding mode controller. The first control law (switching control) enforces the system to the sliding surface. The fundamental task is to design the switching control law defined by a user and to maintain the system state trajectory on this surface as shown in Figure 3.1. In the figure e and $\dot{e}$ indicate the tracking error and first-time derivative of the tracking error, respectively. Choosing an appropriate switching control law influences the dynamic performance of the system. To make this choice, Lyapunov stability theorem is commonly used to determine the stability of closed-loop systems. The second control law (equivalent control) is used when the system is in the sliding phase.

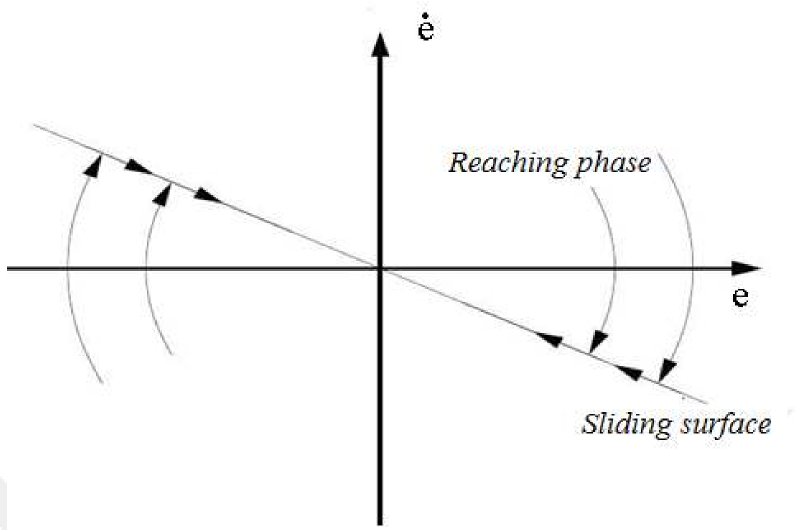

Figure 3.1. Reaching and sliding phases of the SMC

In order to design a sliding mode controller, let us consider the dynamical equations of the single input-single output non-linear system given in Equation (2.18) (Tang and Cai, 2011) where $f(x,t)$ and $g(x,t)$ are nonlinear functions; $x=[x_1\ x_2]^T$, $x(t)$ as state vector; $u(t)$ is control input; $d(x,t)$ is the sum of uncertainties and disturbances, $d(x,t)$ is assumed to be bounded as $|d(x,t)| \le d_{\max}$ where $d_{\max}$ is a positive constant.

For the purpose of finding control signal $u(t)$, tracking error and its first and second time derivatives, respectively, can be defined as follows:

$$e(t)=x_1(t)-r(t) \tag{3.1}$$

$$\dot{e}(t)=\dot{x}_1(t)-\dot{r}(t) \tag{3.2}$$

$$\ddot{e}(t)=\dot{x}_2(t)-\ddot{r}(t) \tag{3.3}$$

where $e(t)$ is tracking error, $r(t)$ is reference signal, and $x_1(t)$ is the output signal.

The sliding surface can be described as

$$s(t)=\left(\lambda+\frac{d}{dt}\right)^{n-1}e(t) \tag{3.4}$$

where *n* denotes the order of uncontrolled system, $n\geq 2$, and λ is a positive constant, $\lambda\in R^{+}$, used as a tuning parameter which determines the slope of switching manifold. If the system is assumed to be second-order ($n=2$), then Equation (3.4) becomes

$$s(t)=\lambda e(t)+\dot{e}(t). \tag{3.5}$$

While $s(t)$ comes close to the sliding surface, the control action decreases, too. The sliding mode is defined as existence of the system on the sliding surface.

The derivative of the sliding surface given in Equation (3.5) is

$$\dot{s}(t)=\lambda\dot{e}(t)+\dot{x}_2(t)-\ddot{r}(t). \tag{3.6}$$

Substituting $\dot{x}_2(t)$ in Equation (2.18) into above equation yields

$$\dot{s}(t)=\lambda\dot{e}(t)+f(x,t)+g(x,t)u(t)+d(x,t)-\ddot{r}(t). \tag{3.7}$$

Sum of the equivalent control signal $u_{eq}(t)$ and the switching control signal $u_{sw}(t)$ creates the control input $u(t)$:

$$u(t)=u_{eq}(t)+u_{sw}(t). \tag{3.8}$$

The equivalent control is obtained in consequence of $\dot{s}(t)=0$ which makes the state trajectory stay on the sliding surface. For the state trajectory staying on the sliding surface, $\dot{s}(t)=0$ must be provided. For the equivalent control $u_{eq}(t)$ design, if external disturbances and uncertainties are ignored and the derivative of $s(t)$ with respect to time is set to zero, one obtains

$$u_{eq}(t)=-\frac{1}{g(x,t)}\left[\lambda\dot{e}(t)+f(x,t)-\ddot{r}(t)\right]. \tag{3.9}$$

Lyapunov's theorem which is to confirm the stability of a system without solving differential equations is the most popular approach for analysis of nonlinear systems. Then in this step the Lyapunov function can be selected as follows (Rantzer , 2001):

$$V(t)=\frac{1}{2}s^2(t) \tag{3.10}$$

with $V(0)=0$ and $V(\mathrm{t})>0$ for $s(\mathrm{t})=0$. Thus, stability is guaranteed if $\dot{V}(\mathrm{t})\leq 0$ (Kesarkar et al., 2013).

The derivative of $V(\mathrm{t})$ along the trajectories of the system in Equation (2.18) is

$$\dot{V}(t)=s(t)\left[\lambda\dot{e}(t)+f(x,t)+g(x,t)\left(u_{eq}(t)+u_{sw}(t)\right)\right] \\ +s(t)\left[d(x,t)-\ddot{r}(t)\right]. \tag{3.11}$$

Substituting $u_{eq}(t)$ given in Equation (3.9) into Equation (3.11) one has

$$\dot{V}(t)=s(t)\left[\lambda\dot{e}(t)+f(x,t)+d(x,t)-\ddot{r}(t)\right] \\ -s(t)g(x,t)\left[\frac{1}{g(x,t)}\left(\lambda\dot{e}(t)+f(x,t)-\ddot{r}(t)\right)-u_{sw}(t)\right]. \tag{3.12}$$

After making various arrangements on the above equation, the following equation is obtained

$$\dot{V}(t)=s(t)\left[g(x,t)u_{sw}(t)+d(x,t)\right] \tag{3.13}$$

To guarantee the stability of the system in Equation (2.18) a switching control law $u_{sw}(t)$ can be defined as follows:

$$u_{sw}(t)=-\frac{1}{g(x,t)}\beta sign\left(s(t)\right) \tag{3.14}$$

where $\beta\geq d_{\max}\geq\left|d(x,t)\right|$. If the switching control law $u_{sw}(t)$ given in Equation (3.14) is substituted into Equation (3.13), time derivative of Lyapunov function $\dot{V}(t)$ in Equation (3.13) gives $\dot{V}(t)=-\beta s(t)sign\left(s(t)\right)=-\beta\left|s(t)\right|\leq 0.$

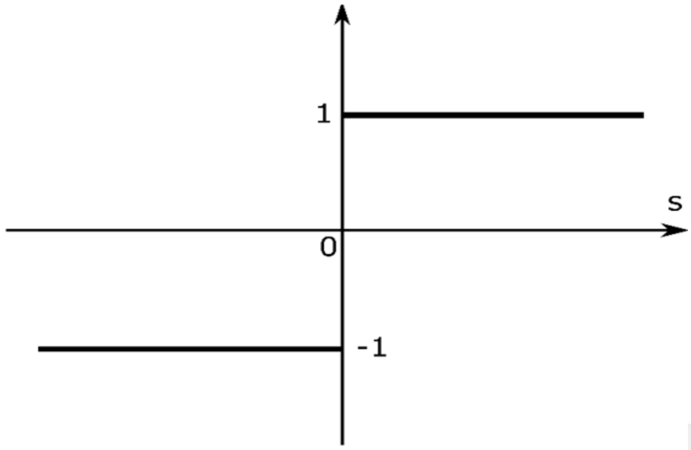

Figure 3.2. Signum function

The $sign(\ )$ shown in Figure 3.2 denotes *signum* function (Utkin, 1992),

$$sign\left(s\left(t\right)\right)=\begin{cases}1, & s\left(t\right)>0\\ 0, & s\left(t\right)=0\\ -1, & s\left(t\right)<0\end{cases}. \tag{3.15}$$

Consequently, $\dot{V}(t)=-\beta\left|s(t)\right|\leq 0$ condition is provided to be ensured $\dot{V}(t)\leq 0$ and the system in Equation (2.18) is asymptotically stable according to Lyapunov theorem.

3.1.1. Chattering Phenomenon

Despite of the advantages of the traditional SMC, there are some disadvantages called by 'chattering'. Chattering arises from undesirable occurrence of oscillations on switching control part with finite frequency and amplitude (Behnamgol, 2015).

There are two possible reasons for producing chattering. First, because the ideal SMC approach requires infinite switching frequency, limited switching frequency can cause chattering (Young et al., 1996). Second, the non-modeled dynamics can cause a high frequency oscillation on the sliding surface (Yu and Kaynak, 2009). The chattering is shown in Figure 3.3 which is highly undesirable for real systems since it may lead unnecessarily large control signal.

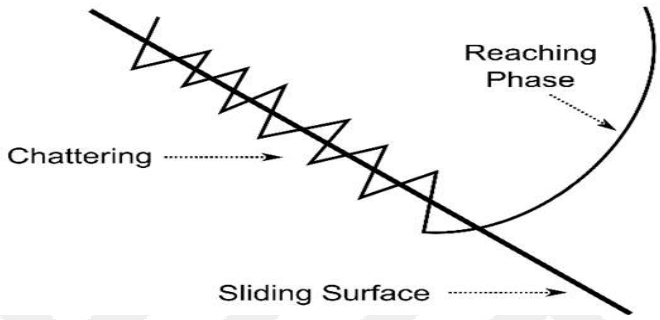

Figure 3.3. Chattering phenomenon in the SMC approach

One of the main problems of SMC is to eliminate chattering. In the literature, to eliminate the chattering, two techniques have been proposed. First of these techniques is the boundary layer solution based on the use of a continuous approximation such as saturation function and tangent function instead of the signum function in the switching control law (Tai and Ahn, 2010). The block diagram of the first-order/traditional sliding mode control system is demonstrated in Figure 3.4.

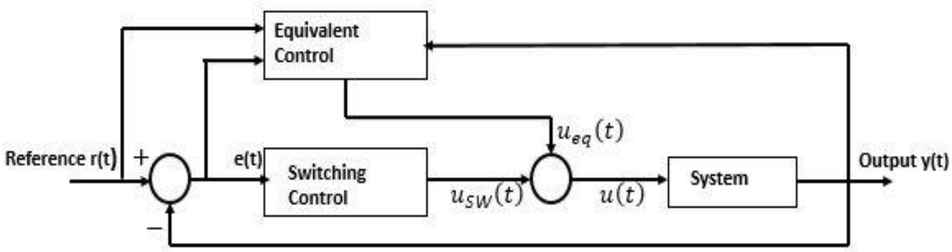

Figure 3.4. Block diagram of the sliding mode controller

Commonly a saturation function has been used instead of signum function in the switching control part. Therefore, Equation (3.14) results in:

$$u_{sw}(t) = -\frac{1}{g(x,t)}\beta sat\left(\frac{s(t)}{\Delta}\right). \tag{3.16}$$

The saturation function shown in Figure 3.5 is defined by

$$\text{sat}\left(\frac{s(t)}{\Delta}\right) = \begin{cases} \dfrac{s(t)}{\Delta} & if \quad \left|\dfrac{s(t)}{\Delta}\right| \le 1 \\ \text{sgn}\left(\dfrac{s(t)}{\Delta}\right) & if \quad \left|\dfrac{s(t)}{\Delta}\right| > 1 \end{cases} \tag{3.17}$$

where Δ denotes a boundary level as shown in Figure 3.6.

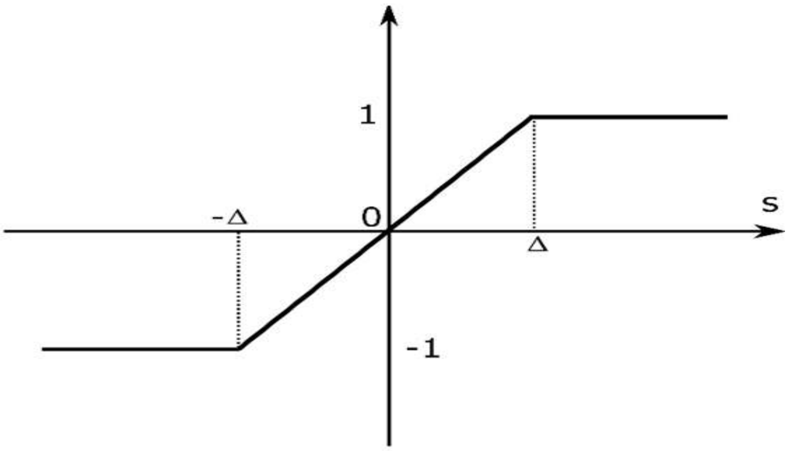

Figure 3.5. Saturation function.

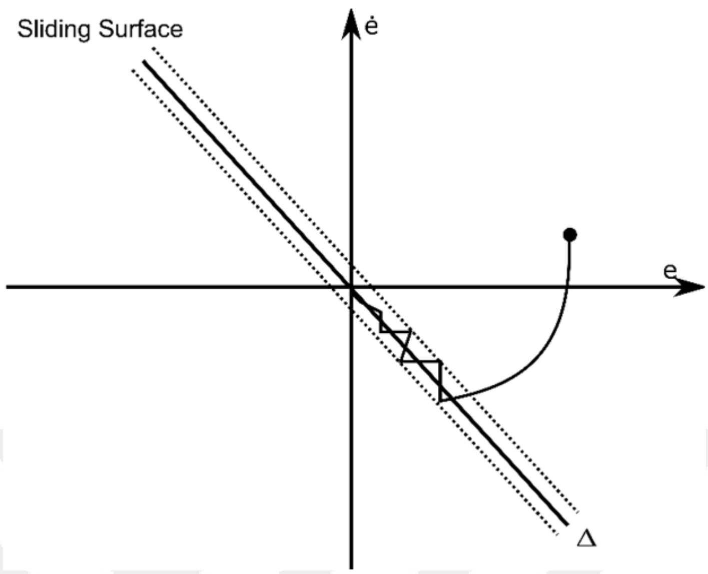

Figure 3.6. Sliding surface with boundary layer

Second of these techniques is a higher-order sliding mode (HOSMC) proposed in order to resolve the chattering phenomenon which is the fundamental disadvantage of the first-order sliding mode control. The *rth* order sliding mode is determined by the equalities $s(t)=\dot{s}(t)=\ddot{s}(t)=...=s^{r-1}(t)=0$.The first-order sliding mode attempts to retain $s(t)=0$ while the second-order sliding mode attempts to retain both $s(t)=0$ and $\dot{s}(t)=0$.

The most used higher order sliding-mode control method is the second-order sliding mode control method. In literature, different second-order sliding mode control algorithms have been proposed. Among them twisting and drift (Levant, 1993), super-twisting (Levant, 1993; Shtessel et al., 2014), quasi-continuous (Levant, 2007) and sub-optimal (Bartolini et al., 2003) are well-known nonmodel-based algorithms.

Among nonmodel-based algorithms, the Super-Twisting Algorithm (STA) provides easy application due to without requirement of the derivative of the sliding surface. STA is preferable because of easy implementation and eliminating the chattering. STA second-order sliding mode control has been aforementioned as subject by many of the studies in recent years. Also, it has taken a significant part in application of control theory problems (Mobayen, 2015).

3.2. Super-Twisting Algorithm Second-Order Sliding Mode Controller

Super Twisting Algorithm decreases chattering in the systems with relative degree 1 with the use of an integral state in the control. STA has a great advantage which does not require information of $\dot{s}(t)$. In a first-order SMC design, the control aim is to move the system state onto sliding surfaces $s(t)=0$. A second-order sliding mode controller (SOSMC) aims at $s(t)=\dot{s}(t)=0$. That is, the system states converge to zero at the intersection of $s(t)=0$ and $\dot{s}(t)=0$ in the state space. Consider sliding variable dynamics given by a system with a relative degree of two:

$$\dot{s}(t)=f(t,s)+u(t) \tag{3.18}$$

where $f(t,s)$ is an unknown bounded perturbation term and globally bounded by $\left|f(t,s)\right| \le \lambda \left|s(t)\right|^{1/2}$ for some constant $\lambda > 0$ and u is the scalar control input. The super-twisting sliding mode controller for perturbation and chattering elimination is given by

$$u(t)=-\lambda\left|s(t)\right|^{1/2} sign\big(s(t)\big)+u_1(t), \tag{3.19a}$$

$$\dot{u}_1(t)=-\alpha sign\big(s(t)\big). \tag{3.19b}$$

Equation (3.20) is obtained using Equation (3.18) and Equation (3.19):

$$\dot{s}(t) = -\lambda |s(t)|^{1/2} sign(s(t)) + u_1(t) + f(t,s). \tag{3.20}$$

In order to guarantee stability of the system with relative degree of two $f(t,s)$ and $u(t)$, Lyapunov function and its derivative with respect to time can be presented as follows, respectively:

$$V(t) = \alpha |s(t)| + \frac{1}{2} u_1^2(t) \tag{3.21a}$$

and

$$\dot{V}(t) = \alpha \frac{s(\mathrm{t})}{|s(\mathrm{t})|} \dot{s}(\mathrm{t}) + \frac{1}{2} 2u_1(t)\dot{u}_1(t). \tag{3.21b}$$

Substituting $\dot{u}_1(t)$ in Equation (3.19b) and $\dot{s}(\mathrm{t})$ in Equation (3.20) into Equation (3.21b) one has

$$\begin{aligned} \dot{V}(t) = \alpha \frac{s(t)}{|s(t)|} &\left[-\lambda |s(t)|^{1/2} sign(s(t)) + u_1(t) + f(t,s) \right] \\ &- u_1(t) \alpha sign(s(t)). \end{aligned} \tag{3.22}$$

Then, using the equations $sign(s(t)) = \frac{|s(t)|}{s(t)}$ and $\frac{|s(t)|}{s(t)} = \frac{s(t)}{|s(t)|}$ the following equation is obtained

$$\dot{V}(t) = -\alpha\lambda |s(t)|^{1/2} + \alpha f(t,s) sign(s(t)) \leq 0 \tag{3.23}$$

where $f(t,s)=\lambda|s|^{\frac{1}{2}}$ and $s(t)$ is given in Equation (3.5). Since $\dot{V}(t)$ is negative definite, the system trajectory will be driven to sliding surface and remain in there until the origin is reached asymptotically. Consequently, the stability of the overall system in Equation (2.18) and Equation (3.19) is guaranteed.

3.3. PID Surface based Second-Order Sliding-Mode Control

Several SOSMC algorithms have been enhanced. Among them super-twisting, twisting, drift, quasi-continuous and sub-optimal are well-known nonmodel-based algorithms. In the nonmodel based second-order sliding mode algorithms, the control input is obtained without the use of the system parameters. Besides of these, a model-based algorithm having systematic solution based on the equivalent approach is presented in the literature (Rhif, 2012). In the model-based algorithm, the equivalent control is obtained by equating the second-time derivative of sliding function to zero and solving for. The switching control can be selected just as in the first-order sliding-mode control.

A dynamic PID sliding surface based second-order sliding surface is selected as follows:

$$\sigma(s)=\left(k_p+\frac{1}{s}k_i+sk_d\right)^{n-1}\chi\left(E(s)\right) \tag{3.24}$$

where n is the order of the system, here it is equal to 2; k_p, k_i and k_d are positive parameters; $\chi\left(E(s)\right)$ is the integral of the tracking error given in Laplace domain

$$\chi\left(E(s)\right)=\left(\frac{1}{s}\right)E(s). \tag{3.25}$$

Setting $n = 2$ and substituting $\chi\left(E(s)\right)$ in Equation (3.25) into Equation (3.24) give

$$\sigma(s) = \frac{1}{s} k_p E(s) + \frac{1}{s^2} k_i E(s) + k_d E(s). \tag{3.26}$$

Though the control input appears in the first time derivative of the sliding surface in the first-order SMC, in the second-order sliding modes the control input appears in the second derivatives of the sliding surface. Thus, the second order derivative of the sliding surface should be taken and converted into a time domain:

$$s^2 \sigma(s) = s k_p E(s) + k_i E(s) + s^2 k_d E(s). \tag{3.27}$$

Time domain representation of Equation (3.27) is as follows:

$$\ddot{\sigma}(t) = k_p \dot{e}(t) + k_i e(t) + k_d \ddot{e}(t). \tag{3.28}$$

To make sure that the system reaches the sliding surface within finite time, $\ddot{\sigma}(t) = 0$ must be provided:

$$\ddot{\sigma}(t) = k_p \dot{e}(t) + k_i e(t) + k_d \ddot{e}(t) = 0. \tag{3.29}$$

Substituting $\ddot{e}$(t) given in Equation (3.3) into above equation, one has

$$\begin{aligned} \ddot{\sigma}(t) &= k_p \dot{e}(t) + k_i e(t) \\ &\quad + k_d \left[f(x,t) + g(x,t) u(t) + d(x,t) - \ddot{r}(t) \right] = 0. \end{aligned} \tag{3.30}$$

Sum of the equivalent control signal $u_{eq}(t)$ and the switching control signal $u_{sw}(t)$ creates the control input $u(t)$:

$$u(t)=u_{eq}(t)+u_{sw}(t). \tag{3.31}$$

The equivalent control is obtained in the consequence of $\ddot{\sigma}(t)=0.$ For the equivalent control $u_{eq}(\mathrm{t})$ design if external disturbances and uncertainties are ignored and the second derivative of $\sigma(t)$ with respect to time is set to zero one obtains

$$u_{eq}(t)=-\frac{1}{k_d g(x,t)}\left[k_p\dot{e}(t)+k_i e(t)+k_d f(x,t)-k_d\ddot{r}(t)\right]. \tag{3.32}$$

Lyapunov function for the stability of the system given in Equation (2.18) can be chosen as follows (Rantzer, 2001):

$$V(t)=\frac{1}{2k_d}\dot{\sigma}^2(t) \tag{3.33}$$

with $V(0)=0$ and $V(t)\geq 0$ for $\dot{\sigma}(t)=0$. Thus, stability of the system given in Equation (2.18) is guaranteed if $\dot{V}(t)\leq 0$.

The time derivative of $V(t)$ along the trajectories of the system in Equation (2.18) is

$$\dot{V}(t)=\frac{1}{k_d}\dot{\sigma}(t)\ddot{\sigma}(t). \tag{3.34}$$

Substituting $\ddot{\sigma}(t)$ given in Equation (3.30) into above equation yields

$$\begin{aligned}\dot{V}(t) &= \frac{1}{k_d}\dot{\sigma}(t)\left[k_p\dot{e}(t)+k_i e(t)\right] \\ &+\dot{\sigma}(t)\left\{f(x,t)+g(x,t)\left[u_{eq}(t)+u_{sw}(t)\right]\right\} \\ &+\dot{\sigma}(t)\left[d(x,t)-\ddot{r}(t)\right].\end{aligned} \tag{3.35}$$

Substituting $u_{eq}(t)$ given in Equation (3.32) into the above equation we obtain

$$\begin{aligned}\dot{V}(t) &= \frac{1}{k_d}\dot{\sigma}(t)\left\{k_p\dot{e}(t)+k_i e(t)+k_d\left[f(x,t)+d(x,t)-\ddot{r}(t)\right]\right\} \\ &+\dot{\sigma}(t)\left[g(x,t)u_{sw}(t)\right] \\ &-\dot{\sigma}(t)\frac{1}{k_d}\left[k_p\dot{e}(t)+k_i e(t)+k_d f(x,t)-k_d\ddot{r}(t)\right].\end{aligned} \tag{3.36}$$

After making various arrangements on the above equation, the following equation is obtained

$$\begin{aligned}\dot{V}(t) &= \dot{\sigma}(t)\left[g(x,t)u_{sw}(t)+\frac{1}{k_d}d(x,t)\right] \\ &\le -\beta\dot{\sigma}(t)\,sign\left(\dot{\sigma}(t)\right) = -\beta\left|\dot{\sigma}(t)\right| \le 0\end{aligned} \tag{3.37}$$

if the switching control function is selected as follows:

$$u_{sw}(t) = -\frac{1}{g(x,t)}\beta sign(\dot{\sigma}(t)) \tag{3.38}$$

provided that $\beta \geq \frac{d_{\max}}{k_d} \geq |d(x,t)|$. This guarantees the stability of the system given in Equation (2.18) in the sense of Lyapunov stability theorem.

3.4. Adaptive Control

One of the challenging tasks in the sliding mode control design is to estimate bounds of uncertainties. In general, these bounds are overestimated which leads to excessive gain. Chattering phenomenon, which is the main drawback of sliding mode control, is important as it could damage actuators and systems.

A first way to reduce the chattering is the use of a boundary layer: In this case, many approaches have proposed adequate tuning of controller gains (Slotine and Sastry 1983). A second way to decrease the chattering phenomenon is the use of higher order sliding mode controller (Levant 1993, 2003, 2007; Bartolini et al., 2003; Laghrouche et al., 2007; Plestan et al., 2010). However, in these control approaches, knowledge of bounds of uncertainties is required. In absence of bounds of uncertainties, adaptive sliding mode is used in purpose of obtaining an as small as possible dynamical adaptation of the control gain which is sufficient to counteract the uncertainties/perturbations. As recalled previously, this problem is an exciting challenge for applications given that, in many cases, gains are also overestimated, which gives larger control magnitude and larger chattering. New methodologies for adaptive sliding mode control has been used in the literature (Plestan et al., 2010; Shtessel et al., 2014). In this thesis, an adaptive SMC is proposed in Chapter 4 to determine the uncertainty limits of the system.

3.5. Fault tolerant Control

During the control design process there might be some unknown disturbances and some uncertainties arising from creating an approximate mathematical model used for the controller design (Alwi and Edwards, 2008). In control design process it is important to ensure the closed-loop stability of the overall system under aforementioned unsuitable conditions. Additionally, operating safety, reliability, and availability of the system have a significant importance. This importance become greater when it comes to fields like aircrafts and reactors which are safety critical plants. Field of fault tolerant control systems is based on safety critical systems like aircraft for the initial research (Alwi and Edwards, 2008).

Fault Tolerant Control (FTC) schemes take an important place in safety critical systems. FTC schemes aspire to preserve overall system stability and achieve an acceptable performance in spite of faults and failures within the system (Wang et al., 2012).

FTC systems can be classified as passive fault tolerant control (PFTC) systems or active fault tolerant control (AFTC) systems.

In PFTC systems the controller is of a fixed structure and is designed off-line. Due to the fact that PFTC systems do not require up-to-date fault information, PFTC methods are computationally more attractive. In passive fault tolerant control schemes, the idea is to design the controller using robust control techniques such that the closed-loop system response is robust against certain classes of uncertainties and presumed system faults.

AFTC systems react to faults/failures actively by reconfiguring control actions so that stability and acceptable performance of the system can be maintained. In certain circumstances, degraded performance may have to be accepted. The structure of an AFTC system is usually more complex compared to PFTC systems but can deal with a wider class of faults.

A fault is a sudden event and can occur in any part of the system. As shown in the Figure 3.7., it can also be classified as actuator fault, sensor fault, or component fault, depending upon the location of occurrence.

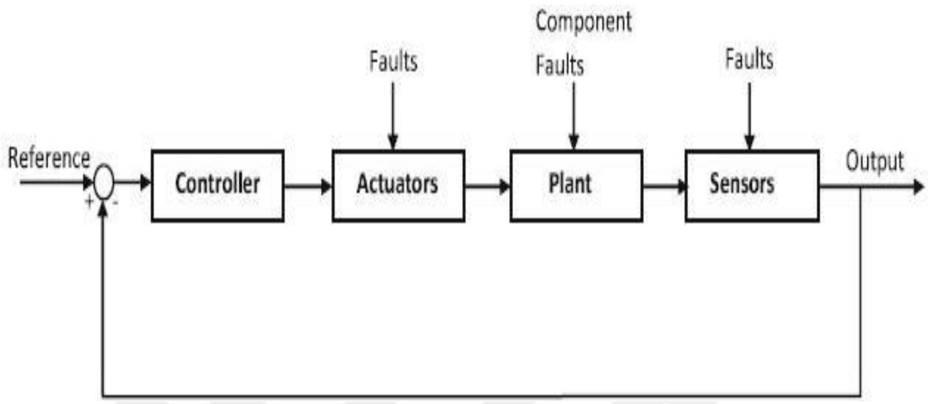

Figure 3.7 Classification of faults

3.5.1. Actuator faults

Actuators represent an interface between the controller commands and the system to be controlled. When a fault occurs, the actuator works with reduced capability as compared to its normal operating/fault-free condition. In a post fault condition, the actuator will only be partially effective in achieving the required controller demand, which may affect the overall performance of the system. Actuator faults may occur due to, for instance, a drop in voltage supply, increased resistance, hydraulic leakages etc.

In the literature, different representations have been used to model actuator faults and failures. For example, to model an actuator fault/failure, the state-space model can be written as

$$\dot{\boldsymbol{x}}(t) = A\boldsymbol{x}(t) + B\Sigma(t)u(t) + B\big(I - \Sigma(t)\big)\bar{u}(t) \tag{3.39}$$

where $A \in R^{n \times n}$; $B \in R^{n \times m}$; $\Sigma(t) = diag(\theta_1(t), \ldots, \theta_m(t))$ and $\theta_i(t) \in [0\ 1]$; $\bar{u}(t)$ is an uncontrollable offset vector, (If $\theta_i(t) = 1$ then the ith actuator is functioning normally, whereas if $\theta_i(t) = 0$ ith actuator has a failure, i.e. the control action from the failed actuator is equal to $\bar{u}(t)$) (Alwi and Edwards, 2008).

3.5.2. Sensor faults

Sensors are used in the control system to measure and convert the physical quantities of interest into a signal. A fault in the sensor means the sensor is measuring incorrectly. Sensor faults can degrade the feedback system performance even in the presence of a well-designed controller. Therefore, it is important to detect and isolate sensor faults at an early stage.

3.5.3. Component faults

If faults do not belong to the category of actuator or sensor these type of faults can be considered as a component fault. A component fault occurs in the plant components. As a result the input/output dynamical behavior of the controlled system will be altered. Component faults can in turn result in a change in the physical parameters of the system and can reduce the overall performance of the system.

A component fault may introduce changes in the system matrix and can be represented in the following form:

$$\dot{x}(t) = (A + \Delta A(t))x(t) + B(t)u(t) \tag{3.40}$$

where $\Delta A(t)$ represents a change in the system matrix A.

In this thesis, component faults are studied regardless of in which component or how many faults occur.

4. CONTROLLER DESIGN

In this thesis, we propose a SMC for an electromechanical system with uncertainties and faults. We proceed by solving the problems that arise during the SMC design phases, step by step. In the most basic SMC, there is the chattering problem. This can be solved either with the saturation function or with the high-order (second-order) SMC. Second-order SMC is preferred because it gives better results than the SMC with the saturation function. There are two ways to make the controller second-order. The first of these is non-model based algorithm (super-twisting algorithm) SOSMC and the second is model-based algorithm (PID surface-based) SOSMC. Since our system contains faults and this fault is on system parameters, model-based PID based SOSMC which uses system parameters is preferred instead of non-model based SOSMC which does not use system parameters. Adaptive PID based SOSMC has been chosen to determine the limits of the uncertainties in the system. In addition, fault-tolerant adaptive PID based SOSMC has been selected to find the fault added to the system. The problems are thus solved step by step.

4.1. Adaptive Dynamic First-order Fault-Tolerant Sliding Mode Control Design

As introduced in Section 3.5. Fault Tolerant Control (FTC) schemes take an important place in safety critical systems. FTC schemes aspire to preserve overall system stability and achieve an acceptable performance in spite of faults and failures within the system. The designed and proposed active fault tolerant controllers actively react to faults/failures by reconfiguring control actions so that the stability and performance of the system can be maintained.

In this part of the thesis, active first and second-order Adaptive Dynamic Fault Tolerant Sliding Mode Controllers, respectively, are designed and proposed against component fault problems. The designed and proposed methods are evaluated experimentally using the experimental system described in Chapter 2. The designed and proposed controllers are compared with the traditional SMC with the signum function.

The damaged electromechanical system model is obtained adding fault functions on the model of electromechanical system given in Equation (2.18). The following is a damaged electromechanical system model to be introduced:

$$\begin{aligned} \dot{x}_1(t) &= x_2(t) \\ \dot{x}_2(t) &= f_1(x,t) + g_1(x,t)u(\mathrm{t}) + d(x,t). \end{aligned} \tag{4.1}$$

$f_1(x,t)$ and $g_1(x,t)$ are obtained by adding fault functions to the system parameters:

$$\begin{aligned} f_1(x,t) &= f(x,t) + \eta_1(x,t) \\ g_1(x,t) &= g(x,t) + \eta_2(x,t) \end{aligned} \tag{4.2}$$

where $\eta_1(x,t)$ and $\eta_2(x,t)$ are fault functions. The fault functions can be given by

$$\begin{aligned} \eta_1(x,t) &= \eta x_2(t) + \eta x_1(t) \\ \eta_2(x,t) &= \eta(t) \end{aligned} \tag{4.3}$$

where η is unknown damaged/fault degree and $0 \le \eta \le 1$.

Equation (4.1), together with Equation (4.2) and Equation (4.3), refers to the damaged version of the electromechanical system given in Equation (2.18). Thus, if $\eta(t)=0$ Equation (2.18) is equal to Equation (4.1).

In order to design an adaptive dynamic fault-tolerant sliding-mode control (ADFTSMC) for the electromechanical system given in Equation (4.1), a dynamic sliding surface is chosen as follows:

$$s(t)=Te(t)+\dot{e}(t)+Hu(t) \tag{4.4}$$

where T , H are positive constants and $e(t)$ is tracking error.

Tracking error for the system given in Equation (4.1) which is a modified version of Equation (2.18) can be determined as follows:

$$e(t)=x_1(t)-r(t) \tag{4.5}$$

where $r(t)$ is reference trajectory.

The first and second-order derivatives of the tracking error, respectively, are

$$\begin{aligned} &\dot{e}(t)=\dot{x}_1(t)-\dot{r}(t) \\ &\ddot{e}(t)=\dot{x}_2(t)-\ddot{r}(t). \end{aligned} \tag{4.6}$$

In order to guarantee that the system reaches the sliding-mode surface within a finite time $\dot{s}(t)$ is chosen as follows:

$$\dot{s}(t) = -p_1 s(t) - p_2 sign(s) \tag{4.7}$$

where p_1 and p_2 are positive constants.

Let us design the equivalent control by setting the time derivative of the sliding surface in Equation (4.4) to the chosen $\dot{s}(t)$ given in Equation (4.7):

$$\dot{s}(t) = T\dot{e}(t) + \ddot{e}(t) + H\dot{u}(t) = -p_1 s(t) - p_2 sign(s). \tag{4.8}$$

Substituting $\ddot{e}(t)$ in second part of Equation (4.6) into Equation (4.8) and setting $\dot{s}(t) = 0$ guarantee that the state trajectory stays on the sliding surface:

$$T\dot{e}(t) + \dot{x}_2(t) - \ddot{r}(t) + H\dot{u}(t) = -p_1 s(t) - p_2 sign(s). \tag{4.9}$$

Substituting $\dot{x}_2(t)$ given by Equation (4.1) into the above equation, one has

$$\begin{aligned} &T\dot{e}(t) + f_1(x,t) + g_1(x,t)u(t) + d(x,t) - \ddot{r}(t) \\ &+ H\dot{u}(t) = -p_1 s(t) - p_2 sign(s). \end{aligned} \tag{4.10}$$

Substituting $f_1(x,t)$ and $g_1(x,t)$ in Equation (4.2) into Equation (4.10) gives

$$\begin{aligned} &T\dot{e}(t) + f(x,t) + \eta_1(x,t) \\ &+ \left[g(x,t) + \eta_2(x,t) \right] u(t) + d(x,t) - \ddot{r}(t) \\ &+ H\dot{u}(t) = -p_1 s(t) - p_2 sign(s). \end{aligned} \tag{4.11}$$

If the unknown parameters η_1 and η_2 are replaced by their estimates $\hat{\eta}_1$ and $\hat{\eta}_2$ respectively, the following equation is obtained

$$\begin{aligned} &T\dot{e}(t)+f(x,t)+\hat{\eta}_1(x,t) \\ &+\left[g(x,t)+\hat{\eta}_2(x,t)\right]u(t)+d(x,t)-\ddot{r}(t) \\ &+H\dot{u}(t)=-p_1 s(t)-p_2 sign\left(s(t)\right). \end{aligned} \tag{4.12}$$

Collecting and rearranging $\dot{u}(t)$ terms on the left-hand-side in Equation (4.12) yield

$$\begin{aligned} \dot{u}(t)=&\frac{1}{H}\left[-p_1 s(t)-p_2 sign\left(s(t)\right)-T\dot{e}(t)\right]-\frac{1}{H}\left[d(x,t)-\ddot{r}(t)\right] \\ &-\frac{1}{H}\left\{f(x,t)+\hat{\eta}_1(x,t)+\left[g(x,t)+\hat{\eta}_2(x,t)\right]u(t)\right\} \end{aligned} \tag{4.13}$$

where $\hat{\eta}_1(x,t)$ and $\hat{\eta}_2(x,t)$ are the estimations of $\eta_1(x,t)$ and $\eta_2(x,t)$, respectively:

$$\begin{aligned} &\hat{\eta}_1(x,t)=\hat{\eta}x_2(t)+\hat{\eta}x_1(t) \\ &\hat{\eta}_2(x,t)=\hat{\eta}(t) \end{aligned} \tag{4.14}$$

where $\hat{\eta}(t)$ is the estimation of $\eta(t)$. In order to guarantee the stability of the controlled system given in Equation (4.1), let us select Lyapunov function as follows:

$$V(t)=\frac{1}{2}s^2(t)+\frac{1}{2}\frac{1}{Y}\tilde{\eta}^2(t)\geq 0$$
$$\tilde{\eta}(t)=\eta(t)-\hat{\eta}(t) \tag{4.15}$$

where $\tilde{\eta}(t)$ is the estimation error and Y is positive constant. With the calculation of the first order derivative of Lyapunov function in the first part of Equation (4.15), the following equation is obtained

$$\dot{V}(t)=s(t)\dot{s}(t)+\dot{\tilde{\eta}}(t)\frac{1}{Y}\tilde{\eta}(t). \tag{4.16}$$

Time derivative of $\tilde{\eta}(t)$ given in the second part of Equation (4.15) is obtained in the following:

$$\dot{\tilde{\eta}}(t)=\dot{\eta}(t)-\dot{\hat{\eta}}(t). \tag{4.17}$$

In Equation (4.17), $\eta(t)$ is constant and for this reason the time derivative of $\eta(t)$ is equal to zero. Thus, Equation (4.17) results in

$$\dot{\tilde{\eta}}(t)=-\dot{\hat{\eta}}(t). \tag{4.18}$$

Substituting $\dot{s}(t)$ in Equation (4.8) into Equation (4.16) and using Equation (4.1) and Equation (4.6) one has

$$\begin{aligned}\dot{V}(t) &= s(t)\left[T\dot{e}(t)+f_1(x,t)+g_1(x,t)u(t)\right] \\ &\quad +s(t)\left[d(x,t)-\ddot{r}(t)+H\dot{u}(t)\right] \\ &\quad -\dot{\hat{\eta}}(t)\frac{1}{Y}\tilde{\eta}(t).\end{aligned} \tag{4.19}$$

After necessary adjustments for Equation (4.19), the following equation is obtained

$$\begin{aligned}\dot{V}(t) &= s(t)\left[f_1(x,t)+g_1(x,t)u(t)\right] \\ &\quad +s(t)\left[T\dot{e}(t)+d(x,t)-\ddot{r}(t)+H\dot{u}(t)\right]-\dot{\hat{\eta}}(t)\frac{1}{Y}\tilde{\eta}(t).\end{aligned} \tag{4.20}$$

Substituting $f_1(x,t)$ and $g_1(x,t)$ in Equation (4.2) into Equation (4.20) yields

$$\begin{aligned}\dot{V}(t) &= s(t)\left\{\left[f(x,t)+\eta_1(x,t)\right]+\left[g(x,t)+\eta_2(x,t)\right]u(t)\right\} \\ &\quad +s(t)\left[T\dot{e}(t)+d(x,t)-\ddot{r}(t)+H\dot{u}(t)\right] \\ &\quad -\dot{\hat{\eta}}(t)\frac{1}{Y}\tilde{\eta}(t).\end{aligned} \tag{4.21}$$

Substituting $\dot{u}(t)$ given in Equation (4.13) into Equation (4.21) leads to

$$\begin{aligned}\dot{V}(t) &= s(t)\left\{\left[f(x,t)+\eta_1(x,t)\right]+\left[g(x,t)+\eta_2(x,t)\right]u(t)\right\} \\ &\quad -s(t)\left\{\left[f(x,t)+\hat{\eta}_1(x,t)\right]+\left[g(x,t)+\hat{\eta}_2(x,t)\right]u(t)\right\} \\ &\quad +s(t)\left[-p_1s(t)-p_2sign(s)\right]-\dot{\hat{\eta}}(t)\frac{1}{Y}\tilde{\eta}(t).\end{aligned} \tag{4.22}$$

After making various arrangements in the above equation, the following equation is obtained

$$\begin{aligned}\dot{V}(t) = & s(t)\left[f(x,t)+\eta_1(x,t)\right] \\ & + s(t)\left\{\left[g(x,t)+\eta_2(x,t)\right]u(t)\right\} \\ & - s(t)\left[f(x,t)+\hat{\eta}_1(x,t)\right] \\ & - s(t)\left\{\left[g(x,t)+\hat{\eta}_2(x,t)\right]u(t)\right\} \\ & + s(t)\left[-p_1 s(t)-p_2 sign(s)\right]-\dot{\hat{\eta}}(t)\frac{1}{Y}\tilde{\eta}(t).\end{aligned} \tag{4.23}$$

After the necessary adjustments in the above equation, the following equation is obtained

$$\begin{aligned}\dot{V}(t) = & s(t)\left[\eta_1(x,t)-\hat{\eta}_1(x,t)\right] \\ & + s(t)\left\{\left[\eta_2(x,t)-\hat{\eta}_2(x,t)\right]u(t)\right\} \\ & + s(t)\left[-p_1 s(t)-p_2 sign(s)\right]-\dot{\hat{\eta}}(t)\frac{1}{Y}\tilde{\eta}(t).\end{aligned} \tag{4.24}$$

Substituting $\eta_1(x,t)$ and $\eta_2(x,t)$ in Equation (4.3) and their estimations given in Equation (4.14) into above equation, one has

$$\begin{aligned}\dot{V}(t) = & s(t)\left[(\eta-\hat{\eta})x_2(t)+(\eta-\hat{\eta})x_1(t)+(\eta-\hat{\eta})u(t)\right] \\ & + s(t)\left[-p_1 s(t)-p_2 sign(s)\right]-\dot{\hat{\eta}}(t)\frac{1}{Y}\tilde{\eta}(t).\end{aligned} \tag{4.25}$$

Rearranging Equation (4.25) yields

$$\dot{V}(t) = \tilde{\eta}(t)\left\{s(t)\left[x_2(t)+x_1(t)+u(t)\right]-\dot{\hat{\eta}}(t)\frac{1}{Y}\right\} \\ +s(t)\left[-p_1 s(t)-p_2 sign(s)\right]. \tag{4.26}$$

All the terms including $\tilde{\eta}(t)$ are eliminated if the adaptation law to estimate $\eta(t)$ is selected as follows:

$$\dot{\hat{\eta}}(t) = s(t)\left\{\left[x_2(t)+x_1(t)+u(t)\right]Y\right\}. \tag{4.27}$$

As a result, the following condition must be provided to be ensured $\dot{V}(t) \leq 0$ for asymptotic stability of the system in Equation (4.1):

$$\dot{V}(t) = -p_1 s(t)s(t) - p_2\left|s(t)\right| \leq 0. \tag{4.28}$$

Eventually, under the conditions: $V(0)=0$ if $s(t)=0$ and $\dot{V}(0)=0$ if $\dot{s}(t)=0$ in other cases $\dot{V}(0)\leq 0$ stability of the whole system given in Equation (4.1) with the control in Equation (4.13) and the adaptation law in Equation (4.27) is guaranteed.

4.2. PID Sliding surface based Adaptive Dynamic Second-order Fault-Tolerant Sliding Mode Control Design

In this study, in order to decrease “chattering” a second-order sliding mode control instead of the traditional (first-order) SMC with the signum function is selected. In addition, because a fault function is added on the system parameters, model based second-order sliding mode algorithms must be used. The proposed method for controlling an uncertain damaged system is the proportional-integral-derivative (PID) sliding surface based second-order fault-tolerant sliding mode controller (ADFTSMC). For this controller design dynamic PID based second-order sliding surface is selected as follows:

$$\sigma(s)=\left[k_p+\frac{1}{s}k_i+sk_d\right]^{n-1}\chi\big(E(s)\big)+H\gamma\big(U(s)\big), \tag{4.29}$$

$$\chi\big(E(s)\big)=\left(\frac{1}{s}\right)E(s), \tag{4.30}$$

$$\gamma\big(U(s)\big)=\left(\frac{1}{s}\right)U(s) \tag{4.31}$$

where $\chi\big(E(s)\big)$ is the integral of the tracking error; $\gamma\big(U(s)\big)$ is the integral of the control input given in Laplace domain; n is the order of the system here it is equal to 2; k_p, k_i and k_d are positive coefficients.

Substituting $\chi\big(E(s)\big)$ and $\gamma\big(U(s)\big)$ in Equation (4.30) and Equation (4.31), respectively, into Equation (4.29) gives

$$\sigma(s)=\frac{1}{s}k_pE(s)+\frac{1}{s^2}k_iE(s)+k_dE(s)+\frac{1}{s}HU(s). \tag{4.32}$$

Though the control input appears in the first time derivative of the sliding surface in the first-order (traditional) SMC, in second-order sliding modes the control input appears in the second derivative of the sliding surface.

Time domain representation of Equation (4.32) is as follows:

$$\ddot{\sigma}(t)=k_p\dot{e}(t)+k_i e(t)+k_d\ddot{e}(t)+H\dot{u}(t). \tag{4.33}$$

To make sure that the system given in Equation (4.1) reaches the sliding mode surface within a finite time $\ddot{\sigma}(t)$ is selected as follows:

$$\ddot{\sigma}(t)=-p_1\dot{\sigma}(t)-p_2 sign\left(\dot{\sigma}(t)\right) \tag{4.34}$$

where p_1 and p_2 are positive constants. Afterwards, let us design the equivalent control by setting the second time derivative of the sliding surface in Equation (4.33) to the selected second-time derivative of $\sigma(t)$ in Equation (4.34):

$$k_p\dot{e}(t)+k_i e(t)+k_d\ddot{e}(t)+H\dot{u}(t)=-p_1\dot{\sigma}(t)-p_2 sign\left(\dot{\sigma}(t)\right). \tag{4.35}$$

Substituting $\ddot{e}(t)$ in Equation (4.6) into Equation (4.35), the following equation is obtained:

$$\begin{aligned}&k_p\dot{e}(t)+k_i e(t)+k_d\left[f_1(x,t)+g_1(x,t)u(t)+d(x,t)-\ddot{r}(t)\right]\\&+H\dot{u}(t)=-p_1\dot{\sigma}(t)-p_2 sign\left(\dot{\sigma}(t)\right).\end{aligned} \tag{4.36}$$

For the state trajectory staying on the sliding surface, the equality given above must be provided. Substituting $f_1(x,t)$ and $g_1(x,t)$ in Equation (4.2) into the above equation, the following equation is obtained:

$$\begin{aligned}&k_d\left\{f(x,t)+\eta_1(x,t)+\left[g(x,t)+\eta_2(x,t)\right]u(t)\right\}\\&+k_d\left[d(x,t)-\ddot{r}(t)\right]+k_p\dot{e}(t)+k_ie(t)\\&+H\dot{u}(t)=-p_1\dot{\sigma}(t)-p_2sign\left(\dot{\sigma}(t)\right).\end{aligned} \tag{4.37}$$

In order to make the system given in Equation (4.1) adaptive, the unknown parameters $\eta_1(t)$ and $\eta_2(t)$ in Equation (4.37) is replaced by their estimates $\hat{\eta}_1(t)$ and $\hat{\eta}_2(t)$, respectively, then the time derivative of the control input is obtained in the following:

$$\begin{aligned}&\dot{u}(t)=\left[-p_1\dot{\sigma}(t)-p_2sign\left(\dot{\sigma}(t)\right)-k_p\dot{e}(t)-k_ie(t)\right]\\&-\frac{k_d}{H}\left\{f(x,t)+\hat{\eta}_1(x,t)+\left[g(x,t)+\hat{\eta}_2(x,t)\right]u(t)\right\}\\&-\frac{k_d}{H}\left[d(x,t)-\ddot{r}(t)\right]\end{aligned} \tag{4.38}$$

where $\hat{\eta}_1(x,t)$ and $\hat{\eta}_2(x,t)$ are the estimations of $\eta_1(x,t)$ and $\eta_2(x,t)$, respectively.

$$\begin{aligned}&\hat{\eta}_1(x,t)=\hat{\eta}x_2(t)+\hat{\eta}x_1(t)\\&\hat{\eta}_2(x,t)=\hat{\eta}(t)\end{aligned} \tag{4.39}$$

where $\hat{\eta}(t)$ is the estimation of $\eta(t)$.

A Lyapunov function candidate, which affirms the stability of the system given in Equation (4.1), can be chosen as follows:

$$V(t)=\frac{1}{2}\dot{\sigma}^2(t)+\frac{1}{2}\frac{1}{Y}\tilde{\eta}^2(t)\geq 0 \tag{4.40}$$

$$\tilde{\eta}(t)=\eta(t)-\hat{\eta}(t) \tag{4.41}$$

where $\tilde{\eta}(t)$ is the estimation error.

With the calculation of the first-order time derivative of the Lyapunov function in Equation (4.40) the following equation is obtained:

$$\dot{V}(t)=\dot{\sigma}(t)\ddot{\sigma}(t)+\frac{1}{Y}\dot{\tilde{\eta}}(t)\tilde{\eta}(t)\leq 0. \tag{4.42}$$

Time derivative of $\tilde{\eta}(t)$ given in Equation (4.41) is obtained in the following

$$\dot{\tilde{\eta}}(t)=\dot{\eta}(t)-\dot{\hat{\eta}}(t). \tag{4.43}$$

In the above equation $\eta(t)$ is constant and for this reason the time derivative of $\eta(t)$ is equal to zero. Thus

$$\dot{\tilde{\eta}}(t)=-\dot{\hat{\eta}}(t). \tag{4.44}$$

After necessary adjustment in Equation (4.42) then the following equation is obtained:

$$\dot{V}(t) = \dot{\sigma}(t)\ddot{\sigma}(t) - \frac{1}{Y}\dot{\hat{\eta}}(t)\tilde{\eta}(t) \leq 0. \tag{4.45}$$

Substituting $\ddot{\sigma}(t)$ given in Equation (4.33) into Equation (4.45) yields

$$\dot{V}(t) = \dot{\sigma}(t)\left[k_p\dot{e}(t) + k_i e(t) + k_d\ddot{e}(t) + H\dot{u}(t)\right] - \frac{1}{Y}\dot{\hat{\eta}}(t)\tilde{\eta}(t). \tag{4.46}$$

Substituting $\ddot{e}(t)$ given in Equation (4.6) into the above equation yields

$$\begin{aligned}\dot{V}(t) &= \dot{\sigma}(t)k_d\left[f_1(x,t) + g_1(x,t)u(t) + d(x,t) - \ddot{r}(t)\right] \\ &\quad + \dot{\sigma}\left[k_p\dot{e}(t) + k_i e(t) + H\dot{u}(t)\right] - \frac{1}{Y}\dot{\hat{\eta}}(t)\tilde{\eta}(t).\end{aligned} \tag{4.47}$$

Substituting $f_1(x,t)$ and $g_1(x,t)$ given in Equation (4.2) into Equation (4.47) one has

$$\begin{aligned}\dot{V}(t) &= \dot{\sigma}(t)\left[k_p\dot{e}(t) + k_i e(t) + H\dot{u}(t)\right] - \frac{1}{Y}\dot{\hat{\eta}}(t)\tilde{\eta}(t) \\ &\quad + \dot{\sigma}(t)k_d\left\{f(x,t) + \eta_1(x,t) + \left[g(x,t) + \eta_2(x,t)\right]u(t)\right\} \\ &\quad + \dot{\sigma}(t)k_d\left[d(x,t) - \ddot{r}(t)\right].\end{aligned} \tag{4.48}$$

After necessary adjustment in the above equation we obtain

$$\begin{aligned}\dot{V}(t) &= \dot{\sigma}(t)k_d\left\{f(x,t)+\eta_1(x,t)+\left[g(x,t)+\eta_2(x,t)\right]u(t)\right\}\\ &+\dot{\sigma}(t)k_d\left[d(x,t)-\ddot{r}(t)\right]+\dot{\sigma}(t)\left[H\dot{u}(t)\right]\\ &+\dot{\sigma}(t)\left[k_p\dot{e}(t)+k_ie(t)\right]-\frac{1}{Y}\dot{\hat{\eta}}(t)\tilde{\eta}(t).\end{aligned} \tag{4.49}$$

Substituting $\dot{u}(t)$ given in Equation (4.38) into the above equation yields

$$\begin{aligned}\dot{V}(t) &= \dot{\sigma}(t)k_d\left[f(x,t)+\eta_1(x,t)\right]\\ &+\dot{\sigma}(t)k_d\left\{\left[g(x,t)+\eta_2(x,t)\right]u(t)\right\}\\ &+\dot{\sigma}(t)\left\{H\left[\frac{1}{H}\left[-p_1\dot{\sigma}(t)-p_2sign\left(\dot{\sigma}(t)\right)\right]\right]\right\}\\ &+\dot{\sigma}(t)\left\{H\left[\frac{1}{H}\right]\left(-k_p\dot{e}(t)-k_ie(t)\right)\right\}\\ &+\dot{\sigma}(t)\left\{H\left[-\frac{k_d}{H}\left(f(x,t)+\hat{\eta}_1(x,t)\right)\right]\right\}\\ &+\dot{\sigma}(t)\left\{H\left[-\frac{k_d}{H}\right]\left[g(x,t)+\hat{\eta}_2(x,t)\right]u(t)\right\}\\ &+\dot{\sigma}(t)\left\{H\left[-\frac{k_d}{H}\left(d(x,t)-\ddot{r}(t)\right)\right]\right\}\\ &+\dot{\sigma}(t)\left[k_p\dot{e}(t)+k_ie(t)\right]-\frac{1}{Y}\dot{\hat{\eta}}(t)\tilde{\eta}(t)\\ &+\dot{\sigma}(t)k_d\left[d(x,t)-\ddot{r}(t)\right].\end{aligned} \tag{4.50}$$

Equation (4.50) can be arranged as follows:

$$\begin{aligned}\dot{V}(t) = \dot{\sigma}(t)k_d\left[\eta_1(x,t)+\eta_2(x,t)u(t)\right] \\ -\dot{\sigma}(t)k_d\left[\hat{\eta}_1(x,t)+\hat{\eta}_2(x,t)u(t)\right] \\ +\dot{\sigma}(t)\left[-p_1\dot{\sigma}(t)-p_2 sign(\dot{\sigma}(t))\right]-\frac{1}{Y}\dot{\hat{\eta}}(t)\tilde{\eta}(t).\end{aligned} \tag{4.51}$$

After necessary adjustment in Equation (4.51), the following equation is obtained:

$$\begin{aligned}\dot{V}(t) = \dot{\sigma}(t)k_d\left\{\left[\eta_1(x,t)-\hat{\eta}_1(x,t)\right]+\left[\eta_2(x,t)-\hat{\eta}_2(x,t)\right]u(t)\right\} \\ +\dot{\sigma}(t)\left[-p_1\dot{\sigma}(t)-p_2 sign(\dot{\sigma}(t))\right]-\frac{1}{Y}\dot{\hat{\eta}}(t)\tilde{\eta}(t).\end{aligned} \tag{4.52}$$

Substituting $\eta_1(x,t)$ and $\eta_2(x,t)$ in Equation (4.3) and their estimations given in Equation (4.14) into the above equation one has

$$\begin{aligned}\dot{V}(t) = \dot{\sigma}(t)k_d\left[(\eta-\hat{\eta})x_2(t)+(\eta-\hat{\eta})x_1(t)+(\eta-\hat{\eta})u(t)\right] \\ +\dot{\sigma}(t)\left[-p_1\dot{\sigma}(t)-p_2 sign(\dot{\sigma}(t))\right]-\frac{1}{Y}\dot{\hat{\eta}}(t)\tilde{\eta}(t).\end{aligned} \tag{4.53}$$

Equation (4.53) can be rearranged as follows:

$$\begin{aligned}\dot{V}(t) = \tilde{\eta}(t)\left\{\dot{\sigma}(t)k_d\left[x_2(t)+x_1(t)+u(t)-\frac{1}{Y}\dot{\hat{\eta}}(t)\right]\right\} \\ +\dot{\sigma}(t)\left[-p_1\dot{\sigma}(t)-p_2 sign(\dot{\sigma}(t))\right].\end{aligned} \tag{4.54}$$

All the terms in Equation (4.54) including $\tilde{\eta}(t)$ are eliminated if the adaptation law to estimate $\eta(t)$ is selected as follows:

$$\dot{\hat{\eta}}(t) = k_d \dot{\sigma}(t)\left\{\left[x_2(t) + x_1(t) + u(t)\right]Y\right\}. \tag{4.55}$$

As a result, the following condition must be provided to be ensured $\dot{V}(t) \leq 0$ for stability of the system in Equation (4.1) with the control in Equation (4.38) and the adaptation law in Equation (4.55):

$$\dot{V}(t) = -p_1 \dot{\sigma}(t)\dot{\sigma}(t) - p_2 \left|\dot{\sigma}(t)\right| \leq 0 \tag{4.56}$$

$\dot{V}(0) = 0$ if $\dot{\sigma}(t) = 0$ in other cases $\dot{V}(t) \leq 0$.

Consequently, the stability of the overall system given in Equation (4.1) is guaranteed in the sense of Lyapunov theory.

5. EXPERIMENTAL APPLICATION AND DISCUSSION

This chapter is divided into two sections.

In the first section, it is aimed to conduct the basis of our thesis by repeating the commonly used SMC algorithms existing in the literature. These controllers are Traditional SMC with Signum and Saturation Functions given in Equation (3.8), Super-Twisting Algorithm Second-Order SMC given in Equation (3.19a) and Equation (3.19b) and PID-Based Second-Order SMC given in Equation (3.31), respectively. No fault function have been added to the system in these designed controllers. So, the electromechanical system without fault given in Equation (2.18) is used. The performances of the designed controllers are compared with each other by means of chattering.

In the second section, a fault function has been added to the system in Equation (2.18). In this way the electromechanical system is transformed to the damaged electromechanical system with fault in Equation (4.1). Then, the designed Adaptive Dynamic First-Order Fault-Tolerant Controller given in Equation (4.13) and the proposed Adaptive Dynamic Second-Order Fault-Tolerant Controller given in Equation (4.38) are compared with the Traditional SMC with the Signum Function given in Equation (3.8) for the damaged electromechanical system in Equation (4.1). The responses of the traditional SMC with the Signum Function and the designed and proposed controllers against the fault occurred in the system are compared. The experimental study is performed for the system described in Chapter 2 but the one in Equation (4.1), not in Equation (2.18). Stability of all controllers are guaranteed in the sense of Lyapunov stability theorem. The robustness of the designed and proposed controllers has been observed by testing them under different speed values. The tracking performances of the controllers are obtained for the selected shaft speeds of 1200 rpm and 1800 rpm. For all experiments, the initial state condition $x(0)=\left[x_1 \;\; x_2\right]^T=\left[0 \;\; 0\right]^T$ of the electromechanical system are used and experiment time is chosen as *Time (t) = 2 sec*. In order to avoid high-frequency measurement noise, a low-pass filter with the transfer function of $G(s)=\dfrac{250}{(s+250)}$ is used.

5.1. Experimental Applications of Basic SMC Algorithms

5.1.1. Traditional SMC with Signum and Saturation Functions

In this part of the thesis, the performance of the Traditional SMC with the signum function is compared with that of the Traditional SMC with the saturation function by means of chattering. The controller parameters are given in Table 5.1.

Table 5.1. Parameters of the Traditional SMC

Parameter	**Value**
λ	20
β	1.2×10^{6}
Δ	100

Figure 5.1 shows the control signal of Traditional SMC given in Equation (3.8) with different switching control laws given in Equation (3.14) and Equation (3.16) for a set point 1200rpm. It is obvious that the signum function used in the switching control law produces chattering. On the other hand it's clearly shown that the saturation function used in the switching control law reduces chattering. The control signal of Traditional SMC with the Saturation function is bounded in the range of |1-1.2|V while the control signal of Traditional SMC with the Signum function is bounded in the range of |0.8-1.4|V at steady-state.

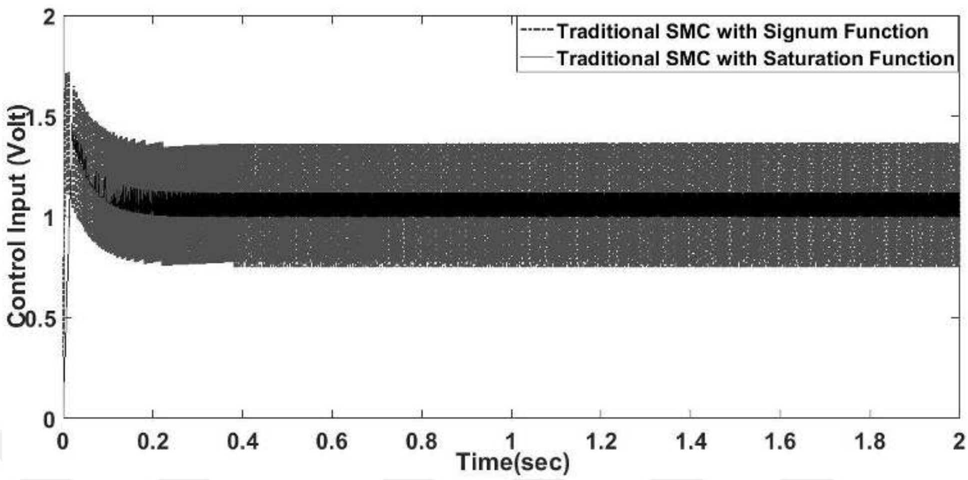

Figure 5.1. Control signals for the traditional SMC with signum and saturation functions for set point 1200 rpm

Figure 5.2 also shows the switching control signal u_{sw} with the signum function given in Equation (3.14) and u_{sw} with the saturation function given in Equation (3.16) for observing the chattering more clearly. When using Equation (3.16) instead of Equation (3.14) in the switching control law, chattering at the control input is significantly reduced.

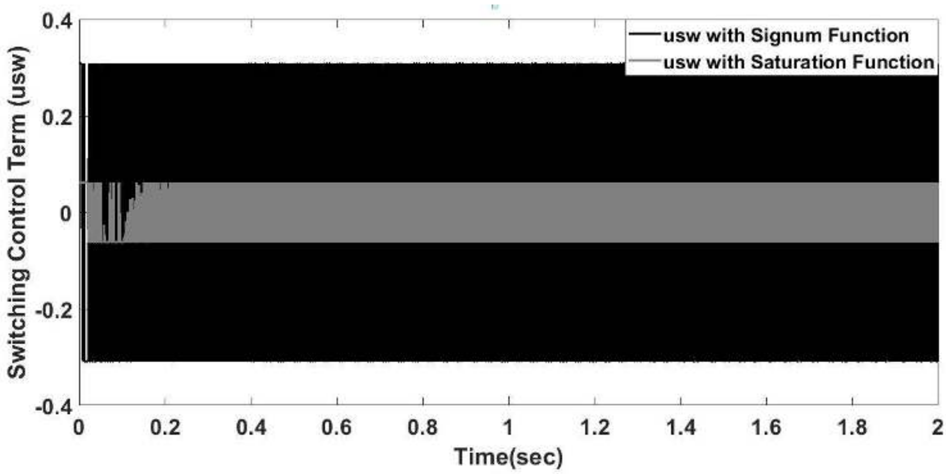

Figure 5.2. Switching control terms for traditional SMC with signum and saturation functions for set point 1200 rpm

Fig 5.3 shows step response of the traditional SMC with the signum function given in Equation (3.15) and the saturation function given in Equation (3.17) for set point 1200 rpm, respectively. From the figure, it is obviously seen that although the traditional SMC with the signum function exhibits faster speed response than the traditional SMC with the saturation function, it shows much oscillations to be able to track the reference signal against motor parameter variation and external disturbances. However, the SMC with the saturation function reveals neither oscillation nor overshoot. The settling time and steady-state errors are about 0.24 sec and 10 rpm, respectively, for the traditional SMC with saturation function. It is clear that the traditional SMC with the saturation function has less output variation from the trajectory in steady state compared with the traditional SMC with the signum function which deviates approximately 50 rpm from the desired speed.

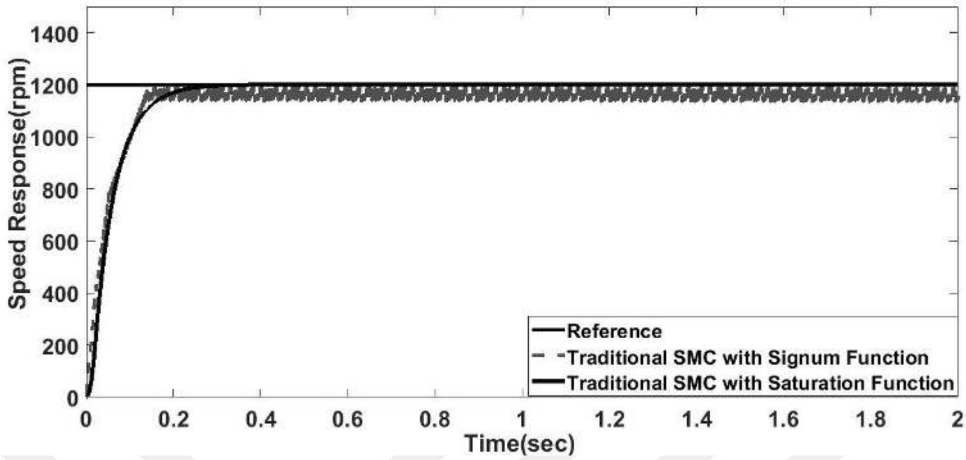

Figure 5.3. Step responses for the traditional SMC with signum and saturation functions for set point 1200 rpm

Fig 5.4a and Fig 5.4b show sliding surfaces of the traditional SMC given in Equation (3.5) with the signum function in Equation (3.15) and the saturation function in Equation (3.17) used in different switching control laws in Equation (3.14) and Equation (3.16), respectively, for set point 1200 rpm. The sliding functions converge to zero in a finite time despite of uncertainties and noises in the control input. The variations in the sliding function directly affect the switching control and effect of the signum function can be clearly seen. For the sliding surface with the saturation function initial values and variations around the desired point are small in magnitude as compared to those of the sliding surface with the signum function.

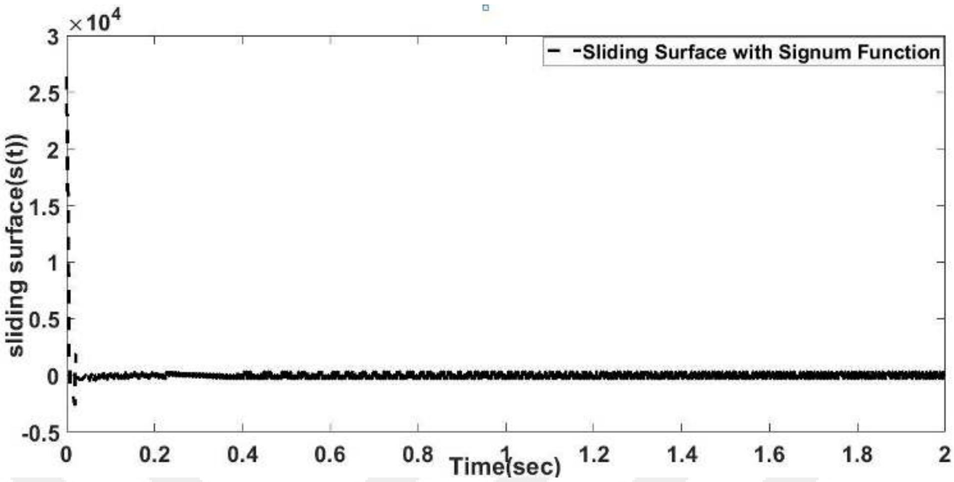

Figure 5.4. (a). Sliding surface for the traditional SMC with the signum function for set point 1200 rpm

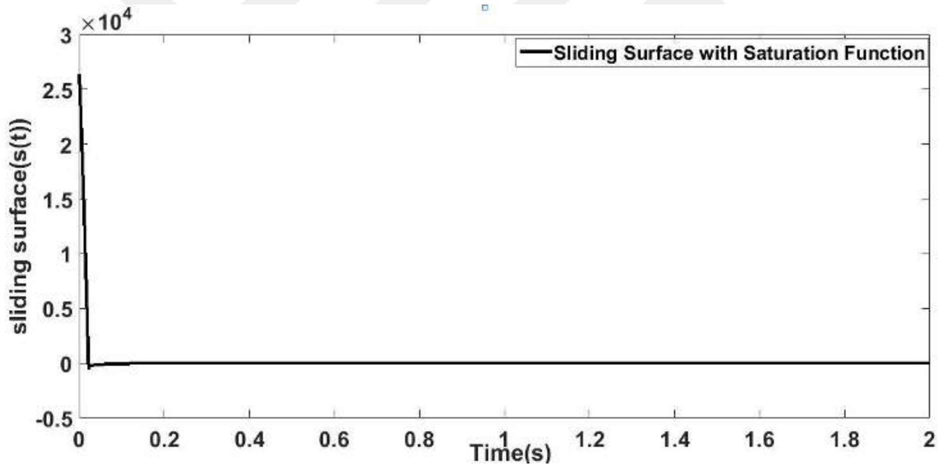

Figure 5.4. (b). Sliding surface for the traditional SMC with the saturation function for set point 1200 rpm

Considering the sliding surface as $s(t)$ and derivative of $s(t)$ as $\dot{s}(t)$ given in Equation (3.5) and Equation (3.6), respectively, the sliding surfaces of the controller versus time derivatives of the sliding surfaces are shown in Figure 5.5. The sliding surface with the saturation function shows expected behavior with small variations in both $s(t)$ and $\dot{s}(t)$ and yields significantly reduced chattering produced by switching control in Equation (3.16).

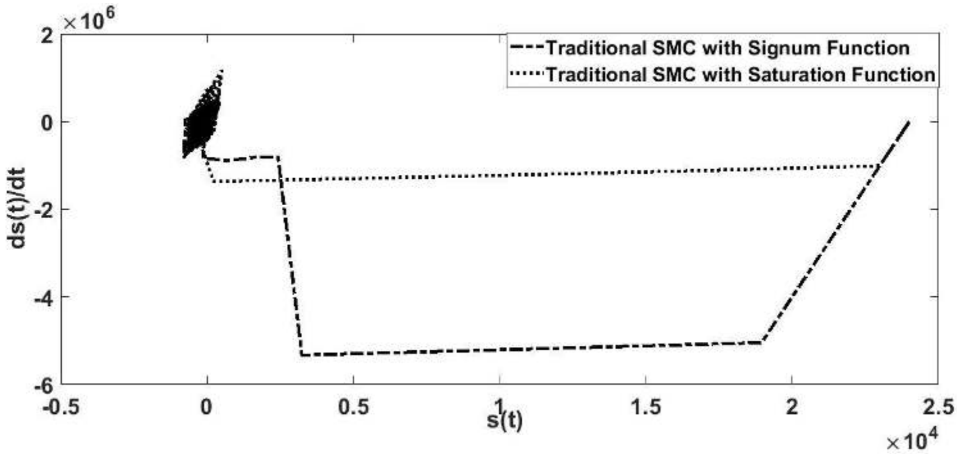

Figure 5.5. Sliding surfaces versus their first-time derivative changes on the traditional SMC for set point 1200 rpm

Similarly, the errors of the controller versus time derivatives of the errors given in Equation (3.3) are shown in Figure 5.6. The main objective of the controller is to force the system states to zero in a finite time and keep them at that point. Since the sliding functions of the controller are based on the errors and their first-time derivatives, it is expected that the sliding functions also converge to the equilibrium point ($e(t) = \dot{e}(t) = 0$). A large error deviation in magnitude is measured at the output of the traditional SMC with the signum function. A small error deviation is measured from the output of the traditional SMC with the saturation function.

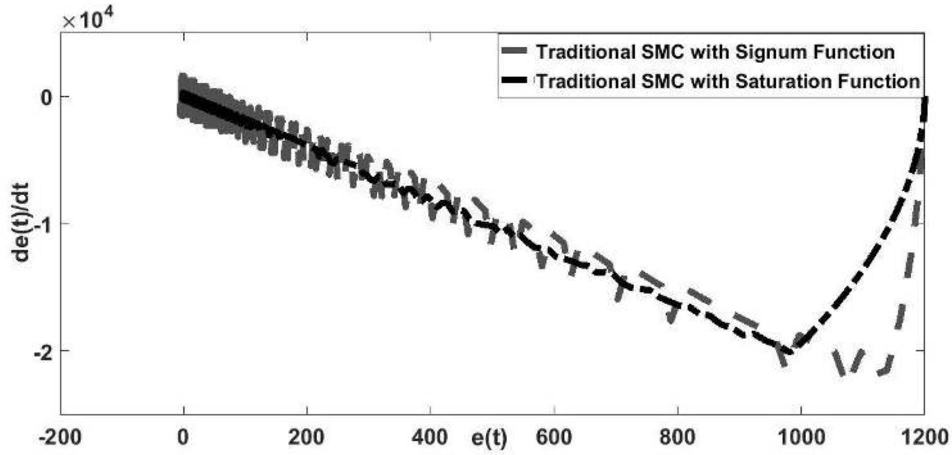

Figure 5.6. Error functions versus their first-time derivative changes on the traditional SMC for set point 1200 rpm

Figure 5.7 shows the control signals given in Equation (3.8) of the traditional SMC with the different switching control laws given in Equation (3.14) and in Equation (3.16), respectively, for a set point 1800 rpm. Similar to that at 1200 rpm, the signum function used in the switching control law produces chattering. On the other hand it's clearly shown that the saturation function used in the switching control law reduces chattering. The control signal of the Traditional SMC with the saturation function is bounded in the range of |1.6-1.7|V while the control signal of the Traditional SMC with the Signum function is bounded in the range of |1-2.25|V at steady-state. It is observed that chattering increases at 1800 rpm compared to 1200 rpm.

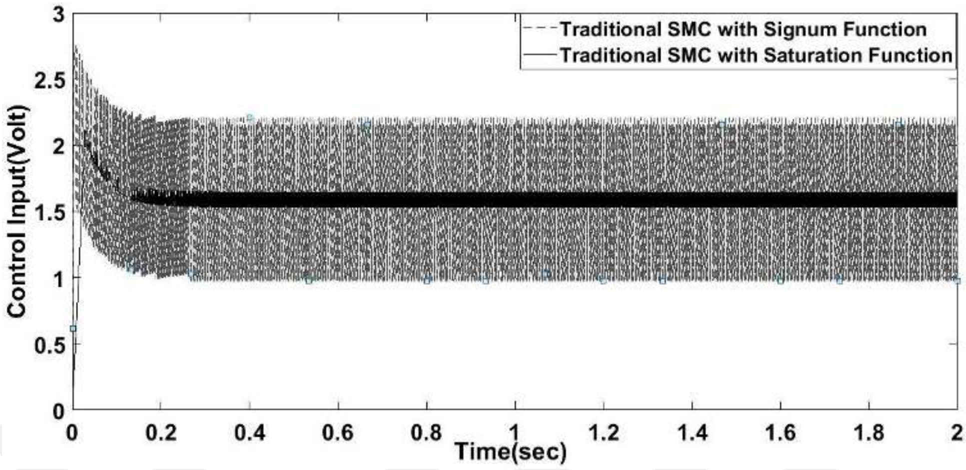

Figure 5.7. Control signals for the traditional SMC with signum and saturation functions for set point 1800 rpm

Figure 5.8 also shows the switching control signals u_{sw} with the signum function given in Equation (3.14) and u_{sw} with the saturation function given in Equation (3.16) for observing the chattering more clearly. When using Equation (3.16) instead of Equation (3.14) in the switching control law, chattering at the control input is significantly reduced.

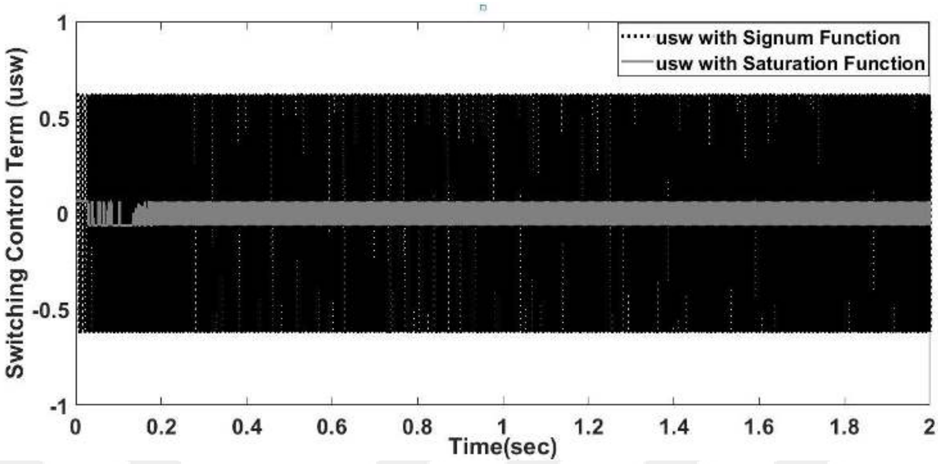

Figure 5.8. Switching control terms u_{sw} for the traditional SMC with signum and saturation functions for set point 1800 rpm

Fig 5.9 shows step responses of the SMC with the signum function given in Equation (3.14) and the saturation function given in Equation (3.16) for a set point 1800 rpm, respectively. It is seen that chattering increases at 1800 rpm compared to 1200 rpm. From the figure, it is obviously seen that although the traditional SMC with the signum function exhibits faster speed response than the traditional SMC with the saturation function, it shows much oscillations to be able to track the reference signal against motor parameter variation and external disturbances. However, the SMC with the saturation function reveals neither oscillation nor overshoot. The settling time and steady-state errors are about 0.22 sec and 5 rpm, respectively, for the traditional SMC with the saturation function. It is clear that the traditional SMC with saturation function has less output variation from the trajectory in steady state compared with the traditional SMC with the signum function which deviates approximately 65 rpm from the desired speed.

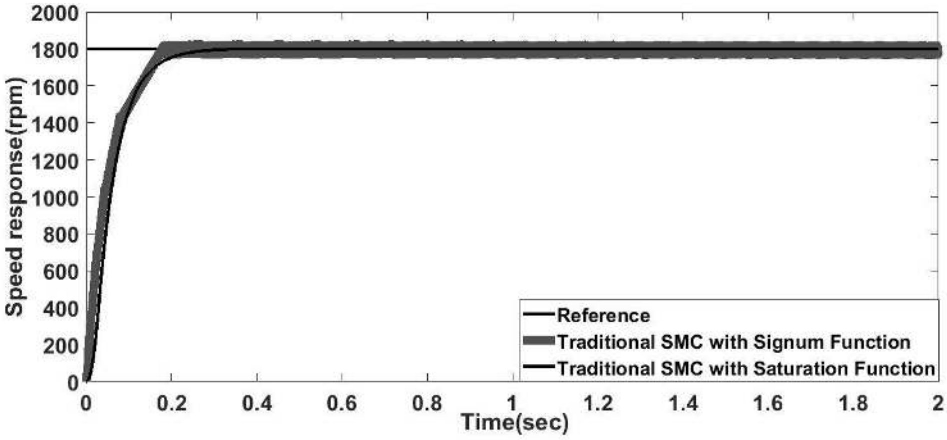

Figure 5.9. Step responses for the traditional SMC with signum and saturation functions for set point 1800 rpm

Figure 5.10a and Figure 5.10b show the sliding surfaces of the traditional SMC given in Equation (3.5) with the signum function in Equation (3.15) and the saturation function in Equation (3.17) used in the different switching control laws in Equation (3.14) and in Equation (316), respectively, for a set point 1800 rpm. Figure 5.10 shows that the sliding functions with the different switching control laws of the controllers converges to zero in a finite time when using Equation (3.5) and varies around zero with different magnitudes. The variations in the sliding function directly affect the switching control and effect of the signum function can be clearly seen. For the sliding surface with the saturation function initial values and variations around the desired point are small in magnitude as compared to the sliding surface with the signum function.

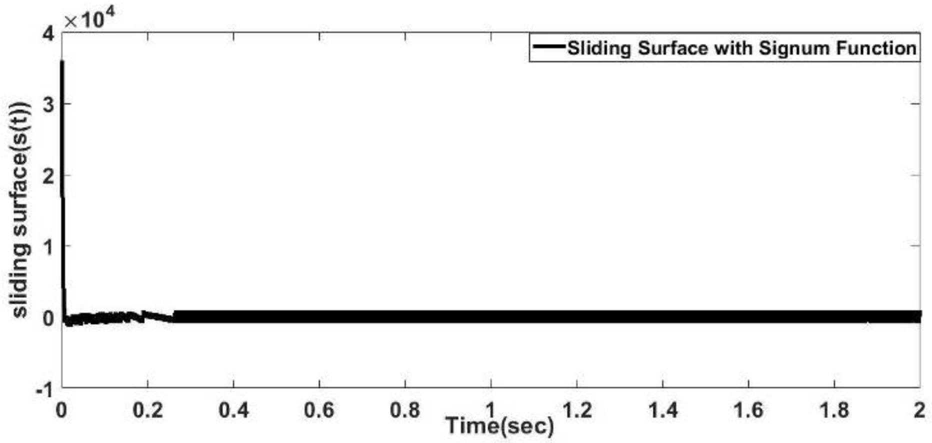

Figure 5.10. (a). Sliding surface for the traditional SMC with signum function for set point 1800 rpm

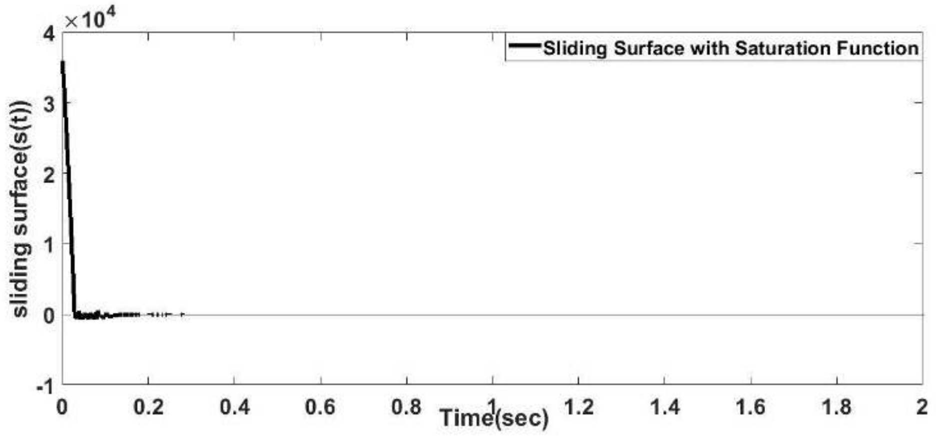

Figure 5.10. (b). Sliding surface for the traditional SMC with saturation function for set point 1800 rpm

Considering the sliding surface as $s(t)$ and derivative of $s(t)$ as $\dot{s}(t)$ given in Equation (3.5) and Equation (3.6), respectively, the sliding surfaces of the controller versus time derivatives of the sliding surfaces are shown in Figure 5.11. The sliding surface with the saturation function shows expected behavior with small variations in both $s(t)$ and $\dot{s}(t)$ which yields significantly reduced chattering produced by switching control in Equation (3.16).

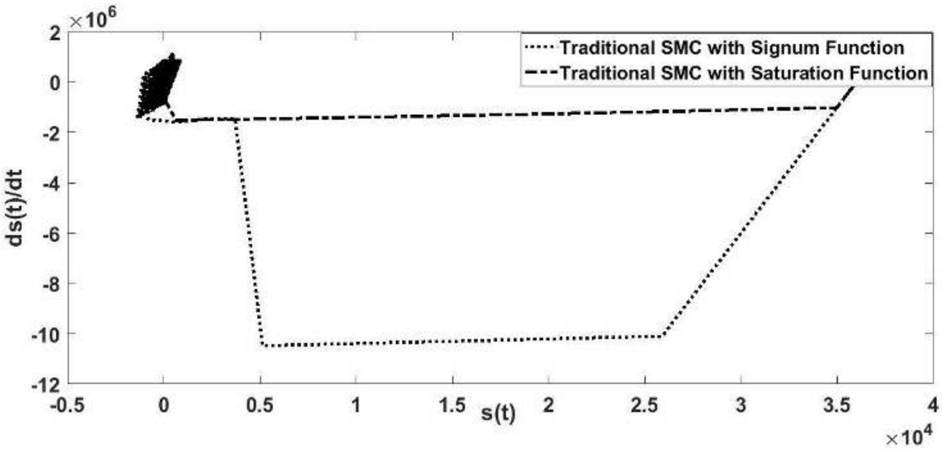

Figure 5.11. Sliding surfaces versus their first-time derivative changes on the traditional SMC for set point 1800 rpm.

As a result of this subsection, we can say that the first-order (traditional) SMC with the saturation function exhibits better performance than one with the signum function in view of chattering even if their steady-state and transient performances are similar.

5.1.2. Super-Twisting Algorithm Second-Order SMC and Traditional SMC

In this part of the thesis, the performance of the super-twisting algorithm second-order SMC is compared with that of the traditional SMC with the signum function by means of chattering. In this subsection, all experimental results are performed using the signum function given in Equation (3.15.) The controller parameters are given in Table 5.2.

Table 5.2. Parameters of the Super-Twisting Algorithm Second-Order SMC

Parameter	**Value**
λ	20
α	0.015

The control inputs produced by the controllers are illustrated in Figure 5.12. The figure shows the experimental results of the control signals in Equation (3.8) of the traditional SMC with the signum function in Equation (3.15) and those of the control signal $u(\mathrm{t})$ given in Equation (3.19) of the super-twisting second-order SMC for a set point 1200 rpm. The control signal of the super-twisting second-order SMC is bounded in the range of |1-1.15|V while the control signal of the traditional SMC with the signum function is bounded in the range of |0.8-1.4|V at steady-state. It is obvious that the super-twisting second-order SMC with the signum function considerably reduces the chattering phenomenon in comparison with the traditional SMC with the signum function.

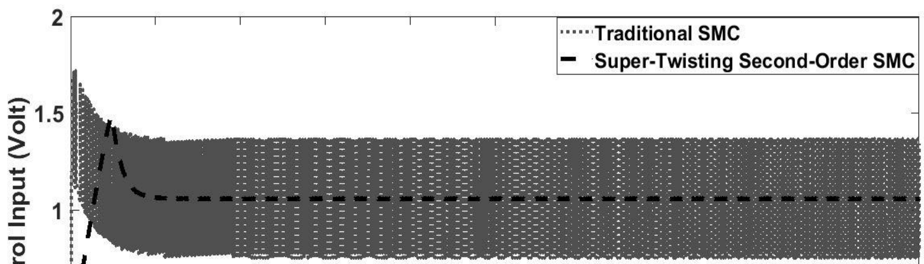

Figure 5.12. Control signals for the traditional SMC with signum function and super-twisting second-order SMC for set point 1200 rpm

Fig 5.13 shows the experimental responses of the traditional SMC with the signum function and super-twisting second-order SMC for a set point 1200 rpm. The super-twisting second-order SMC and the traditional SMC with the signum function both have reached the desired reference value as seen in the figure. From the figure, it is obviously seen that although the traditional SMC with the signum function exhibits faster speed response than super-twisting second-order SMC, it shows much oscillations to be able to track the reference signal against motor parameter variation and external disturbances. The settling time and steady-state errors are about 0.22 sec and 10 rpm, respectively, for the super-twisting second-order SMC. It is clear that the super-twisting second-order SMC has less output variation from the trajectory in steady state compared with the traditional SMC with the signum function which deviates approximately 100 rpm from the desired speed.

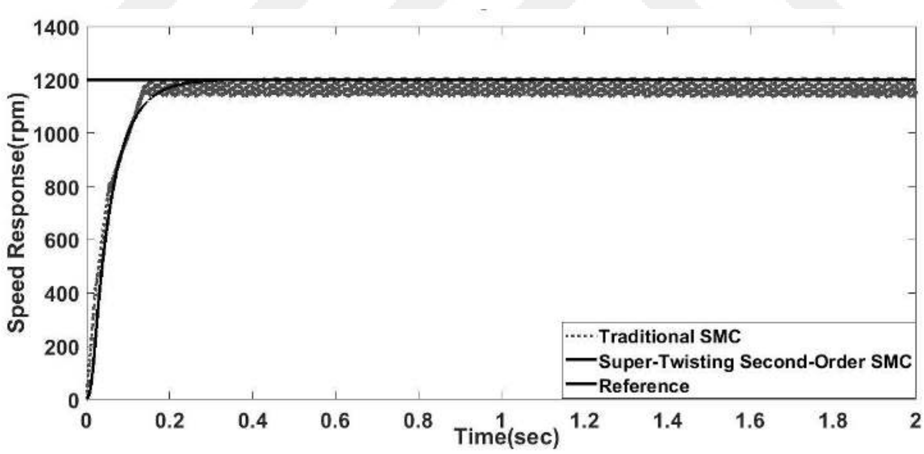

Figure 5.13. Step responses for the super-twisting second-order SMC and the traditional SMC with signum function for set point 1200 rpm

Figure 5.14a and Figure 5.14b show both sliding surfaces in Equation (3.5) of the traditional SMC in Equation (3.8) with the signum function given in Equation (3.15) and the super-twisting second-order SMC given in Equation (3.19) for a set point 1200 rpm. The sliding surfaces converge to zero in a finite time despite of uncertainties and noises in the control input. For the sliding surface of the super-twisting second-order SMC initial values and variations around the desired point are small in magnitude as compared to the sliding surface of the traditional SMC with the signum function.

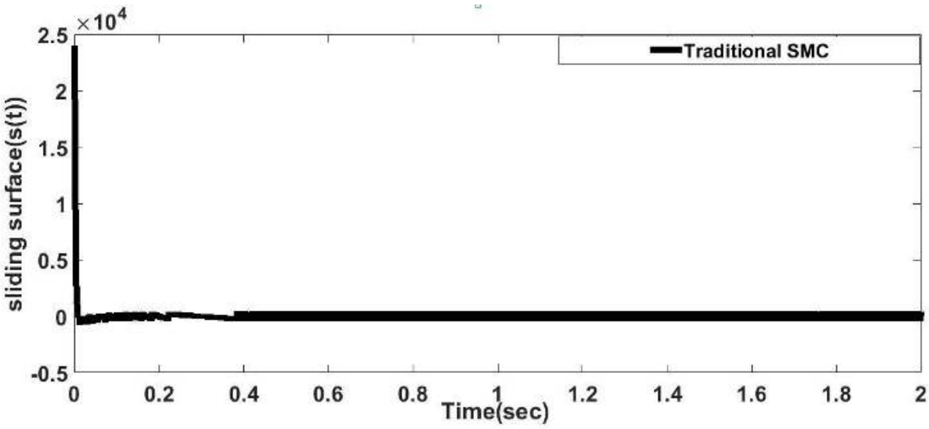

Figure 5.14. (a). Sliding surface for the traditional SMC with signum function for set point 1200 rpm

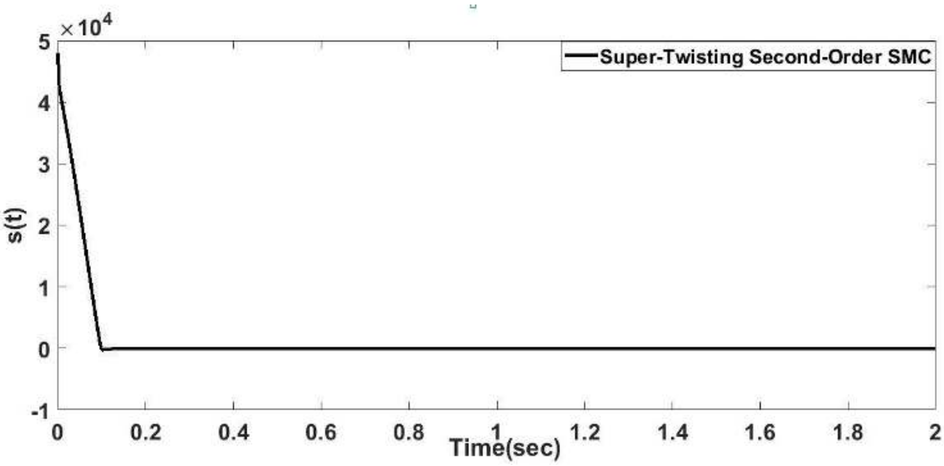

Figure 5.14. (b). Sliding surface for the super-twisting second-order SMC for set point 1200 rpm

Considering the sliding surface $s(t)$ in Equation (3.5) of the traditional SMC and the sliding surface $s(t)$ in Equation (3.5) of the super-twisting SMC and derivative of $s(t)$ as $\dot{s}(t)$ given in Equation (3.6) of the traditional SMC and given in Equation (3.18) of the super-twisting SMC, respectively, the sliding surfaces of the controllers versus time derivatives of the sliding surfaces are shown in Figure 5.15. The sliding surface of the super-twisting second-order SMC shows behavior with small variations in both $s(t)$ and $\dot{s}(t)$ which yields significantly reduced chattering produced by the switching control in Equation (3.19).

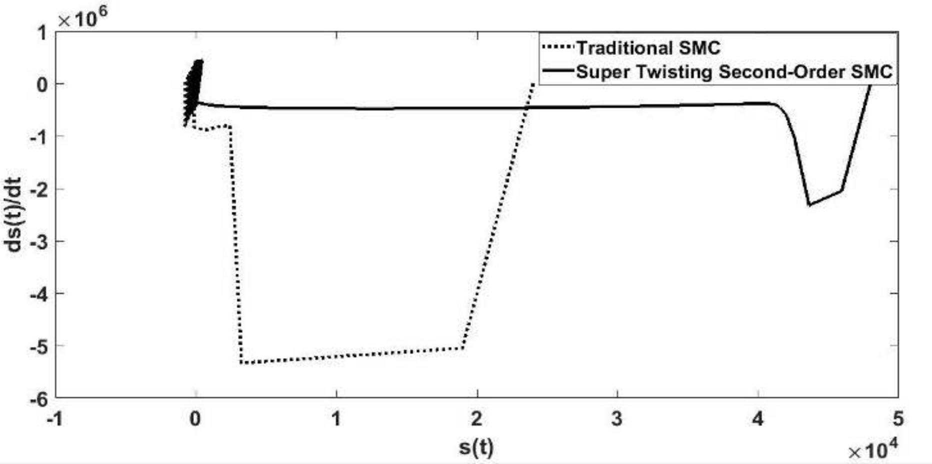

Figure 5.15. Sliding surfaces versus their first-time derivative changes on the traditional SMC with signum function and super-twisting second-order SMC for set point 1200 rpm

Figure 5.16 shows the experimental results of the control signals of the traditional SMC given in Equation (3.8) and the super-twisting second-order SMC given in Equation (3.19) for a set point 1800 rpm. The control signal of the super-twisting second-order SMC is bounded in the range of |1.6-1.65|V while the control signal of the traditional SMC with the signum function is bounded in the range of |1-2.25|V at steady-state. It is obvious that the super-twisting second-order SMC considerably reduces the chattering phenomenon in comparison with the traditional SMC.

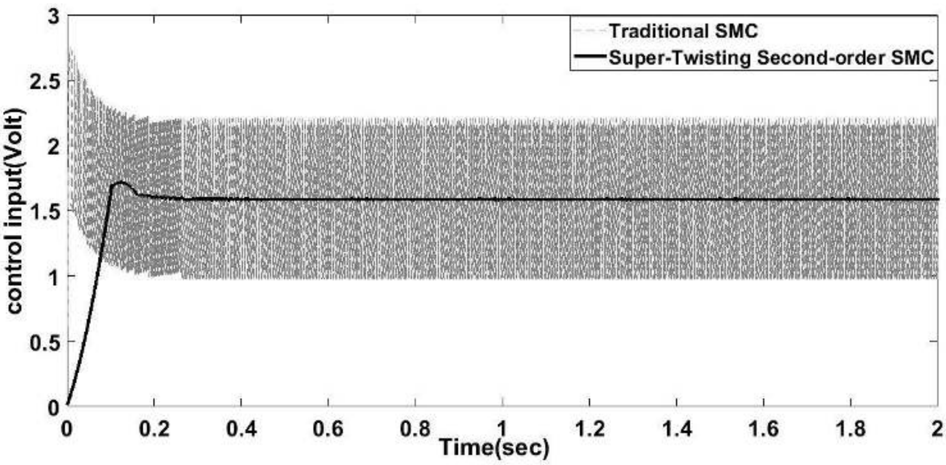

Figure 5.16. Control signals for the traditional SMC with signum function and super-twisting second-order SMC for set point 1800 rpm

Fig 5.17 shows the experimental responses of the traditional SMC and super-twisting second-order SMC for a set point 1800rpm. The super-twisting second-order SMC and traditional SMC have reached the desired reference value as seen in the figure. From the figure, it is obviously seen that although the traditional SMC with the signum function exhibits faster speed response than super-twisting second-order SMC, it shows much oscillations to be able to track the reference signal against motor parameter variation and external disturbances. The super-twisting second-order SMC reveals neither oscillation nor overshoot. The settling time and steady-state errors are about 0.21sec and 14 rpm, respectively, for the super-twisting second-order SMC. It is clear that the super-twisting second-order SMC has less output variation from the trajectory in steady-state compared with the traditional SMC with the signum function which deviates approximately 105 rpm from the desired speed.

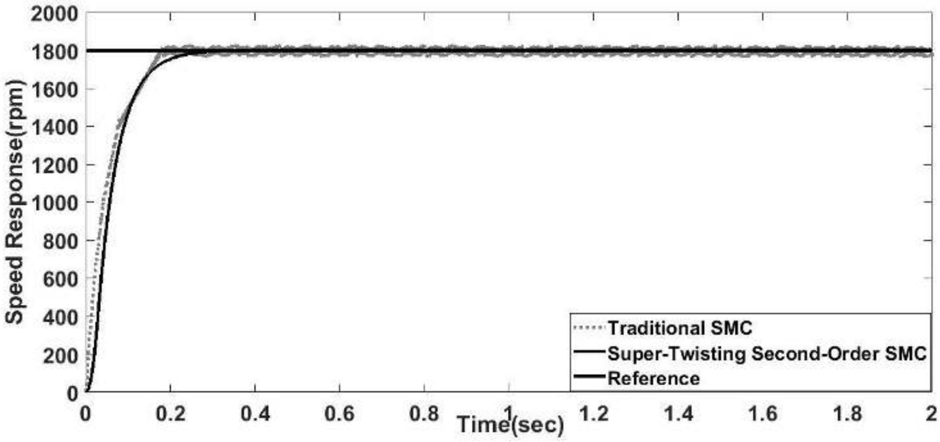

Figure 5.17. Step responses for the super-twisting second-order SMC and the traditional SMC with signum function for set point 1800 rpm

Figure 5.18a and Figure 5.18b show both sliding surfaces in Equation (3.5) of the traditional SMC in Equation (3.8) with the signum function given in Equation (3.15) and the super-twisting second-order SMC given in Equation (3.19) for a set point 1800 rpm. The sliding surfaces converge to zero in a finite time despite of uncertainties and noises in the control input. For the sliding surface of the super-twisting second-order SMC initial values and variations around the desired point are small in magnitude as compared to the sliding surface of the traditional SMC with the signum function.

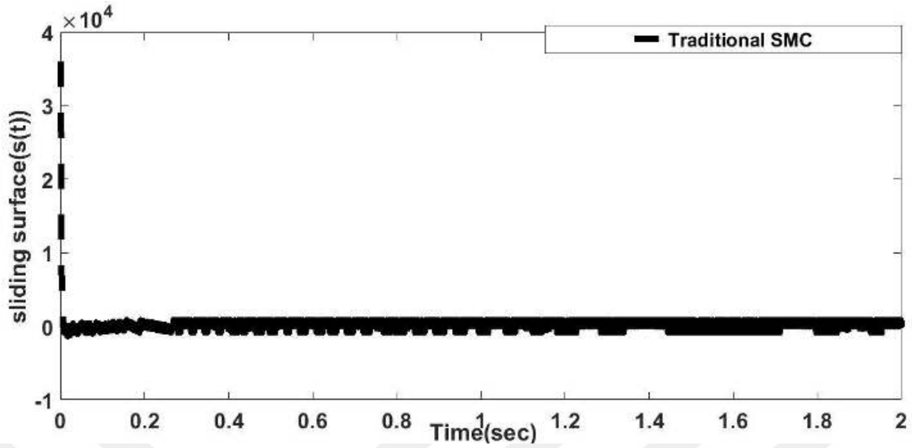

Figure 5.18. (a). Sliding surface for the traditional SMC with signum function for set point 1800 rpm

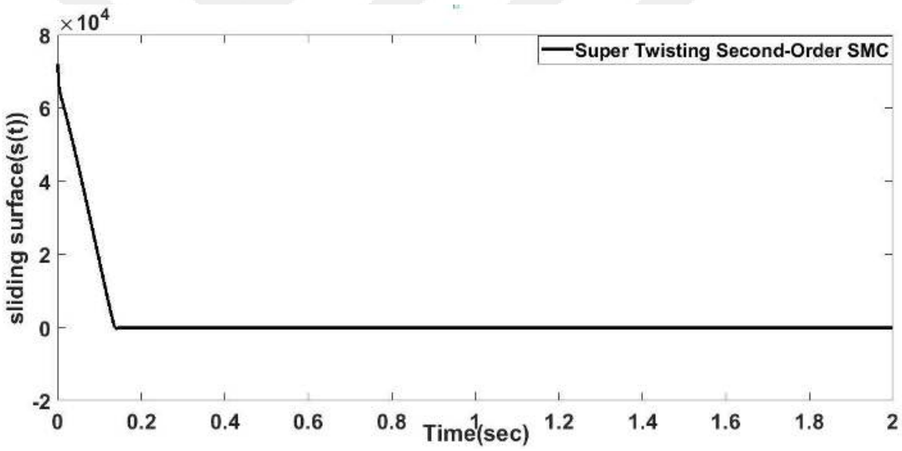

Figure 5.18. (b). Sliding surface for the super-twisting second-order SMC for set point 1800 rpm

Considering the sliding surface $s(t)$ in Equation (3.5) of the traditional SMC and the sliding surface $s(t)$ in Equation (3.5) of the super-twisting SMC and derivative of $s(t)$ as $\dot{s}(t)$ given in Equation (3.6) of the traditional SMC and given in Equation (3.18) of the super-twisting SMC, respectively, the sliding surfaces of the controllers versus time derivatives of the sliding surfaces are shown in Figure 5.19. The sliding surface of the super-twisting second-order SMC shows behavior with small variations in both $s(t)$ and $\dot{s}(t)$ which yields significantly reduced chattering produced by the switching control in Equation (3.19).

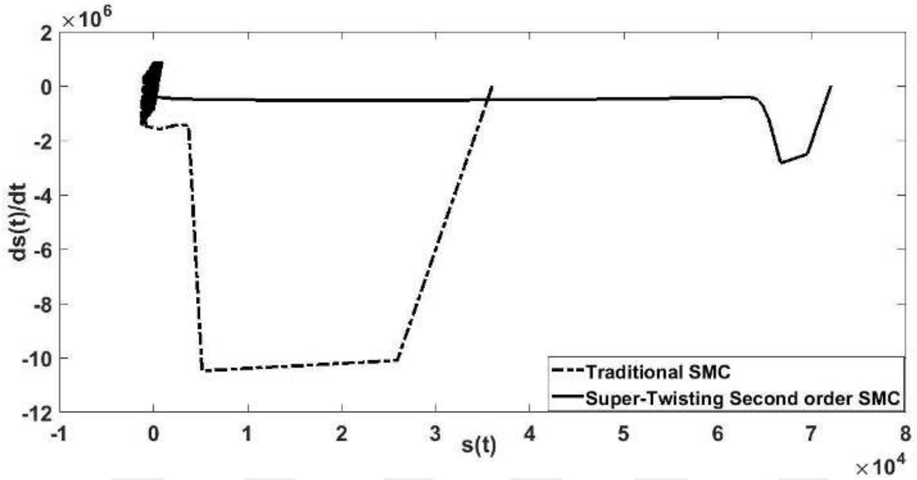

Figure 5.19. Sliding surfaces versus their first-time derivative changes on the traditional SMC with signum function and super-twisting second-order SMC for set point 1800 rpm

As a conclusion of this subsection the nonmodel-based super-twisting algorithm second-order SMC with the signum function is superior to the model-based first-order (traditional) SMC according to chattering elimination.

5.1.3. PID-Based Second-Order SMC and Traditional SMC

In this part of the thesis, the performance of the PID-based second-order SMC is compared with that of the traditional SMC with the signum function by means of chattering. The controller parameters are given in Table 5.3.

Table 5.3. Parameters of the PID based Second-order SMC

Parameter	**Value**
k_p	1.5
k_i	0.0012
k_d	0.02
β	1.2×10^6

Figure 5.20 shows the experimental results of the control signal of the traditional SMC with the signum function given in Equation (3.8) and the control signal of the PID-based second-order SMC given in Equation (3.31) for a set point 1200 rpm. The control signal of the PID-based second-order SMC is bounded in the range of |1-1.16|V in steady-state while the control signal of the traditional SMC with the signum function is bounded in the range of |0.8-1.4|V in steady-state. From the figure it is seen the fact that there is much chattering on the control signal of the traditional SMC with the signum function than those of the PID-based second-order SMC with the signum function.

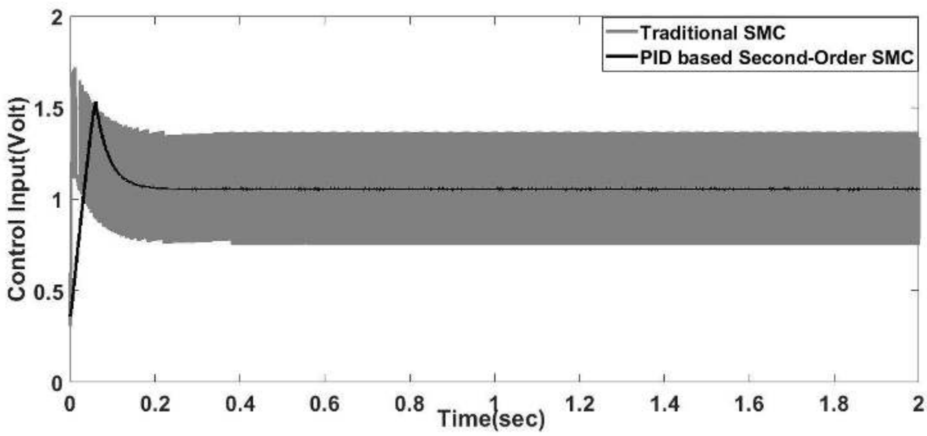

Figure 5.20. Control signals for the traditional SMC with signum function and the PID based second-order SMC for set point 1200 rpm

Figure 5.21 shows the experimental results of velocities of the traditional SMC with the signum function and PID-based second-order SMC for a set point 1200 rpm. The PID-based second-order SMC and the traditional SMC with the signum function have reached the desired reference value as seen in the figure. The PID-based second-order SMC reveals neither oscillation nor overshoot. However, the traditional SMC with the signum function oscillates under the reference. From the figure, it is obviously seen that the PID-based second-order SMC exhibits faster speed response than traditional SMC with the signum function, it also shows no oscillation to be able to track the reference signal against motor parameter variation and external disturbances. The settling time and steady-state errors are about 0.19 sec and 17 rpm, respectively, for the PID-based second-order SMC. It is clear that the PID-based second-order SMC has less output variation from the trajectory in steady state compared with the traditional SMC with the signum function, which deviates approximately 100 rpm from the desired speed. The traditional SMC with the signum function has much chattering effect on its output speed.

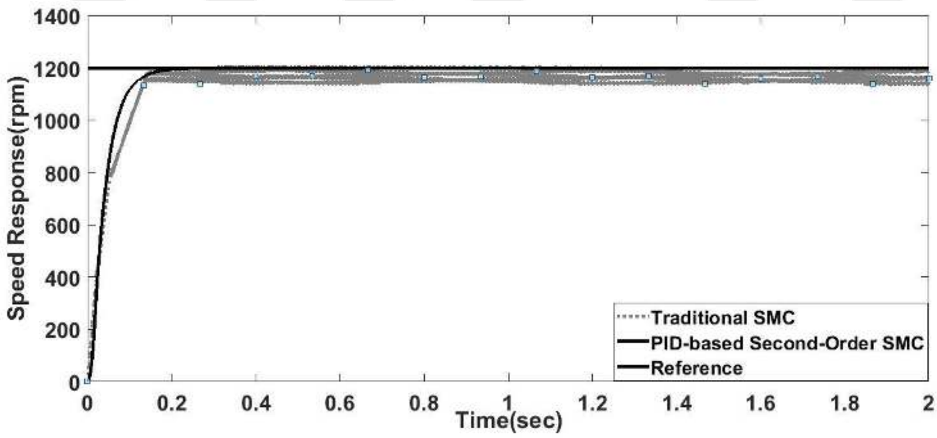

Figure 5.21. Step responses for PID-based second-order SMC and the traditional SMC with signum function for set point 1200 rpm

Figure 5.22a and Figure 5.22b show the sliding surfaces of the traditional SMC with the signum function and the PID-based second-order SMC for a set point 1200 rpm. The sliding functions converge to zero in finite time when using

Equation (3.5) and two times integral $\left(\int_0^t \int_0^t \ddot{\sigma}(\tau) d\tau d\tau \right)$ of Equation (3.28). Initial values and variations around the desired point of the sliding surface of the PID-based second-order SMC are small in magnitude as compared to those of the sliding surface of the traditional SMC with the signum function.

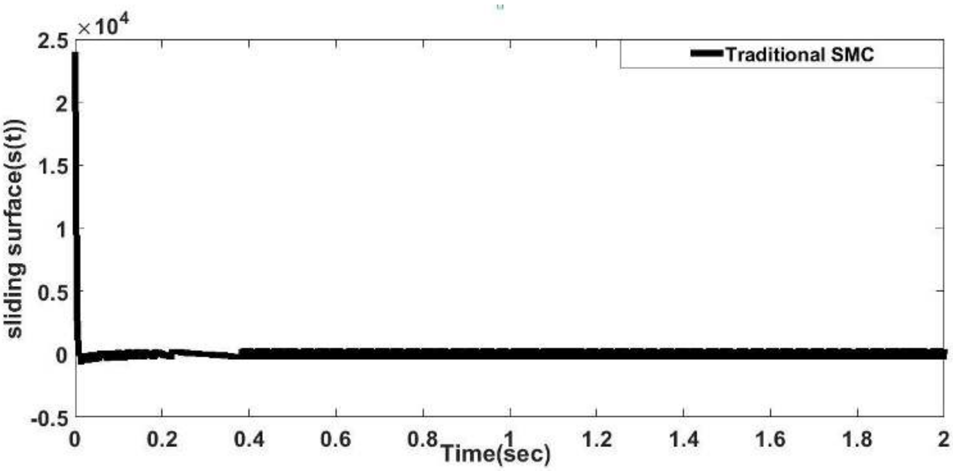

Figure 5.22 (a). Sliding surfaces for the traditional SMC with signum function for set point 1200 rpm

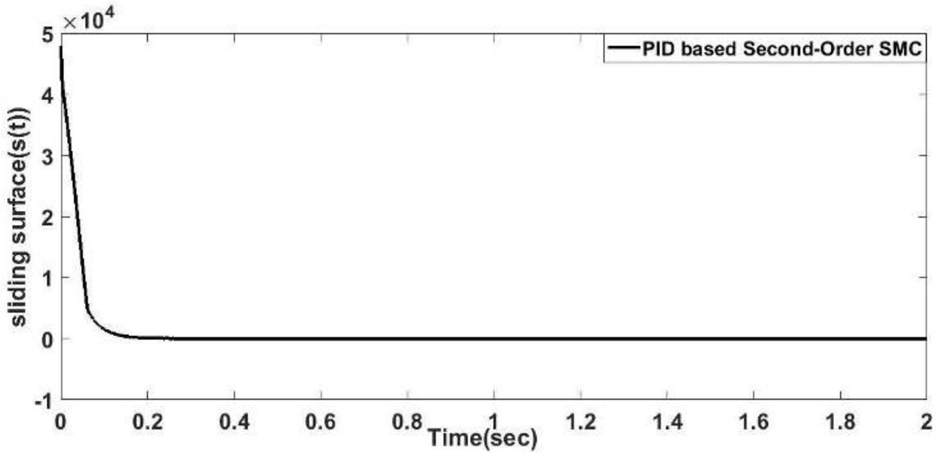

Figure 5.22. (b). Sliding surfaces for the PID-based second-order SMC for set point 1200 rpm

Considering the sliding surface as $s(t)$ and derivative of $s(t)$ as $\dot{s}(t)$, the sliding surfaces of the controllers versus time derivatives of the sliding surfaces are shown in Figure 5.23. The sliding surface of the PID-based second-order SMC shows behavior with small variations in both $s(t)$ and $\dot{s}(t)$ which yields significantly reduced chattering produced by the switching control in Equation (3.38).

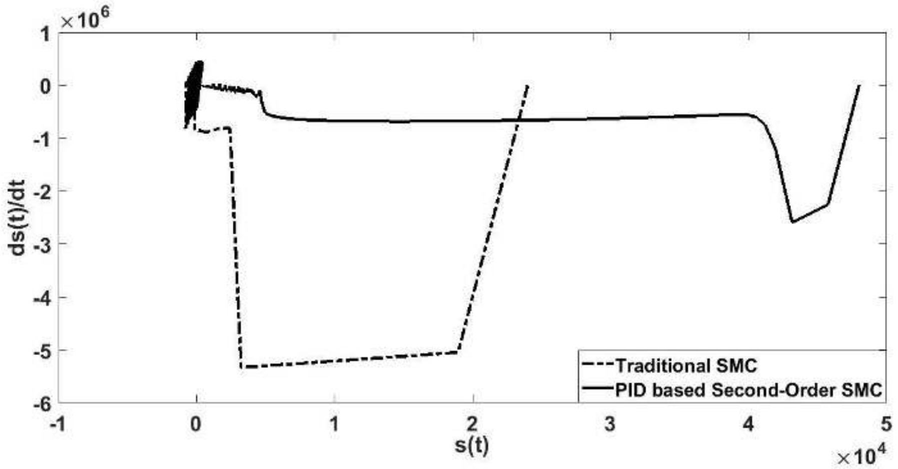

Figure 5.23. Sliding surface versus their first-time derivative changes on the traditional SMC with signum function and PID-based second-order SMC for set point 1200 rpm

Figure 5.24 shows the experimental results of the control signal of the traditional SMC with the signum function given in Equation (3.8) and the control signal of the PID-based second-order SMC given in Equation (3.31) for a set point 1800 rpm. The control signal of the PID-based second-order SMC is bounded in the range of |1-2.25|V while the control signal of Traditional SMC with Signum function is bounded in the range of| 0.8-1.65|V at steady-state. It is obvious that the PID-based second-order SMC considerably reduces the chattering phenomenon in comparison with the traditional SMC with the signum function. It is also seen that chattering increases on the PID-based second-order SMC at 1800 rpm as compared to 1200 rpm.

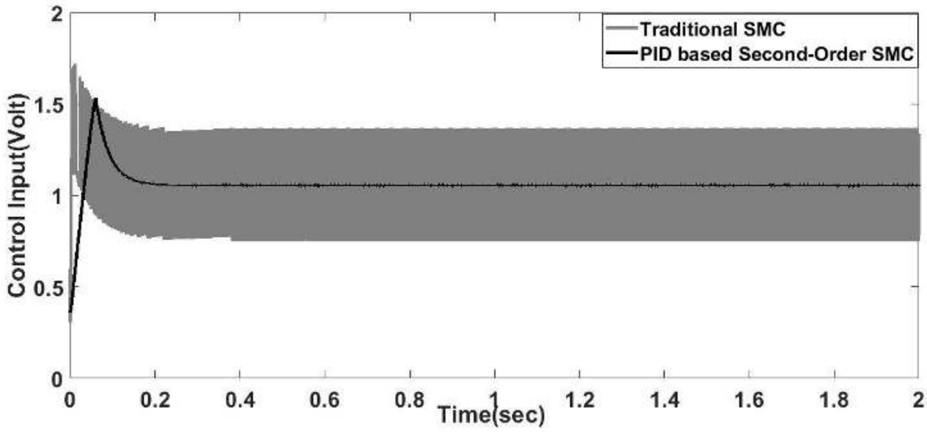

Figure 5.24. Control signals for the traditional SMC with signum function and the PID-based second-order SMC for set point 1800 rpm

Fig 5.25 shows the experimental results of the velocities of the traditional SMC with the signum function and the velocities of PID-based second-order SMC for a set point 1800 rpm. The PID-based second-order SMC and the traditional SMC with the signum function have reached the desired reference value as seen in the figure. The PID-based second-order SMC reveals neither oscillation nor overshoot while the traditional SMC with the signum function has oscillation. From the figure, it is clearly seen that the PID-based second-order SMC exhibits faster speed response than the traditional SMC with the signum function. It also shows no oscillation to be able to track the reference signal against the motor parameter variations and external disturbances. The settling time and steady-state errors are about 0.19 sec and 14 rpm, respectively, for the PID-based second-order SMC. It is clear that the PID-based second-order SMC has less output variation from the trajectory in steady state compared with the traditional SMC with the signum function that deviates approximately 105 rpm from the desired speed.

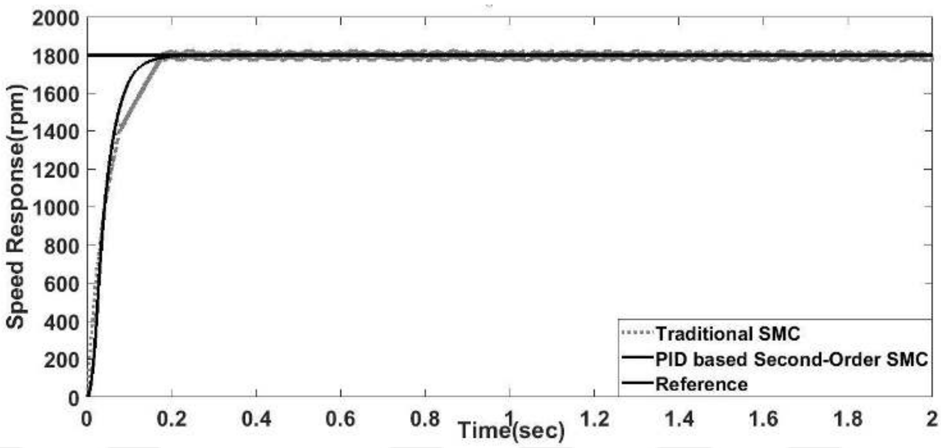

Figure 5.25. Step responses for PID-based second-order SMC and the traditional SMC with signum function for set point 1800 rpm

Figure 5.26a and Figure 5.26b show the sliding surfaces of the traditional SMC with the signum function and the PID-based second-order SMC for a set point 1800 rpm. The sliding functions converge to zero in finite time when using Equation (3.5) and two times integral $\left(\int_0^t\int_0^t \ddot{\sigma}(\tau)d\tau d\tau\right)$ of Equation (3.28). Initial values and variations around the desired point of the sliding surface of the PID-based second-order SMC are small in magnitude as compared to the sliding surface of the traditional SMC with the signum function.

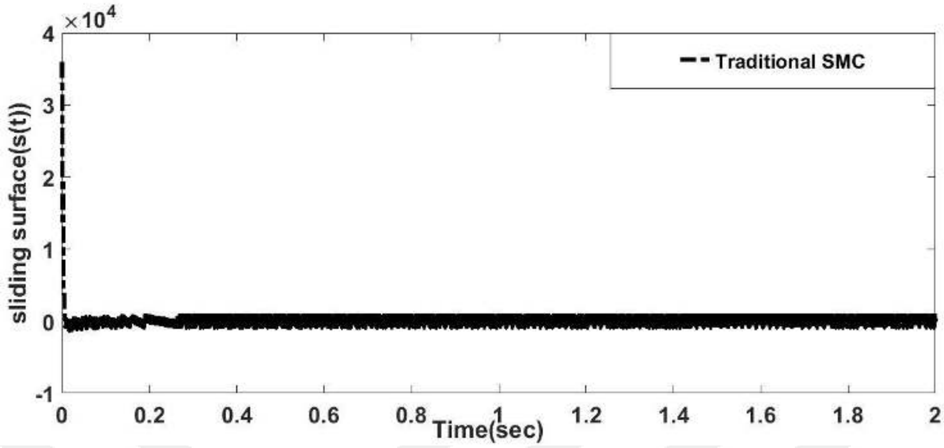

Figure 5.26. (a). Sliding surface for the traditional SMC with signum function for set point 1800 rpm

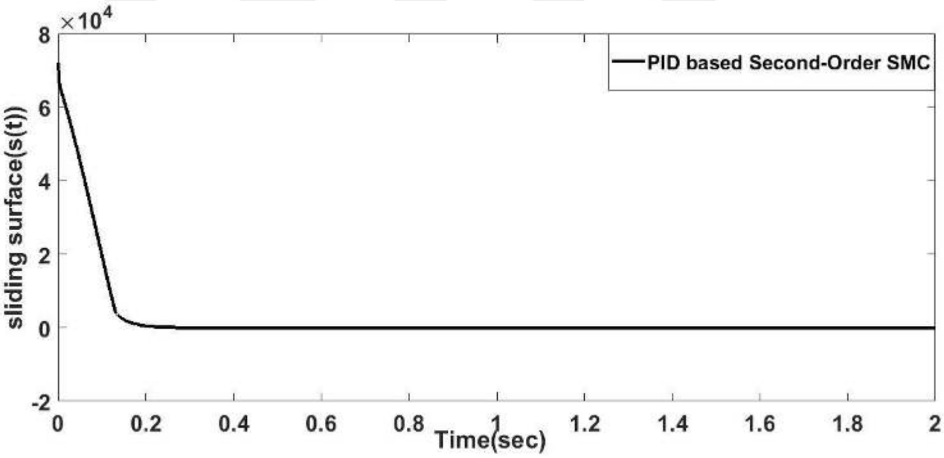

Figure 5.26. (b). Sliding surface for the PID-based second-order SMC for set point 1800 rpm

The sliding surfaces of the controllers versus time derivatives of the sliding surfaces are shown in Figure 5.27. The magnitudes of the sliding surfaces converge to zero and remain nearly stable at that value as already stated in. The sliding surface of the PID-based second-order SMC shows behavior with small variations in both $s(t)$ and $\dot{s}(t)$ which yields significantly reduced chattering produced by the switching control in Equation (3.31).

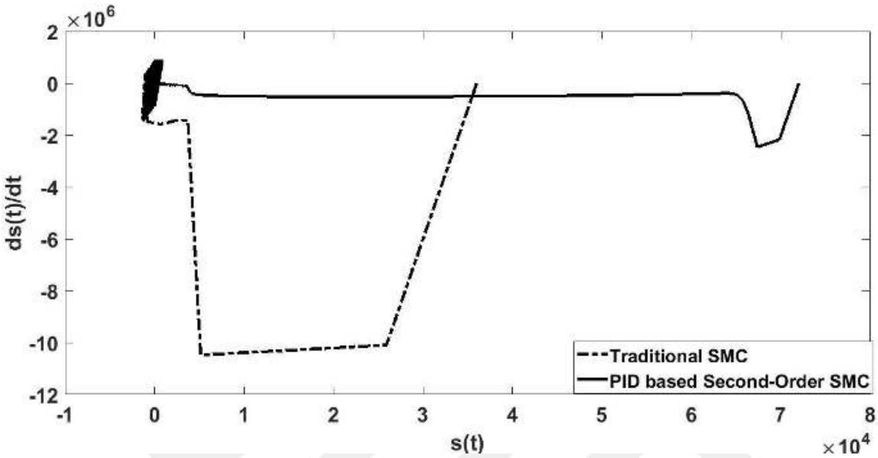

Figure 5.27. Sliding surfaces versus their first-time derivative changes on the traditional SMC with the signum function and PID-based second-order SMC for set point 1800 rpm

We can conclude that the PID-based second-order SMC with the signum function manages successfully the chattering more efficiently than the traditional SMC with the signum function on the electromechanical system with uncertainties and disturbances but without fault.

Experimental results of the adaptive dynamic fault-tolerant first-order and PID-based second-order SMCs designed and proposed, respectively, in order to be able to cope with faults will report in next subsection.

5.2. Adaptive Dynamic First and Second-Order Fault-Tolerant SMCs

In this part of the thesis, experimental results of the adaptive dynamic PID sliding surface based first and second-order fault-tolerant sliding mode controllers given in Equation (4.13) and Equation (4.38), respectively, for speed control of the electromechanical system in Equation (4.1) under uncertainties and disturbances are to report. The thesis aims to show how to utilize the robust properties of second-order adaptive dynamic sliding mode control on the problem of component fault. The Lyapunov theorem is used for affirming the design and stability of the closed-loop system. The presented adaptive dynamic first and second-order fault-tolerant sliding mode controllers and the traditional sliding mode controller with the signum function are compared with each other and the results are discussed. The experimental results of the designed and proposed fault-tolerant controllers, concerning parametric uncertainties and disturbances, acquire suitable tracking performance and show more robustness than the traditional SMC with the signum function.

In order to add a fault function to the real electromechanical system, a magnet in the experiment set is used. This magnet imposes certain values of load on the system and this load constitutes a fault function. The amount of load on the system may increase or decrease with the position of the magnet. While the system given in Equation (4.1) is under a certain load, the designed controllers given in Equation (3.8), Equation (4.13) and Equation (4.38) are tested and compared with each other. As shown in the adaptive fault gain figures, the loads added to the system have been found by using the adaptation laws given in Equation (4.27) and Equation (4.55). These loads are as follows: $\eta = 0.5$, $\eta = 0.8$, $\eta = 1$. To test the performances of the designed and proposed controllers, control inputs and speed responses are considered and compared with each other. The parameters of the traditional SMC with the signum function presented in Table 5.1 are utilized and the parameters of the first and second order ADFTSMCs given in Table 5.4 are used.

Table 5.4. Parameters of the first and second-order ADFTSMCs

Parameter	**Value**
H	0.01
Y	0.0000007
p_1	1×10^{5}
p_2	5×10^{-5}
T	20
k_p	30
k_d	10
k_i	1

Estimations of η are computed using Equation (4.27) for the first-order ADFTSMC and Equation (4.55) for the second-order ADFTSMC. In all experiments regarding to first and second-order ADFTSMCs initial conditions of the estimations of the fault gains to solve Equation (4.27) and Equation (4.55) are set to zero $\hat{\eta}(0)=0.$ If we consider the adaptation laws in Equation (4.27) and in Equation (4.55) there is small difference between them. That is the term in the bracket $\{[x_2(t)+x_1(t)+u(t)]Y\}$ is the same but the terms outside of the bracket are different a little which are $s(t)$ in Equation (4.27) and $k_d\dot{\sigma}(t)$ in Equation (4.55).

5.2.1. Adaptive Fault Gain 0.5 and Set Point 1200 rpm

In this part, the experimental results under a set point 1200 rpm and for a fault gain η = 0.5 are reported below. The variations of the adaptive fault gains, η, adding to the system given in (4.1) are shown in Figure 5.28.

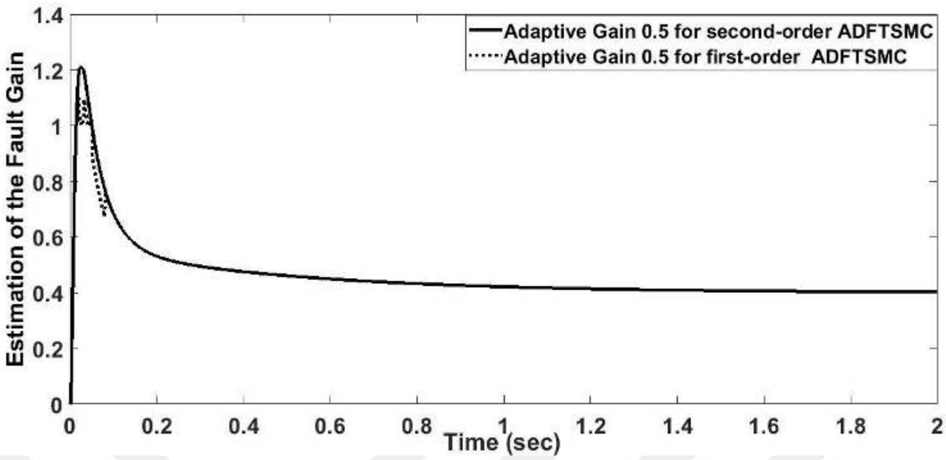

Figure 5.28. Adaptive fault gains $\eta = 0.5$ for set point 1200 rpm

When the load is 0.5, the control input is shown in Figure 5.29. As seen in the figure, the chattering is clearly observed when the traditional SMC with the signum function given in Equation (3.8) is used. Although the first order ADFTSMC given in Equation (4.13) reduces the chattering problem compared to the traditional SMC with the signum function given in Equation (3.8), the problem remains. However, the second-order ADFTSMC given in Equation (4.38) significantly eliminates the chattering problem. The control signal of the second-order ADFTSMC is bounded in the range of |1.10-1.15|V while the control signal of the first order ADFTSMC is bounded in the range of |1-1.25|V and the control signal of the Traditional SMC with the Signum function is bounded in the range of |0.8-1.4|V at steady-state.

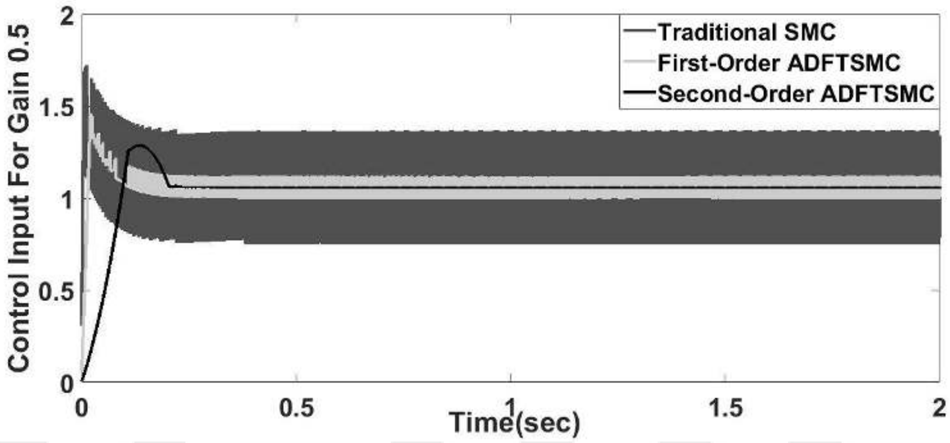

Figure 5.29. Control signals for traditional SMC with signum function, first-order ADFTSMC and second-ADFTSMC for set point 1200 rpm, adaptive fault gain $\eta = 0.5$.

Fig 5.30. shows step responses of the traditional SMC with the signum function given in Equation (3.8), first order ADFTSMC given in Equation (4.13) and second order ADFTSMC given in Equation (4.38) for a set point 1200 rpm and adaptive fault gain $\eta = 0.5$. All controllers reveal neither oscillation nor overshoot. As seen, the traditional SMC with the signum function does not reach the desired reference value and remains at 1100 rpm which causes a steady-state error of 8.3 percent in the controlled system. The first-order and second-order ADFTSMCs given in Equation (4.13) and Equation (4.38), respectively, have reached the desired reference value as seen in the figure. The figure shows that the second-order ADFTSMC is 0.19 sec faster in settling time than the first-order ADFTSMC. The steady-state errors are about 5 rpm and 9 rpm, respectively, for the second-order ADFTSMC and first-order ADFTSMC. These results show that the proposed second-order ADFTSMC performs better and faster than the designed first-order ADFTSMC.

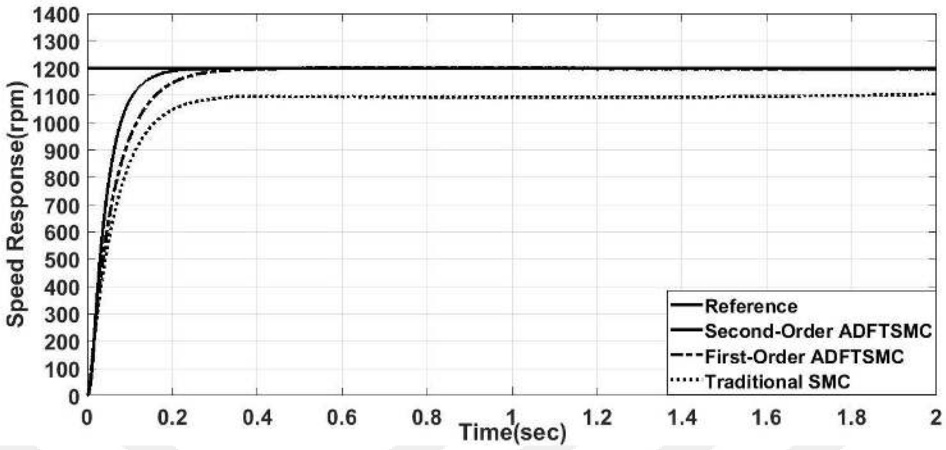

Figure 5.30. Speed responses for the traditional SMC with signum function, first-order ADFTSMC and second-ADFTSMC for set point 1200 rpm, adaptive fault gain $\eta = 0.5$.

5.2.2. Adaptive Fault Gain 0.8 and Set Point 1200 rpm

In this part, the experimental results under a set point 1200 rpm and for a fault gain $\eta = 0.8$ are reported below. The variations of the adaptive fault gains, η, adding to the system given in (4.1) are shown in Figure 5.31. One can observe from the figure that there is a small difference between the curves which is arised from the terms $s(t)$ in Equation (4.27) and $k_d \dot{\sigma}(t)$ in Equation (4.55). If we examine the equations mentioned above in detail, we would see integral of the error in Equation (4.55) different from Equation (4.27).

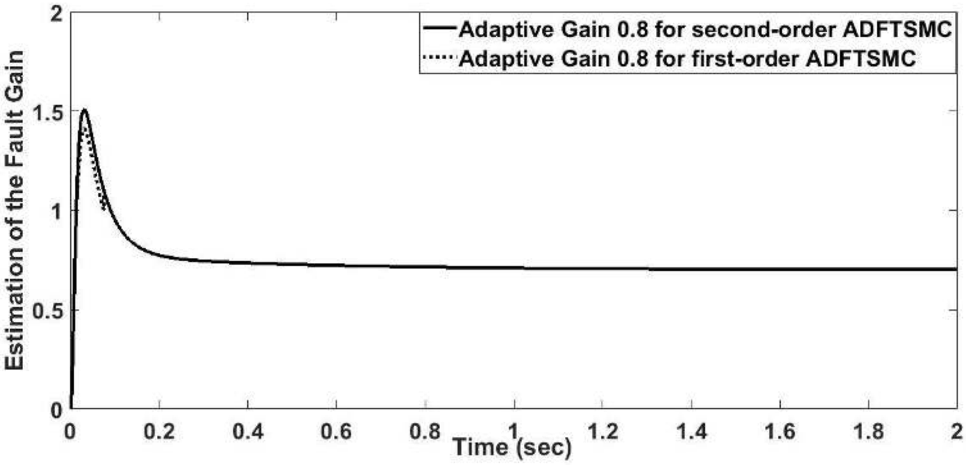

Figure 5.31. Adaptive fault gain $\eta = 0.8$ and set point 1200 rpm

When the load is $\eta = 0.8$, the control input graphics of the controllers are shown in Figure 5.32. It is observed that when the load value is 0.8, the chattering problem increases more than when the load value is 0.5. In the traditional SMC with the signum function given in Equation (3.8), chattering is much higher than the designed first and the proposed second-order ADFTSMCs given in Equation (4.13) and given in Equation (4.38), respectively. Chattering problem in the first-order ADFTSMC decreases compared to the traditional SMC with the signum function but continues. However, the second-order ADFTSMC manages to eliminate the chattering problem again. The control signal of the second-order ADFTSMC is bounded in the range of |1.10-1.15|V while the control signal of the first-order ADFTSMC is bounded in the range of |0.9-1.25|V and the control signal of the traditional SMC with the signum function is bounded in the range of |0.6-1.6|V at steady-state.

If we investigate the control inputs given by Equation (4.13) and Equation (4.38) for the first and second-order ADFTSMC, respectively, we would become aware of the sliding surface $s(t)$ and the derivative of the sliding surface $\dot{\sigma}(t)$ which are almost only one difference between Equation (4.13) and Equation (4.38).

The integral of the sliding surface $\dot{\sigma}(t)$ reduces the chattering on the control signal of the second-order ADFTSMC.

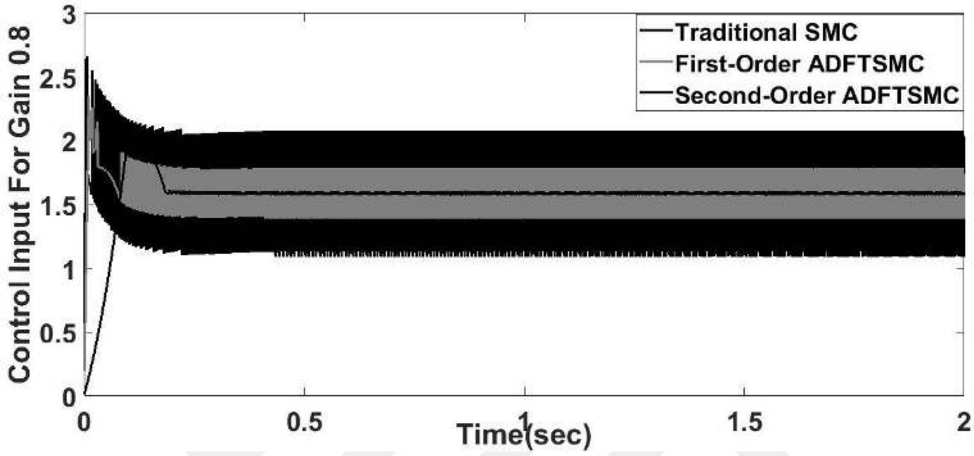

Figure 5.32. Control signals for the traditional SMC with signum function, first-order ADFTSMC and second-ADFTSMC for set point 1200 rpm, adaptive fault gain $\eta = 0.8$

Fig 5.33 shows step responses of the traditional SMC with the signum function given in Equation (3.8), first-order ADFTSMC given in Equation (4.13) and second-order ADFTSMC given in Equation (4.38) for a set point 1200 rpm and adaptive fault gain $\eta = 0.8$. All controllers reveal neither oscillation nor overshoot. It seems that the traditional SMC does not approach the reference value and remains at 1050 rpm. This corresponds to a 12.5 percent steady-state error in the system. As seen, the steady-state error percentage is 4.2 percent higher than the case where the load is 0.5. The designed first and proposed second-order ADFTSMCs given in Equation (4.13) and Equation (4.38), respectively, as in the case where the load value is 0.8 have reached the desired reference value as seen in the figure. The figure shows that the second-order ADFTSMC is 0.21 sec faster on settling time than the first-order ADFTSMC. As shown in the same way, the steady-state errors are about 6 rpm and 11 rpm, respectively, for the second-order ADFTSMC and first-order ADFTSMC. These results show that the proposed second-order ADFTSMC performs better and faster than the first-order ADFTSMC.

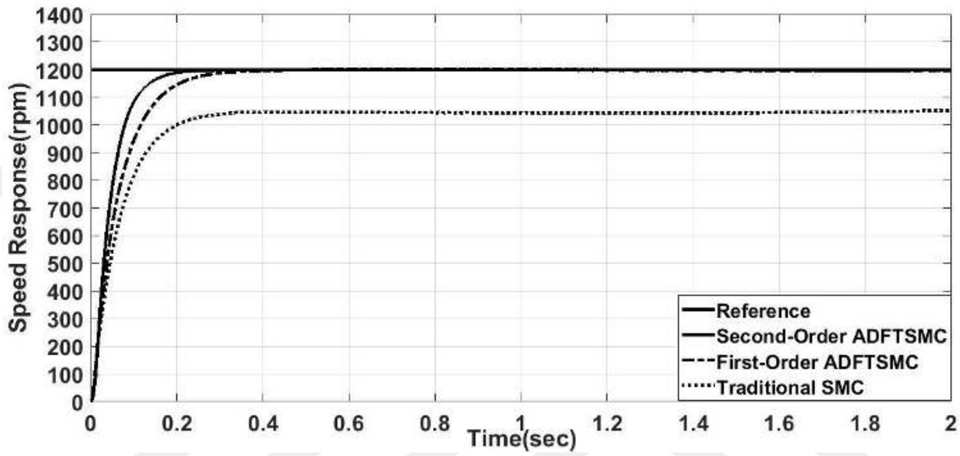

Figure 5.33. Speed responses for the traditional SMC with signum function, first-order ADFTSMC and second-ADFTSMC for set point 1200 rpm, adaptive fault gain $\eta = 0.8$

5.2.3. Adaptive Fault Gain 1 and Set Point 1200 rpm

In this part, the experimental results under a set point 1200 rpm and for a fault gain $\eta = 1$ are reported below. The variations of the adaptive fault gains, η adding to the system given in (4.1) are shown in Figure 5.34.

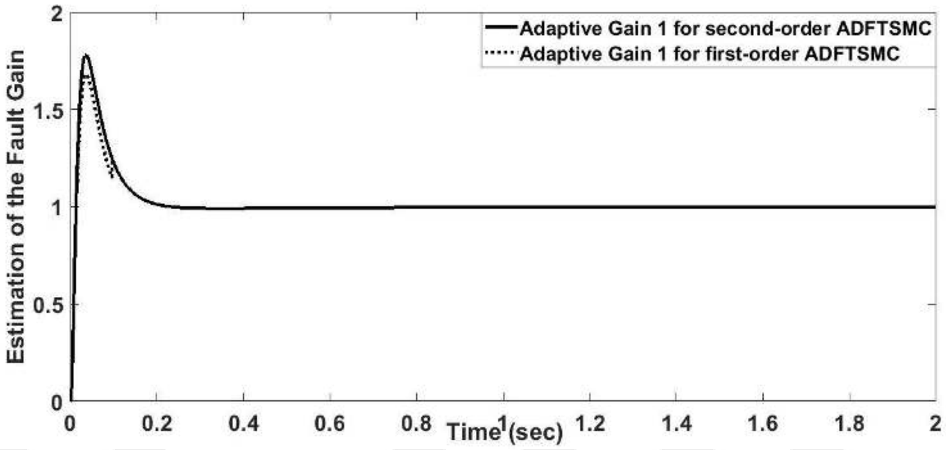

Figure 5.34. Adaptive fault gain $\eta = 1$ for set point 1200 rpm

Figure 5.35 shows the control input graphs of the controllers that are the proposed and designed in case the adaptive fault gain $\eta = 1$. As seen in the figure, the chattering is clearly observed when the traditional SMC with the signum function given in Equation (3.8) is used. It is observed that when adaptive fault gain $\eta = 1$, the chattering problem in the traditional SMC with the signum function increases even more than when the adaptive fault gain $\eta = 0.8$. Although the first order ADFTSMC given in Equation (4.13) reduces the chattering problem compared to the traditional SMC with the signum function given in Equation (3.8), the problem still remains. However, the second-order ADFTSMCs given in Equation (4.38) manages to eliminate the chattering problem again. The control signal of the second-order ADFTSMC is bounded in the range of |1.10-1.15|V while the control signal of the first-order ADFTSMC is bounded in the range of |0.85-1.25|V and the control signal of the traditional SMC with the signum function is bounded in the range of |0.5-1.65|V at steady-state.

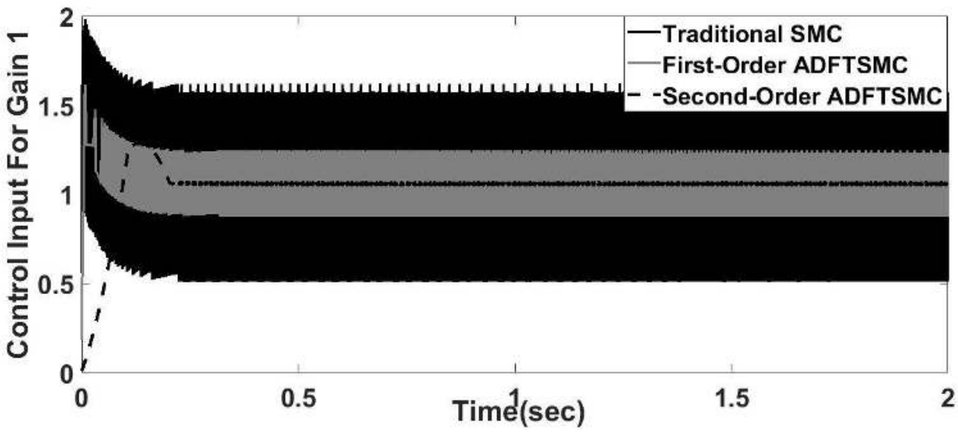

Figure 5.35. Control signals for traditional SMC with signum function, first-order ADFTSMC and second-ADFTSMC for set point 1200 rpm, adaptive fault gain $\eta = 1$

Figure 5.36 shows step responses of the traditional SMC with the signum function given in Equation (3.8), first order ADFTSMC given in Equation (4.13) and second order ADFTSMC given in Equation (4.38) for a set point 1200 rpm and adaptive fault gain $\eta = 1$. All controllers reveal neither oscillation nor overshoot. As seen, the traditional SMC with the signum function does not reach the desired reference value again and remains at 1000 rpm which causes a steady-state error of 16.6 percent in the system. The first-order and second-order ADFTSMC given in Equation (4.13) and Equation (4.38), respectively, have reached the desired reference value as seen in the figure. As can be seen, the error percentage is 8.3 percent more when the load value is 0.5 and 4.1 percent higher when the load value is 0.8. The figure shows that the second-order ADFTSMC is 0.19 sec faster on settling time than the first-order ADFTSMC. The steady-state errors are about 8 rpm and 13 rpm, respectively, for the second-order ADFTSMC and first-order ADFTSMC. These results show that the proposed second-order ADFTSMC performs better and faster than the designed first order ADFTSMC.

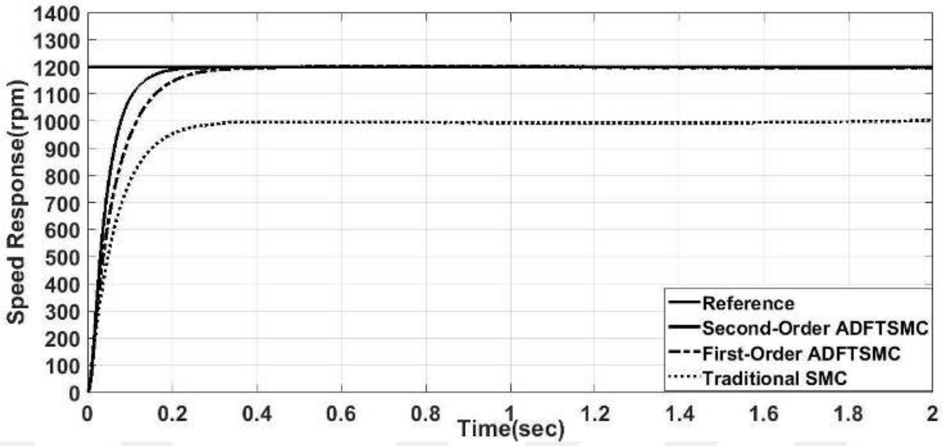

Figure 5.36. Speed responses for the traditional SMC with signum function, first-order ADFTSMC and second-ADFTSMC for set point 1200 rpm, adaptive fault gain $\eta = 1$

5.2.4. Adaptive Fault Gain 0.5 and Set Point 1800 rpm

In this part, some results under set point 1800 rpm and for a fault gain = 0.5 are given below. When the load is $\eta = 0.5$, the control input graph is shown in Figure 5.37. As seen in the figure, the chattering is clearly observed when the traditional SMC with the signum function given in Equation (3.8) is used. Although the first-order ADFTSMC given in Equation (4.13) reduces the chattering problem compared to the traditional SMC with the signum function given in Equation (3.8), the problem still remains. However, the second-order ADFTSMC given in Equation (4.38) significantly eliminates the chattering problem. The control signal of the second-order ADFTSMC is bounded in the range of |1.6-1.65|V while the control signal of the first-order ADFTSMC is bounded in the range of |1.5-1.75|V and the control signal of the traditional SMC with the signum function is bounded in the range of |1.2-1.85|V at steady-state. As expected, the chattering is the most on the control signal of the traditional SMC with the signum function among three controllers but it is the least on the second-order ADFTSMC.

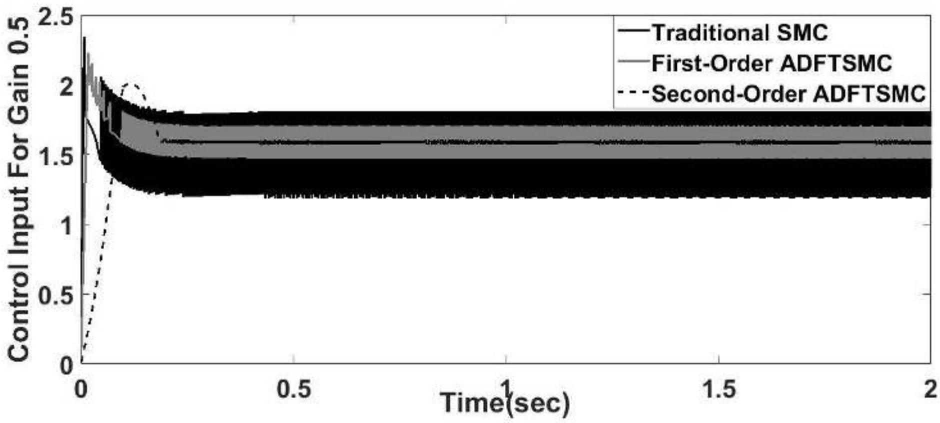

Figure 5.37. Control signals for the traditional SMC with signum function, first-order ADFTSMC and second-ADFTSMC for set point 1800 rpm, adaptive fault gain $\eta = 0.5$

Fig 5.38 shows step responses of the traditional SMC with the signum function given in Equation (3.8), first-order ADFTSMC given in Equation (4.13) and second-order ADFTSMC given in Equation (4.38) for a set point 1800 rpm and adaptive fault gain $\eta = 0.5$. Although the proposed second order ADFTSMC reveals neither oscillation nor overshoot, the first-order ADFTSMC reveals 2.77 percent overshoot and the traditional SMC with the signum function reveals 5.55 percent undershoot. As seen from the figure, the traditional SMC with the signum function does not reach the desired reference value and remains at 1700 rpm which causes a steady-state error of 5.55 percent in the controlled system. The first-order and second-order ADFTSMC given in Equation (4.13) and Equation (4.38), respectively, have reached the desired reference value as seen in the figure. The figure shows that the second-order ADFTSMC is 0.1 sec faster on settling time than the first-order ADFTSMC. The steady-state errors are about 5 rpm and 12 rpm, respectively, for the second-order ADFTSMC and first-order ADFTSMC. These results show that the proposed second-order ADFTSMC performs better and faster than the designed first-order ADFTSMC.

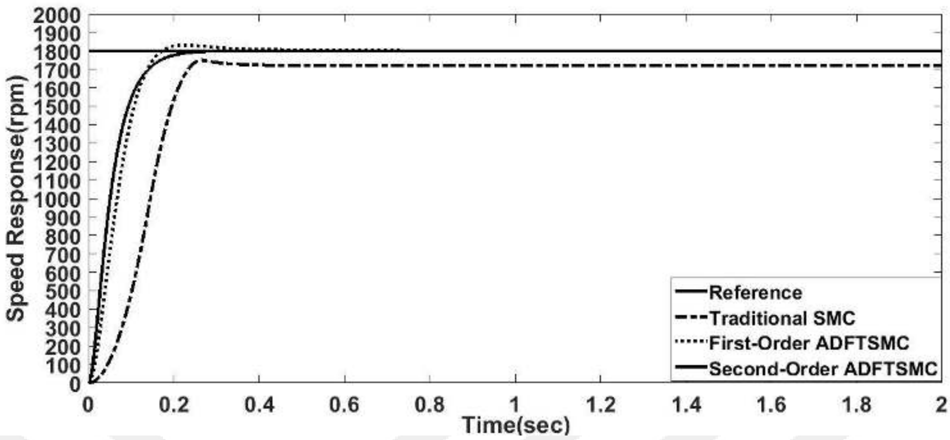

Figure 5.38. Speed responses for the traditional SMC with signum function, first-order ADFTSMC and second-ADFTSMC for set point 1800 rpm, adaptive fault gain $\eta = 0.5$

5.2.5. Adaptive Fault Gain 0.8 and Set Point 1800 rpm

In this part of the thesis, some experimental results for a set point 1800 rpm and for a fault gain = 0.8 are reported. When the load is $\eta = 0.5$, the control input graph is shown in Figure 5.39. As seen in the figure, the chattering is clearly observed when the traditional SMC with the signum function given in Equation (3.8) is used. Although the first-order ADFTSMC given in Equation (4.13) reduces the chattering problem compared to the traditional SMC with signum function given in Equation (3.8), the problem continuous to remain. However, the second-order ADFTSMCs given in Equation (4.38) significantly eliminates the chattering problem. The control signal of the second-order ADFTSMC is bounded in the range of |1.6-1.65|V while the control signal of the first-order ADFTSMC is bounded in the range of |1.55-1.85|V and the control signal of the traditional SMC with the signum function is bounded in the range of |1.2-2.1|V at steady-state. The proposed second-order ADFTSMC achieves to decrease chattering on the control signals the best among three controllers.

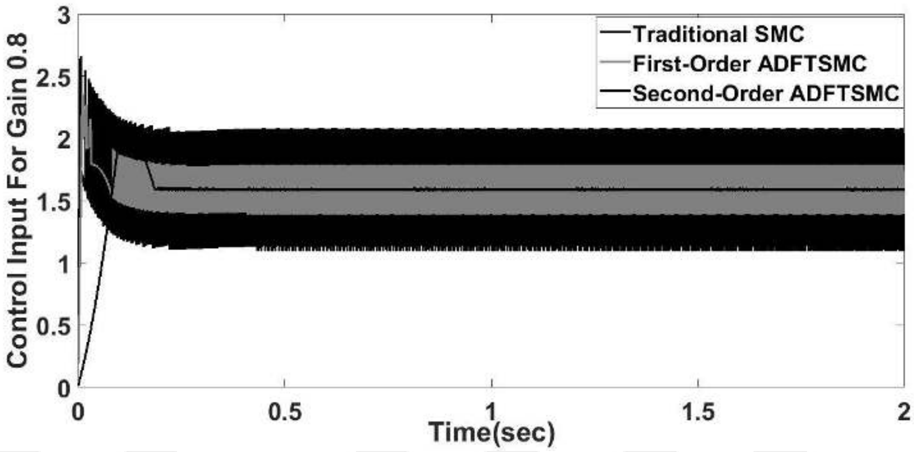

Figure 5.39. Control signals for the traditional SMC with signum function, first-order ADFTSMC and second-ADFTSMC for set point 1800 rpm, adaptive fault gain $\eta = 0.8$

Fig 5.40 shows step responses of the traditional SMC with the signum function given in Equation (3.8), first-order ADFTSMC given in Equation (4.13) and second-order ADFTSMC given in Equation (4.38) for a set point 1800 rpm and adaptive fault gain $\eta = 0.8$. Although the proposed second-order ADFTSMC reveals neither oscillation nor overshoot, the first-order ADFTSMC reveals 2.65 percent overshoot and the traditional SMC with the signum function reveals 11.11 percent undershoot. As seen from the figure, the traditional SMC with the signum function does not reach the desired reference value and remains at 1600 rpm which causes a steady-state error of 11.11 percent in the system. As seen, the steady-state error percentage is 5.56 percent higher than the case where the load is 0.5. The first-order and second-order ADFTSMC given in Equation (4.13) and Equation (4.38), respectively, have reached the desired reference value as seen in the figure. The figure shows that the second-order ADFTSMC is 0.1 sec faster on settling time than the first-order ADFTSMC. The steady-state errors are about 5 rpm and 11 rpm, respectively, for the second-order ADFTSMC and first-order ADFTSMC. These results show that the proposed second-order ADFTSMC performs better and faster than the first-order ADFTSMC and the traditional SMC with the signum function on its switching control part.

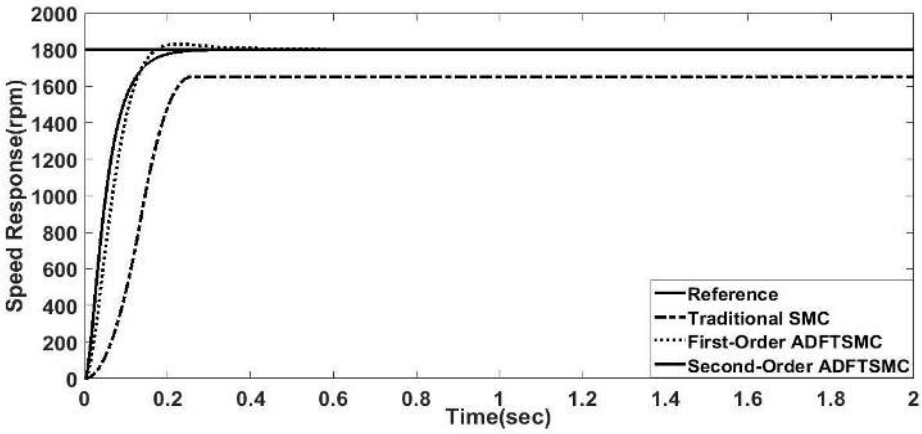

Figure 5.40. Speed responses for the traditional SMC with signum function, first-order ADFTSMC and second-ADFTSMC for set point 1800 rpm, adaptive fault gain $\eta = 0.8$

5.2.6. Adaptive Fault Gain 1 and Set Point 1800 rpm

In this part, the experimental results under a set point 1800 rpm and for a fault gain $\eta = 1$ are reported below. When the load is $\eta = 1$, the control input graph is shown in Figure 5.41. As seen in the figure, the chattering is clearly observed when the traditional SMC with signum function given in Equation (3.8) is implemented to the electromechanical system in Equation (4.1). Although the first order ADFTSMC given in Equation (4.13) reduces the chattering problem compared to the traditional SMC with signum function given in Equation (3.8), the problem remains. However, the second order ADFTSMC given in Equation (4.38) significantly eliminates the chattering problem. The control signal of the second order ADFTSMC is bounded in the range of |1.6-1.65|V while the control signal of first order ADFTSMC is bounded in the range of |1.25-1.85|V and the control signal of Traditional SMC with the Signum function is bounded in the range of |1-2.2|V at steady-state.

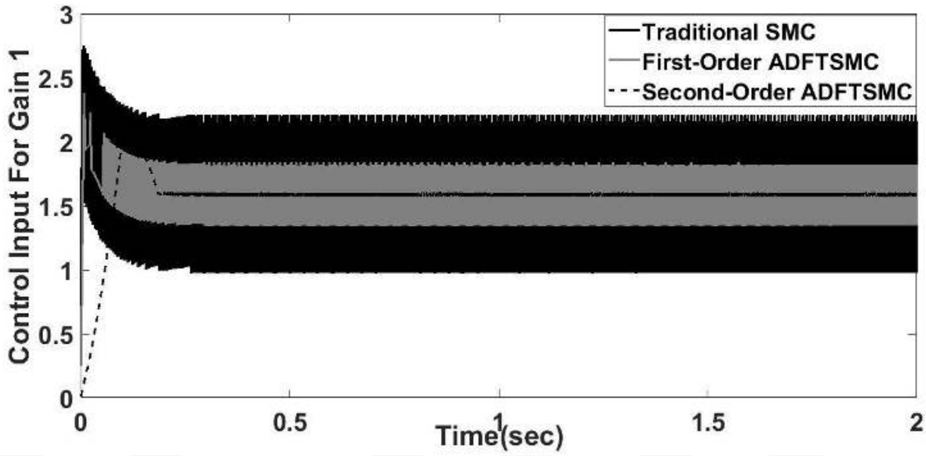

Figure 5.41. Control signals for the traditional SMC with signum function, first-order ADFTSMC and second-ADFTSMC for set point 1800 rpm, adaptive fault gain $\eta = 1$

Fig 5.42 shows step responses of the traditional SMC with the signum function given in Equation (3.8), first-order ADFTSMC given in Equation (4.13), and second-order ADFTSMC given in Equation (4.38) for a set point 1800 rpm and adaptive fault gain $\eta = 1$ The designed first and proposed second-order ADFTSMC's reveal 1.65 percent and 2.7 percent overshoots, respectively, and the traditional SMC with the signum function reveals 16.6 percent undershoot. If we concede from the fast transient-response by changing some non-adaptable parameters of the controllers in order to alleviate the overshoot on the response, we would obtain also better transient response for the second-order ADFTSMC than the others. As seen, the traditional SMC with the signum function does not reach the desired reference value and remains at 1500 rpm which causes a steady-state error of 16.6 percent in the controlled system. As can be observed from the figure, the steady-state error percentage is 5.49 percent higher than the case where the load is 0.8 and 11.05 percent higher than the case where the load is 0.5. It can be said that as the load added to the system increases, the steady-state error increases proportionally. The first-order and second-order ADFTSMCs given in Equation

(4.13) and Equation (4.38), respectively, have reached the desired reference value as seen in the figure. The figure shows that the second-order ADFTSMC is 0.18 sec faster on settling time than the first-order ADFTSMC. The steady-state errors are about 4 rpm and 13 rpm, respectively, for the second-order ADFTSMC and first-order ADFTSMC. These results show that the proposed second-order ADFTSMC performs better and faster than the first-order ADFTSMC.

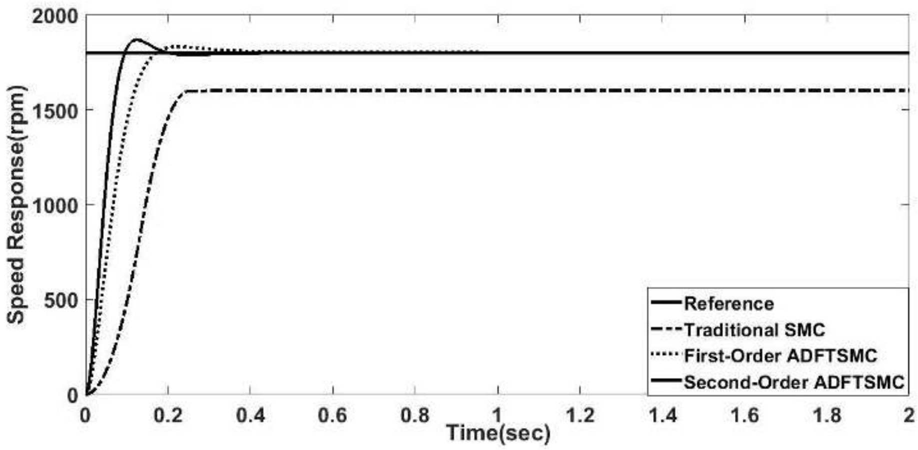

Figure 5.42. Speed responses for the traditional SMC with signum function, first-order ADFTSMC and second-ADFTSMC for set point 1800 rpm, adaptive fault gain $\eta = 1$

This subsection has presented the conclusion that the proposed ADFTSMC performs better in transient and steady-state regimes and also in chattering reduction than the other controllers.

6. CONCLUSION

In this thesis, a first-order and a second-order adaptive dynamic fault-tolerant sliding mode control (ADFTSMC) methods are designed and proposed to control electromechanical systems under faults occurred in the system to be controlled. First, in order to compare chattering eliminations of the first-order (traditional) sliding mode controllers with the signum function and with the saturation function, they are designed and tested. As reported in literature, the traditional SMC with the saturation function reduces the chattering on the control signal more than one with the signum function. Afterwards, the second-order (super-twisting algorithm) SMC is compared with the traditional SMC with the signum function. It is seen that the super-twisting algorithm SMC performs better than the traditional SMC with signum function in view of chattering. Due to the fact that the component fault which is studied in this thesis occurs on system parameters instead of the super-twisting algorithm SMC which is the non-model based, the PID-based second-order SMC is preferred.

In order to confirm the effectiveness of the designed and proposed ADFTSMCs, they are applied to a real electromechanical system given in Chapter 2. The designed and proposed first and second-order ADFTSMCs keep the advantages of the traditional SMC about coming through uncertainties, dead-zones, disturbances and chattering and overcome the fault that may be occurred in the system. It is also aimed to improve chattering reduction of the proposed controller by making it a second order.

The experimental results show that, the second-order ADFTSMC is more effective compared to the first-order ADFTSMC in terms of fault-tolerant and chattering reduction attributes. Also, the experimental results prove that, on average, the second-order ADFTSMC provides more robust control in terms of reducing the chattering 8 times than the first-order ADFTSMC and 23 times than the first-order (traditional) SMC at steady-state. Furthermore, the traditional SMC with the signum function does not reach the desired reference value in all results and causes, on average, a steady-state error of 12 percent in the controlled system. Moreover, the experimental results show that the second-order ADFTSMC, on average, is 0.18 sec faster on settling time than the first-order ADFTSMC.

This study provides a basis for the application of the ADFTSMC to the real electromechanical systems. In addition, by applying the designed and proposed controllers on a real system, it is aimed to show the applicability of the controllers on systems that are more complex such as quadrotor helicopter, missile system, robotic manipulators. In future studies, it is aimed to test the designed and proposed controllers on a more complex system. It is also planned to make the designed and proposed controllers fractional-order.

REFERENCES

Akpolat, Z., & Gokbulut, M. (2003). Discrete time adaptive reaching law speed control of electrical drives. Electrical Engineering, 85(1), 53-58.

Alwi, H. and Edwards, C., 2006. Sliding mode FTC with on-line control allocation. In Decision and Control, 45th IEEE Conference on (pp. 5579-5584). IEEE.

Alwi, H. and Edwards, C., 2008. Fault tolerant control using sliding modes with on-line control allocation. Automatica, 44(7): 1859-1866.

Alwi, H., and Edwards, C., 2008. Fault detection and fault-tolerant control of a civil aircraft using a sliding-mode-based scheme. IEEE Transactions on Control Systems Technology, 16(3), 499-510.

Aydin, M. N. and Coban, R., 2016. Sliding mode control design and experimental application to an electromechanical plant. In Power and Electrical Engineering of Riga Technical University (RTUCON), 57th International Scientific Conference on (pp. 1-4). IEEE.

Aydin, M. N. and Coban, R., 2017. Second-order sliding mode control design and experimental application to a servo motor.

Aydin, M. N., & Coban, R. (2022). PID sliding surface-based adaptive dynamic second-order fault-tolerant sliding mode control design and experimental application to an electromechanical system. International Journal of Control, 1-10.

Bartolini, G., Pisano, A., Punta, E., & Usai, E. (2003). A survey of applications of second-order sliding mode control to mechanical systems. International Journal of control, 76(9-10), 875-892.

Behnamgol, V., A. R. Vali, and I. Mohammadzaman. "Second Order Sliding Mode Control With Finite Time Convergence." Amirkabir International Journal of Modeling, Identification, Simulation & Control 45.2 (2015): 41-52.

Coban, R. (2017). Backstepping integral sliding mode control of an electromechanical system. *Automatika: časopis za automatiku, mjerenje, elektroniku, računarstvo i komunikacije*, *58*(3), 266-272.

Coban, R. (2019). Adaptive backstepping sliding mode control with tuning functions for nonlinear uncertain systems. International Journal of Systems Science, 50(8), 1517-1529.

Edwards, C., Alwi, H. and Tan, C. P., 2010, October. Sliding mode methods for fault detection and fault tolerant control. In Control and Fault-Tolerant Systems (SysTol), Conference on (pp. 106-117). IEEE.

Edwards, C., Alwi, H. and Tan, C., 2012. Sliding mode methods for fault detection and fault tolerant control with application to aerospace systems. International Journal of Applied Mathematics and Computer Science, 22(1), 109-124.

Edwards, C., Lombaerts, T. and Smaili, H., 2010. Fault tolerant flight control. Lecture Notes in Control and Information Sciences, 399, 1-560.

Fekih, A. and Pilla, P., 2007. A passive fault tolerant control strategy for the uncertain MIMO aircraft model F-18. In System Theory SSST'07. Thirty-Ninth Southeastern Symposium on (pp. 320-325). IEEE.

Hamayun, M. T., Edwards, C. and Alwi, H., 2016. A fault tolerant direct control allocation scheme with integral sliding modes. In Fault Tolerant Control Schemes Using Integral Sliding Modes (pp. 63-79). Springer International Publishing.

Hitachi, Y., 2009. Damage-tolerant control system design for propulsion-controlled aircraft (Doctoral dissertation).

Hu, Q. and XIAO, B., 2011. Fault-tolerant sliding mode attitude control for flexible spacecraft under loss of actuator effectiveness. Nonlinear Dynamics, 64(1-2), 13-23.

Kalayci, M. B., & Yiğit, I. (2015). Pratikte Kullanilan Bazi Kayan Kipli Kontrol Tekniklerinin Teorik Ve Deneysel Incelenmesi. *Journal of the Faculty of Engineering & Architecture of Gazi University*, *30*(1).

Kesarkar, A. A. And Selvaganesan, N., 2013. Fractional control of precision modular servo setup for better limit cycle suppression. In Control Applications (CCA), IEEE International Conference on (pp. 467-471). IEEE.

Laghrouche, S., Plestan, F., & Glumineau, A. (2007). Higher order sliding mode control based on integral sliding mode. Automatica, 43(3), 531-537.

Langlois, N., Guermouche, M., Ali, S. A., & ALI, M. G. S. A. (2015). Super-twisting algorithm for DC motor position control via disturbance observer. *IFAC-PapersOnLine*, *48*(30), 43-48.

Levant, A. (1993). Sliding order and sliding accuracy in sliding mode control. International journal of control, 58(6), 1247-1263.

Levant, A. (2003). Higher-order sliding modes, differentiation and output-feedback control. *International journal of Control*, *76*(9-10), 924-941.

Levant, A. (2007). Principles of 2-sliding mode design. automatica, 43(4), 576-586.

Li, T., Zhang, Y. and Gordon, B. W., 2013. Passive and active nonlinear fault-tolerant control of a quadrotor unmanned aerial vehicle based on the sliding mode control technique. Proceedings of the Institution of Mechanical Engineers, Part I: Journal of Systems and Control Engineering, 227(1), 12-23.

Li, X. and Liu, H. H., 2012. A passive fault tolerant flight control for maximum allowable vertical tail damaged aircraft. Journal of Dynamic Systems, Measurement, and Control, 134(3), 031006.

Lin, W. B., & Chiang, H. K. (2013). Super-twisting algorithm second-order sliding mode control for a synchronous reluctance motor speed drive. *Mathematical Problems in Engineering*, *2013*.

Mobayen, S. (2015). An adaptive chattering-free PID sliding mode control based on dynamic sliding manifolds for a class of uncertain nonlinear systems. Nonlinear Dynamics, 82(1), 53-60.

Mahjoub, S., Mnif, F., & Derbel, N. (2015). Second-order sliding mode approaches for the control of a class of underactuated systems. *International Journal of Automation and Computing*, *12*(2), 134-141.

Park, T., & Park, K. (2009, August). Sliding mode control based on pole-placement method for position control of linear stage. In *2009 ICCAS-SICE* (pp. 5127-5130). IEEE.

Plestan, F., Shtessel, Y., Bregeault, V., & Poznyak, A. (2010). New methodologies for adaptive sliding mode control. International journal of control, 83(9), 1907-1919.

Quintero-Manríquez, E., & Félix, R. A. (2014, August). Second-order sliding mode speed controller with anti-windup for BLDC motors. In *2014 World Automation Congress (WAC)* (pp. 610-615). IEEE.

Rantzer, A., 2001. A dual to Lyapunov's stability theorem. Systems & Control Letters, 42(3), 161-168.

Shtessel, Y., Edwards, C., Fridman, L., & Levant, A. (2014). Sliding mode control and observation (Vol. 10). New York, NY: Springer New York.

Sharifi, F., Mirzaei, M., Gordon, B. W. and Zhang, Y., (2010, October). Fault tolerant control of a quadrotor UAV using sliding mode control. In Control and Fault-Tolerant Systems (SysTol), Conference on (pp. 239-244). IEEE.

Susperregui, A., Tapia, G., & Tapia, A. (2007). Application of two alternative sliding-mode control approaches to DC servomotor position tracking. *IET Electric Power Applications*, *1*(4), 611-621.

Tai, N. T. and Ahn, K. K., 2010. A RBF neural network sliding mode controller for SMA actuator. International Journal of Control, Automation and Systems, 8(6), 1296-1305.

Tan, W., & Packard, A. (2008). Stability region analysis using polynomial and composite polynomial Lyapunov functions and sum-of-squares programming. *IEEE Transactions on Automatic Control*, *53*(2), 565-571.

Van, M. (2018). An enhanced robust fault tolerant control based on an adaptive fuzzy PID-nonsingular fast terminal sliding mode control for uncertain nonlinear systems. IEEE/ASME Transactions on Mechatronics, 23(3), 1362-1371.

Yao, Q. (2020). Adaptive finite-time sliding mode control design for finite-time fault-tolerant trajectory tracking of marine vehicles with input saturation. Journal of the Franklin Institute, 357(18), 13593-13619.

Utkin, V. (1977). Variable structure systems with sliding modes. IEEE Transactions on Automatic control, 22(2), 212-222.

Utkin, V. I., 1992. Sliding modes in optimization and control problems.

Utkin, V., & Lee, H. (2006, June). Chattering problem in sliding mode control systems. In *International Workshop on Variable Structure Systems, 2006. VSS'06.* (pp. 346-350). IEEE.

Utkin, V., Guldner, J. and Shi, J., 2009. Sliding mode control in electro-mechanical systems (Vol. 34). CRC press.

Walcko, K. J., Novick, D. and Nechyba, M. C., 2003. Development of a sliding mode control with extended Kalman filter estimation for subjugator. In Proceedings of the Florida conference on recent advances in robotics.

Wang, T., Xie, W. and Zhang, Y., 2012. Sliding mode fault tolerant control dealing with modeling uncertainties and actuator faults. ISA transactions, 51(3): 386-392.

Xu, S. S. D. (2014, January). Super-twisting-algorithm-based terminal sliding mode control for a bioreactor system. In *Abstract and Applied Analysis* (Vol. 2014). Hindawi.

Young, K. D., Utkin, V. I. and Ozguner, U., 1996. A control engineer's guide to sliding mode control. In Variable Structure Systems, 1996. VSS'96. Proceedings, 1996 IEEE International Workshop on (pp. 1-14). IEEE.

Yu, X. and Kaynak, O., 2009. Sliding-mode control with soft computing: A survey. IEEE transactions on industrial electronics, 56(9), 3275-3285.

Zhao, J., Jiang, B., Shi, P. and He, Z., 2014. Fault tolerant control for damaged aircraft based on sliding mode control scheme. International Journal of Innovative Computing, Information and Control, 10(1), 293-302.

CURRICULUM VITAE

Merve Nilay AYDIN, She received his BSc. from Department of Computer Engineering of Fırat University/Turkey in 2011 and M.Sc from Department of Informatics of Mustafa Kemal University in 2015, respectively. She has been working as a research assistant in Department of Computer Engineering of Iskenderun Teknik University since 2013.